Department of Environment Systems

Graduate School of Frontier Sciences

The University of Tokyo

2017

Master's Thesis

Structure and catalytic stability of zeolites in sub- and supercritical water

Submitted January 26, 2018

Adviser: Professor Oshima Yoshito

Co-Adviser: Professor Tokunaga Tomochika

Apibanborirak Chanwit

47-166641

CONTESTS

Page

LIST OF FIGURES

Page

LIST OF TABLES

Page

LIST OF EQUATIONS

Page

CHAPTER 1 INTRODUCTION

Recently, biomass receive a attention from many researchers to use it as a feedstock for green chemical process to replace current fossil feedstock process such as nature gas and crude oil that will be declined in near future because of its availability and cost elevation (Corma, Iborra, & Velty, 2007; Huber, Iborra, & Corma, 2006). According to recent study, Fossil fuel was estimated to run out before 2100, even if renewable source such as wind and solar and advance technology is applied (Shafiee & Topal, 2009). To reduce the fossil fuel consumption and improve sustainable process, biomass process need to be improved to achieve the economic challenge (Lynd, Wyman, & Gerngross, 1999).

The difference between biomass and fossil feedstocks is the oxygen atom or -OH functional group that exists only in biomass feedstocks. The -OH functional group in biomass provide lower vapor pressure, so liquid phase process will probably play a major role for green chemical process. The polar structure of -OH functional group in biomass also requires ionic liquid solvent to dissolve, and water is the most suitable solvent because it is cheap and able to dissolve the polar organic compound. Especially, water near the critical point (374 ^{o}C) exhibits many useful properties such as high solubility for organic and gaseous compounds, high disassociation of water, and weak hydrogen bond in -OH functional group (Eckert, Liotta, Bush, Brown, & Hallett, 2004; Katritzky, Allin, & Siskin, 1996).

Employing heterogeneous catalyst in sub- and supercritical water is the one possible way to accelerate reaction and decrease the residence time to improve economic challenges. Many researchers have been published the studies of heterogeneously catalysts of biomass conversion in hot compressed water (>200 ^{o}C). These reactions include hydrolysis of cellulose (Luo, Wang, & Liu, 2007), dehydration of monosaccharide to furfural derivatives (Chheda & Dumesic, 2006) and dehydrocyclization of bio-methanol (Ramasamy, Gerber, Flake, Zhang, & Wang, 2014). However, only a few catalyst supports were reported to be stable in sub- and supercritical water due to the severe condition of temperature and pressure. TiO_2 and ZrO_2 are the most general catalyst supports that usually use in sub- and supercritical water due to low solubility in water and hydrothermal stability (Ramasamy et al., 2014). However, the problems are this type of catalyst content precious metal which has a relatively high price, and limiting

property such as absent shape selectivity, lower surface area, and little acidity site comparing with current conventional catalyst.

Zeolites are crystalline aluminosilicate-based compounds with open 3D framework structures composed of SiO_4 and AlO_4^- tetrahedra. They have been widely used as catalyst in many industrial processes because of their selective nature due to their specific pore size, large surface area and high acid density (Čejka, Corma, & Tacey, 2010). Zeolites have shown great conversion and selectivity in many vapor phase petrochemical processes with high stability during severe condition (400-550 ^oC) (Gayubo, Alonso, Valle, Aguayo, & Bilbao, 2010). However, the thermal stability of zeolites in liquid water is interestingly different from vapor phase. While zeolites can sustain long treatments under steam at a temperature around 500 ^oC, they may collapse and lose their crystallinity after only a couple hours in hot liquid water. In recent study of zeolites in hot liquid water (Ravenelle et al., 2010), one framework structures of zeolites, H-ZSM-5, provided no appreciable change in intensity of XRD analysis under steam at autogenic pressure, temperature 150 ^oC and 200 ^oC for 6 hours. However, another framework of zeolites, HY zeolite, was transformed into an amorphous under the same operating condition.

In sub- and supercritical water, most researchers believe that zeolites would completely lose their crystallinity due to the extremely high temperature and pressure. Moreover, liquid water at hot compressed water (>200 ^oC) is much more corrosive due to the high-water dissociation. However, operating in this temperature range also provide the advantage in gasification of biomass and hydration reaction because it can eliminate the surface boundary between organic and water phases. Unfortunately, no publication has been studied on the stability of zeolites within this condition. Only one researcher group (Mo & Savage, 2014) applied the use of H-ZSM-5 in supercritical water for hydrothermal catalytic cracking of fatty acids. The result indicated that the XRD result between fresh and regenerated ones were indistinguishable. However, further investigation such as %crystallinity change, and solubility of silica was unpublished in the report.

The main objective of this research is to investigate the stability of zeolites in sub- and supercritical water in term of structural stability and overall stability. The overall stability is defined as an infinitesimal change of conversion and selectivity to find the opportunity to be applied to practical reaction process. To confirm that the zeolites structure has stability under biomass conversion reaction, scanning electron microscope (SEM) measurements and

transmission electron microscopy (TEM) can be used to observe surface characteristics and morphologies. X-ray diffraction (XRD) measurement results will be used for phase identification of % crystalline changing, and ICP-AES will be used for detecting the solubility of Si and Al in water residual. Moreover, the yield of product, the coking deposit, and acidity is planned to be investigated by GC-FID, TGA analysis, and NH_3-TPD, respectively.

CHAPTER 2 LITERATURE REVIEW

This chapter presents a review on the properties of water under sub- and supercritical water (Chapter2.1) followed by the structure, property, application and stability of zeolite in liquid and vapor phases (Chapter2.2).

2.1 Sub- and supercritical water

According to Franck et al. studied, he defines hot compressed water (HCW) as liquid water which has temperatures >200 ºC (Hirth & Franck, 1993), and pressures are sufficient to compress into liquid state (Hirth & Franck, 1993). For supercritical water (SCW), it is defined as water above critical point at temperatures >374 ºC and pressures >22.1 MPa (see Figure 2-1). In the case of subcritical water (Sub-CW), the definition is various depending on researcher purpose. For example, Ramos et al. defines sub-CW as liquid water, temperature >100 ºC to critical point (Ramos, Kristenson, & Brinkman, 2002), Yu et al. defines sub-CW as liquid water, temperature >150 ºC to critical point (Y. Yu, Lou, & Wu, 2008). However, most of researchers defines sub-CW region as liquid state, temperature between 200 ºC and 374 ºC (Akizuki, Fujii, Hayashi, & Oshima, 2014; Matsumura et al., 2005; Savage, 2009). In this work, the definition of sub-CW also defined as the temperatures ranging between 200 ºC and 374 ºC.

2.1.1 Properties of water in sub- and supercritical condition

Hot compressed water exhibits properties that are quite different from water at room temperature as shown in Figure 2-2. According to Wagner et al. studied (Wagner & Pruß, 2002), the density (ρ) of water slowly decreases from 1000 kg/m^3 at 25 ºC to 625 kg/m^3 at 350 ºC and then sharply drops to 165 kg/m^3 at temperature 400 ºC. The dielectric constant (ε), which is a quantity measuring the ability of a substance to store electrical energy in an electric field, was deeply investigated by Fernandez et al.(Fernández, Goodwin, Lemmon, Levelt Sengers, & Williams, 1997). They found that it constantly drops from 80.5 at temperature 20 ºC to 11.4 at temperature 370 ºC and then sharply drops to lower 2 at temperature 450 ºC. For the dissociation of water(K_W) which is measurement from total concentration of hydronium (H_3O^+) and hydroxide ion (OH^-) (see Equation 1), it has the tendency difference from the other properties. According to Bandura studied (Bandura & Lvov, 2006), the dissociation of water initially increases from 10^{-14} to 10^{-11} at temperature 250 ºC, and keep constant at temperature between 250 – 300 ºC with value around 10^{-11}. At this condition, K_W is nearly 1000 times higher than K_W at room temperature. In contrast, K_W

shapely drop when increasing above supercritical condition even lower than K_W of water at ambient water ($10^{-17.5}$ at 500 ºC).

At above supercritical point, the variation of pressure also effects the property of water as shown in Figure 2-3. The values of density (ρ), dielectric constant (ε), and dissociation of water(K_W) increase with increasing of pressure. As a result, SCW at low pressure is a poor solvent for ionic species like inorganic salts. However, it is completely miscible with most of organic compounds and gas (Weingärtner & Franck, 2005).

Consequently, the properties of water in near critical point performs nearly an idea gas. As a result, the relationship of vapor pressure (P), volume (V), temperature (T) can be estimated by PV= nRT (n is mole, and R is gas constant) like the idea gas(Brunner, 2009).

With increasing of temperature, the solubility of gases in SCW tends to decrease (Akiya & Savage, 2002). However, the solubility of gas and non-polar compounds in Sub-CW increases with increasing if temperature and compete miscible in SCW (Brunner, 2009).

Diffusion rates are high due to low viscosity in SCW which is an excellent medium for homogeneous reaction with high rate of reaction and without limiting of mass transfer. For these reasons, it can prevent side reaction that lead to coke formation or poisoning of catalyst.

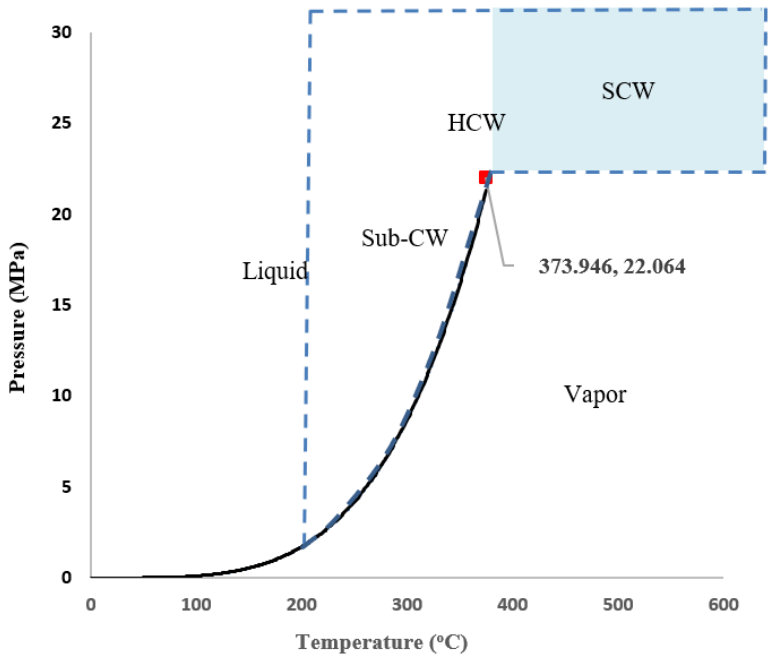

Figure 2-1 Phase diagram of water at sub- and supercritical condition.

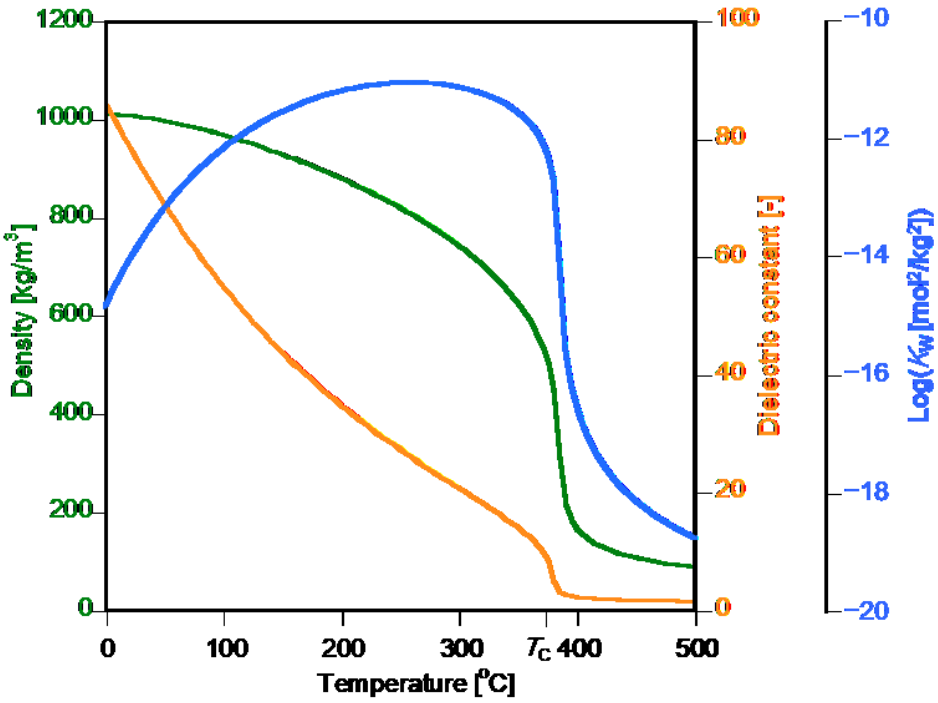

Figure 2-2 Dissociation constant (Kw), density (ρ) and dielectric constant (ε) at 25 MPa as a function of temperature, Adapted from (Peterson et al., 2008).

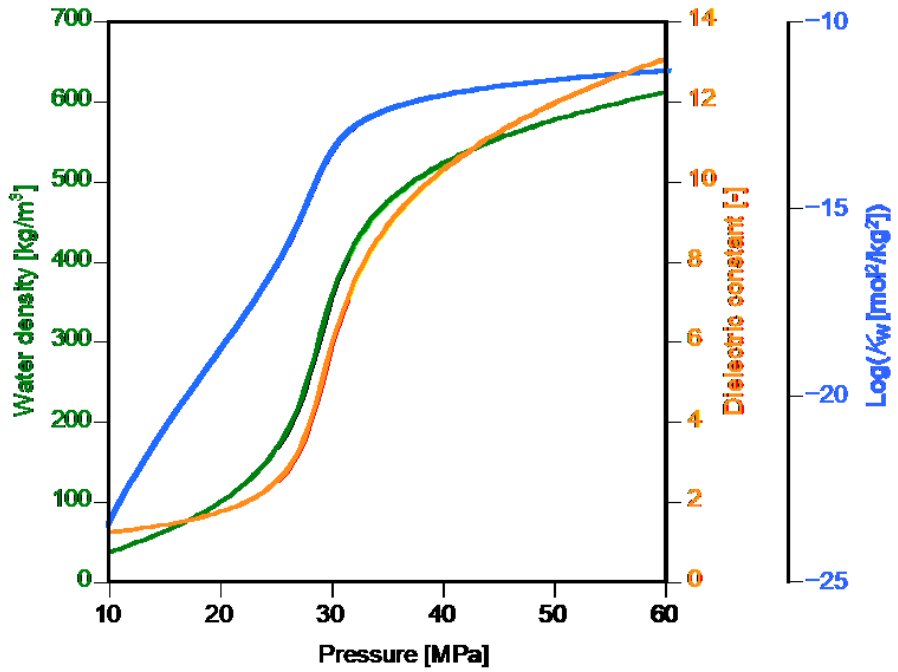

Figure 2-3 The properties of water at Temperature 400 ºC with pressure various from 10 to 60 MPa

Equation 1 Dissociation of water and dissociation constant

$$H_2O \overset{K_w}{\leftrightarrow} H^+ + OH^-$$
$$K_w = [H^+][OH^-]$$

2.1.2 Hydrothermal stability of heterogeneous catalysts

Even though sub- and supercritical water has high K_W and itself act as acid/base catalytic properties, catalysts are frequently used to promote and control the reaction. It has been known for a long time that catalyst can decrease the activation energy and shift the reaction to the equilibrium faster. Nevertheless, the catalysts that can be applied in sub- and supercritical water were limited due to severe condition of temperature and pressure. Moreover, liquid water at near critical water (250-374 ºC) is much more corrosive than liquid water at low temperature due to the high dissociation of water.

In this chapter, the previous study of various catalytic and structural stability (except zeolites see chapter 2.2.4) in sub- and supercritical water were revised as shown a summary in Table 2-1 and Table 2-2, respectively.

Table 2-1 Summary of hydrothermal stability of heterogeneous catalyst in sub-critical water

Catalyst	Reaction	System types	Temperature	Pressure	Time (h)	Stability	Ref.
mesoporous silica SBA-15	Pure water	Closed system	200 °C	Autogenic	12	XRD completely change.	(Pham, Anderson, Johnson, Schmidt-Rohr, & Datye, 2012)
γ-Al_2O_3	Pure water	Closed system	200 °C	Autogenic	10	γ-Al_2O_3→boehmite	(Ravenelle, Copeland, Kim, Crittenden, & Sievers, 2011)
Pt/ γ-Al_2O_3	Glycerol conversion	Open system	220 °C	2.5 MPa	37	γ-Al_2O_3→boehmite Catalytic activity drop (>50%)	(N. Luo, Fu, Cao, Xiao, & Edwards, 2008)
Pt/ γ-Al_2O_3	Lignin in H_2O/ethanol	Closed system	225 °C	Autogenic	10	γ-Al_2O_3 maintain their structure but BET decrease.	(Jongerius et al., 2013)
Pt/ γ-Al_2O_3	Phenol/guaiacol in H_2O/ethanol	Closed system	225 °C	Autogenic	10	γ-Al_2O_3→boehmite	(Jongerius et al., 2013)
Steaming Pt/ SiO_2-Al_2O_3 (Post- treatments)	Pure water/sorbitol conversion	Closed system	200-240 °C	Autogenic (21-36 bars)	2	XRD slightly change by additional of peaks (SiC, kaolinite, and Pt).	(Vilcocq, Cabiac, Especel, Lacombe, & Duprez, 2011)

Table 2-1 Summary of hydrothermal stability of heterogeneous catalyst in sub- critical water (cont.)

Catalyst	Reaction	System types	Temperature	Pressure	Time (h)	Stability	Ref.
Pd on Nb_2O_3 (HY-340), Nb_2O_3-SiO_2	γ-valerolactone to Pentanoic acid	Open system	200 °C	35 bars	12	Conversion of Nb_2O_3 drop to 23% at TOS 68 h. BET and acid site decease	(Pham et al., 2011)
TiO_2-ZrO_2	Sugarcane bagasse, rice husk	Closed system	200-400 °C	34.5 MPa	0.083	High reusability up to 5th cycle without significance drop of yield.	(Chareonlimkun, Champreda, Shotipruk, & Laosiripojana, 2010)
WO_x-ZrO_2	Hydration of cyclohexene	Open system	225-300 °C	15-25 MPa	20 h	XRD slightly change, surface area and pore volume are stable.	(Yuan et al., 2011)
Rutile-TiO_2	Hydration of 1-octene	Open system	250-450 °C	11-33 MPa	NA	XRD patterns were not changed after reaction.	(Akizuki & Oshima, 2012)
Nb_2O_3/carbon	γ-valerolactone to Pentanoic acid	Open system	240 °C	51.3 atm	100 h	Conversion of reaction has high stability at 40%, XRD slightly change of intensity.	(Xiong, Pham, & Datye, 2013)

2.1.2.1 Sub-critical water

Silica. The solubility of Silica in water at temperatures and high pressures has been studied by R.O. Fournier and J.J Rowe(Fournier & Rowe, 1977). They found that Silica has high solubility in water at temperature near- supercritical water. The recent study of mesoporous silica SBA-15 also found similar result. The structure of SBA-15 is completely collapsed under operating at 200 ^{o}C(Pham et al., 2012).

Alumina. Many researchers found that under hydrothermal condition γ-Al_2O_3 will change to boehmite (AlOOH) phase with a significantly decrease acidity and surface area (Ravenelle et al., 2011). For metal-free γ-Al_2O_3, the transformation is completed within 10 h. Even Pt metal significantly prolong the formation of boehmite, the activity of reaction still decreased too fast and unable to maintain the conversion (N. Luo et al., 2008). On the other hand, the presence of large molecular weight compound such as lignin under an ethanol-water mixture can form dissolution-inhibiting and improve the stability (Jongerius et al., 2013). It was also found that vanillin (a lignin-derived compound) can stabilize the aluminum oxide more than phenol due to the larger number of oxygen functionalities that can interact with the alumina. The catalyst operating with lignin reactant showed almost identical XRD result comparing with before reaction. It means that the formation of boehmite does not occur.

Bi-metallic Si and Al support (SiO_2-Al_2O_3). Post-treatment silica-alumina provided higher hydrothermal stability than pure silica or alumina over sorbitol transformation in liquid water at 200 °C. The post-treatment, Streaming or dipping, also plays the important role for stability. In hot liquid water, the modification structure was transformed into a layer of amorphous boehmite, which protected the particle from further hydrolysis (Vilcocq et al., 2011).

Niobia oxide (Nb_2O_3) and Niobia-silica oxide (Nb_2O_3-SiO_2). It found that the decreasing of surface area and acidity side occurred for both Niobia oxide and Niobia-Silica catalysts, the surface loss occurred lower with presence of SiO_2. The addition of SiO_2 (5 wt.%) was found to improve the stability of Niobia–Silica composites. It was concluded that addition of silica to Niobia improves the stability of the support by preventing crystallization(Pham et al., 2011).

Mono- and Bi-metal oxide of Titania, Zirconia, Tungsten (TiO_2, ZrO_2, WO_x). TiO_2-ZrO_2 was found to be stable over dehydration reaction of sugarcane (Chareonlimkun et al., 2010). They investigate the stability of catalyst by reuse the catalysts up to 5^{th} time and found that the total product yields from the spent catalysts were in the range of ± 4% compared to the fresh one. Yuan et al. also investigate bi-metal oxide compound of Tungsten- zirconia oxide (WO_x–ZrO_2) (Yuan et al., 2011). They found that XRD results of fresh and used catalyst are insignificantly different and no obvious growth of extra-framework of WO_2 is observed in XRD pattern. Akizuki and Oshima also applied using Rutile-TiO_2 (Akizuki & Oshima, 2012) which was already confirmed that is stable in supercritical water(J. Yu & Savage, 2001) over hydration of 1-octene in sub- critical water. They found that XRD patterns of TiO_2 of Rutile-TiO_2 are nearly identical from both before and after reaction.

Carbon composites. The hydrothermal stability of Niobia on carbon composites support in liquid water at temperature 240 ºC was investigated by H. Xiong et al(Xiong et al., 2013). They found that the conversion of dehydration of butanol was stable up to 100 h without significance drop of performance when using Niobia on carbon composites prepared by a deposition-precipitation-carbonization method. They also further comparing the same reaction with pure Niobia (HY-340) and found that conversion of reaction shapely drop after 20 h operation.

From overall literature review, it seemed to conclude that hydrothermal stability exists in sub-critical water only transitions metal oxide (TiO_2, ZrO_2, WO_x) and carbon composites material. However, both catalysts types still have the difficulty to apply in actual process reaction. All transitions metal oxide is considered as valuable metal which is expensive, and it still has lower surface area and acidity site comparing with present commercial catalysts. For carbon composites, even it is very attractive supports due to their well define structure, high surface area and abundance of resource, the commercial scale production is still under developing.

Table 2-2 Summary of hydrothermal stability of heterogeneous catalyst in supercritical water

Catalyst	Reaction	System types	Temperature	Pressure	Time (h)	Stability	Ref.
WO_3-TiO_2	Dehydration of glycerol	Open system	400 °C	33 MPa	NA	WO_3 prevents structure TiO_2 change (anatase to rutile)	(Akizuki & Oshima, 2012)
Ir, Pt, Ni and Pt-Ni on γ-Al_2O_3	Reforming of ethylene glycol	Open system	450 °C	250 bars	10	BET decrease (200 to 20 m^2/g), Only Pt-Ni has high stability of conversion.	(de Vlieger et al., 2012; De Vlieger, Mojet, Lefferts, & Seshan, 2012)
TiO_2, ZrO_2, and $CeZrO_2$	Gasification of bio- oil	Closed system	500 °C	300 bars	0.125, 0.25, 0.5	XRD patterns were not changed after reaction.	(Chakinala et al., 2012)
Al_2O_3, SiO_2 and activated carbon	Gasification of bio- oil	Closed system	500 °C	300 bars	0.125, 0.25, 0.5	XRD patterns were changed by additional peak or amorphous appearing	(Chakinala et al., 2012)
MnO_2, TiO_2	Phenol oxidation	Open system	380 °C	250 atm	100 h	All catalysts have highly stable of activity. However, XRD results were changed	(J. Yu & Savage, 2001)

2.1.2.2 Supercritical water

Silica Alumina and activated carbon. It has been proposed that γ-alumina can be transformed to boehmite (γ→δ→θ→α) (Chakinala et al., 2012). They also observed a significant loss of area in BET analysts of silica and activated carbon which indicated that was unstable in supercritical water. Moreover, De Vlieger et al. also confirmed phase change γ-alumina in continuous flow reactor for the reforming of ethylene glycol in supercritical water (De Vlieger et al., 2012), and concluded that γ-alumina is unstable due to the solubility of alumina in product (J. Yu & Savage, 2001). According to Wawrzetz et al. reported, the phase change from γ-Al_2O_3 to boehmite did not cause blocking or deactivation of the catalytic sites in active metal of catalysts(Wawrzetz et al., 2010). The effect of bi-metal loading γ-Al_2O_3 was investigated (De Vlieger et al., 2012). They found that co-metal Pt and Ni loading suppressed the formation of acetic acid in dehydrogenation reaction that responsible for hydroxylation of the Al_2O_3 support.

Mono- and Bi-metal oxide of Titania, Zirconia, Tungsten, Cesium and Manganese (TiO_2, ZrO_2, WO_3, $CeZrO_2$, MnO_2). J.Yu and P. Savage investigated the catalyst activity and stability of MnO_2 and TiO_2 over oxidation of phenol in supercritical water, and they found that both catalyst maintained their activity over 100h operating in continuous flow reactor(J. Yu & Savage, 2001). Moreover, no any metals were detected in the effluent solution. However, the phase transformations were occurred in both catalysts such as changing of anatase TiO_2 into rutile TiO_2, and bulk MnO_2 into Mn_2O_3. To prevent the phase transformations, Akizuki and Oshima suggested that changing of anatase phase to rutile phase in TiO_2 can be suppressed by additional of WO_3 content, and phase transformation is completely suppressed when WO_3 content was increased more than 5 wt. % (Akizuki & Oshima, 2012). Other researchers(Chakinala et al., 2012) also studied the stability of ZrO_2, TiO_2 and Ce-ZrO_2 in supercritical water by investigate surface area (BET) before and after reaction. They found that no significance of surface changed in both ZrO_2 and TiO_2 and slightly increase in Ce-ZrO_2. This indicated that Titania, Zirconia and modified zirconia (Ce–ZrO_2) are stable in supercritical water.

In conclusion, carbon-, TiO_2- and ZrO_2-based materials are supposed to be stable in supercritical water, even though phase transformation occurred. In contrast, Al_2O_3 and SiO_2 are not stable in supercritical water due to high solubility of Si and Al.

2.2 Zeolites

Zeolites are remarkable crystalline aluminosilicates with three-dimensional microporous structures composed by tetrahedral of SiO_4 and AlO_4 link to each other(C Baerlocher, McCusker, & Olson, 2007). This crystalline framework demonstrates highly outstanding performance to improve conversion and selectivity in many chemical, petrochemical, and oil refining process including alkylation, cracking, hydrocracking, and isomerization due to high surface area, well-defined structure, high acidity, and low price(Degnan, Jr., 2000). The relative low price of zeolites started from the discovery of large scale industrial synthesis by Union Carbide in the 1950s(Rabo & Schoonover, 2001).

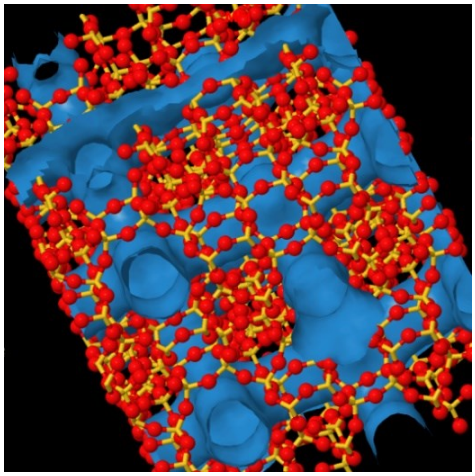

Figure 2-4 Schematic diagram of zeolites structure framework (Captured from Free 3D Drawings software developed by International Zeolite Association (Ch. Baerlocher, 2017))

2.2.1 Structure of zeolites

Zeolites have various structure configuration with different shape and pore size. According to International Zeolite Association (IZA) who keep track and update all zeolite structures, they reported that the discovering framework types have been reported 238 different types of framework structures (2017) which still have new discovering in every year (around 5 structures)(Ch. Baerlocher, 2017). The structure commission of IZA has established the code name systems for zeolites with three-letter codes for open four-connected three-dimensional(3D) framework types. The letter of code name based on the name of the first material possessing the framework type. For example, the code name MFI is derived from ZSM-5 which stands for “Zeolite Socony **M**obil **Fi**ve”. Even though there has been an increasing discovery of new frameworks and patents for their composition, only

around 12 structures of zeolites can find application in commercial processes due to endurance and economic scale production of synthesis zeolites. The example of common structure of zeolites that use in commercial process application was shown in Figure 2-5.

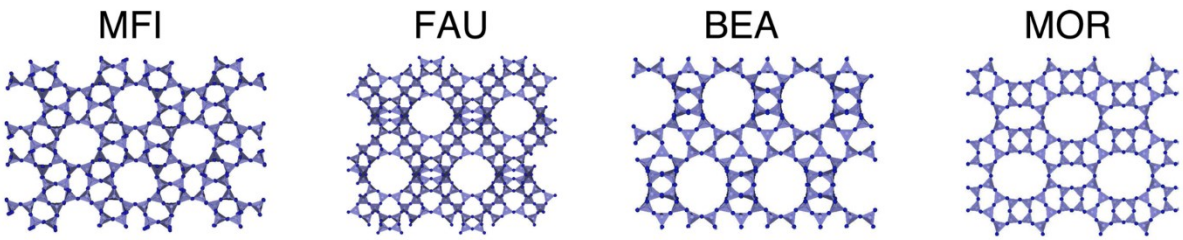

Figure 2-5 Example of zeolites framework structures.

2.2.2 Porous structure

Porous structure of zeolites plays the important roles for creating selective products that does not appear in general support such as Al_2O_3 and SiO_2. In general, zeolites structures construct from AlO_4 and SiO_4 tetrahedra as primary structural unit. However, it also generates secondary structure such as cube, hexagonal, prisms, or cube-octahedra assembled together to create porous structure. The pore diameter of zeolites usually starts from 0.3-1.0 nm with pore volumes 0.1- 0.3 cc/g. The general zeolites pore sizes using oxygen and silica packing models are shown in Figure 2-7. Small size pore consists of Si and O connect to each other in cycle with Si 8 atoms and O 8 atoms, medium size with Si 10 atoms and O 10 atoms, and large pore size with 12 atoms and O 12 atoms. Porous structure of zeolites is illustrated like the molecular sieve properties that excludes larger molecular to pass through or prevent by-product diffuse out of the pore. The example of this advantage is applied in many industrial process applications such as isomerization reaction of para-xylene that the average pore diameter of ZSM-5 (0.55 nm) is smaller than the average kinetic diameter of meta-xylene (0.68 nm), so meta-xylene cannot diffuse out of the pores. Isomerization reaction will occur and convert meta-xylene to para-xylene which has average kinetic diameter lower (0.58 nm). Cyclohexene hydration which utilize as the reaction model in section 4.3 also apply this concept to prevent the condensation reaction of by-product as shown in Figure 2-6.

lists the kinetic diameters of molecules in hydration of cyclohexene

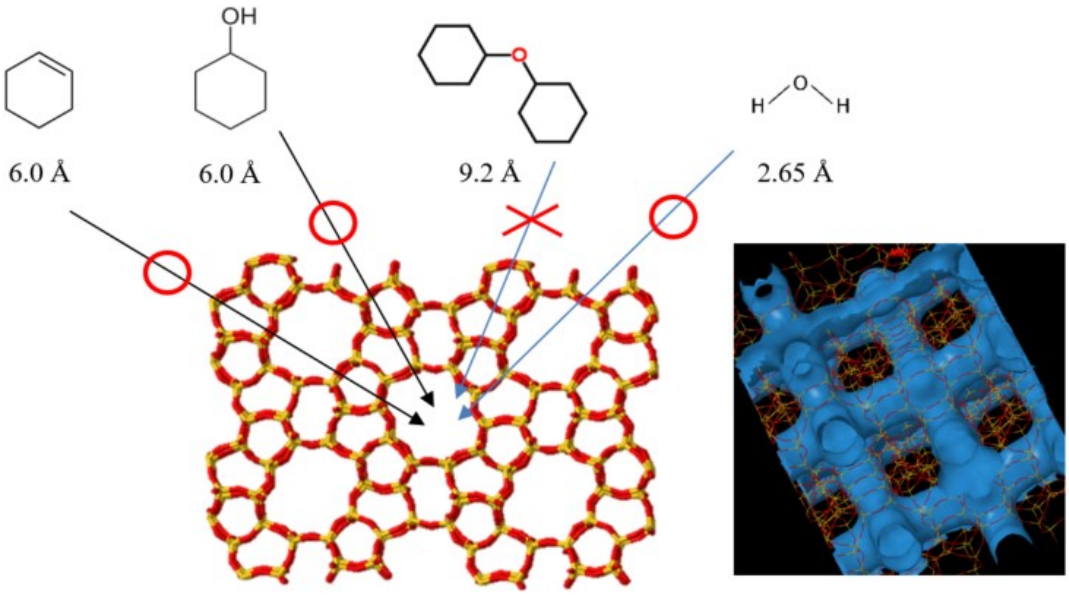

Figure 2-6 Schematic diagram of hydration reaction pass through porous zeolites

The structure of zeolites should be imaged as slightly flexible conformation, with the size and shape of framework corresponding to changing of temperature and substituting of guess species. As shown in previous example, para-xylene can pass thought the porous of ZSM-5, even though the average pore size diameter is smaller than average kinetic diameter of para-xylene.

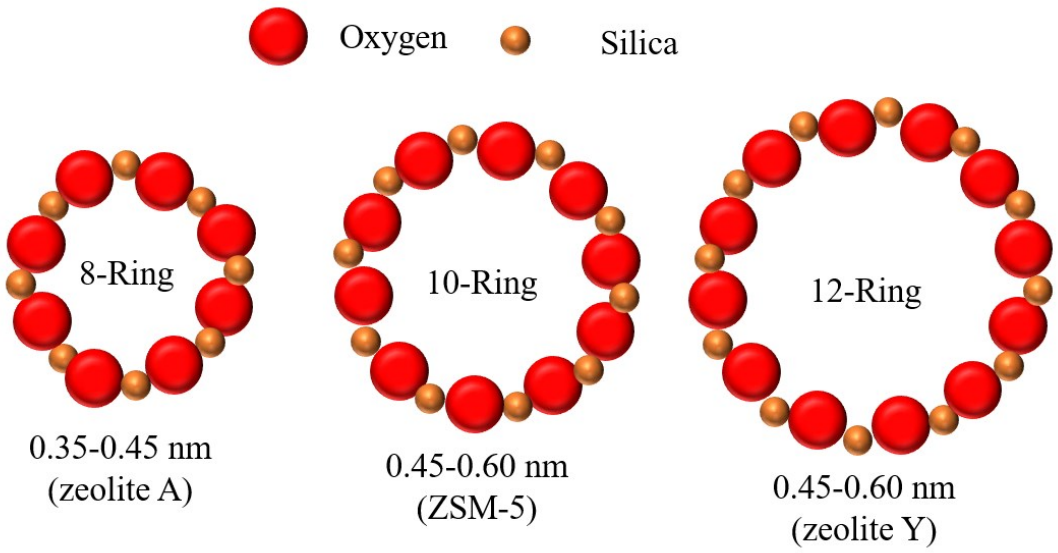

Figure 2-7 Typical zeolite pore sizes demonstrated by oxygen and silica packing model

2.2.3 Acidity

The presence of Al atoms in zeolites creates the negative charges on zeolite framework that requires the positive charges, cations ion, to balance the electroneutrality of the solid. The various cations can be used, and H^+ is normally used as a change balancing-cation. This H^+ also represents as the acid sites. Generally, the acidity of zeolites can be classified in major form as Bronsted acid sites and Lewis acid sites (see Figure 2-8). Bronsted acid is defined as protons(H^+) donation, and Lewis acid is defined as accepting electron pairs which is AlO^+ or metal cations. Extra framework Alumina (EFAl) e.g. AlO^+ is formed during pre-treatment method such as dealumination or dihydroxylation of H^+

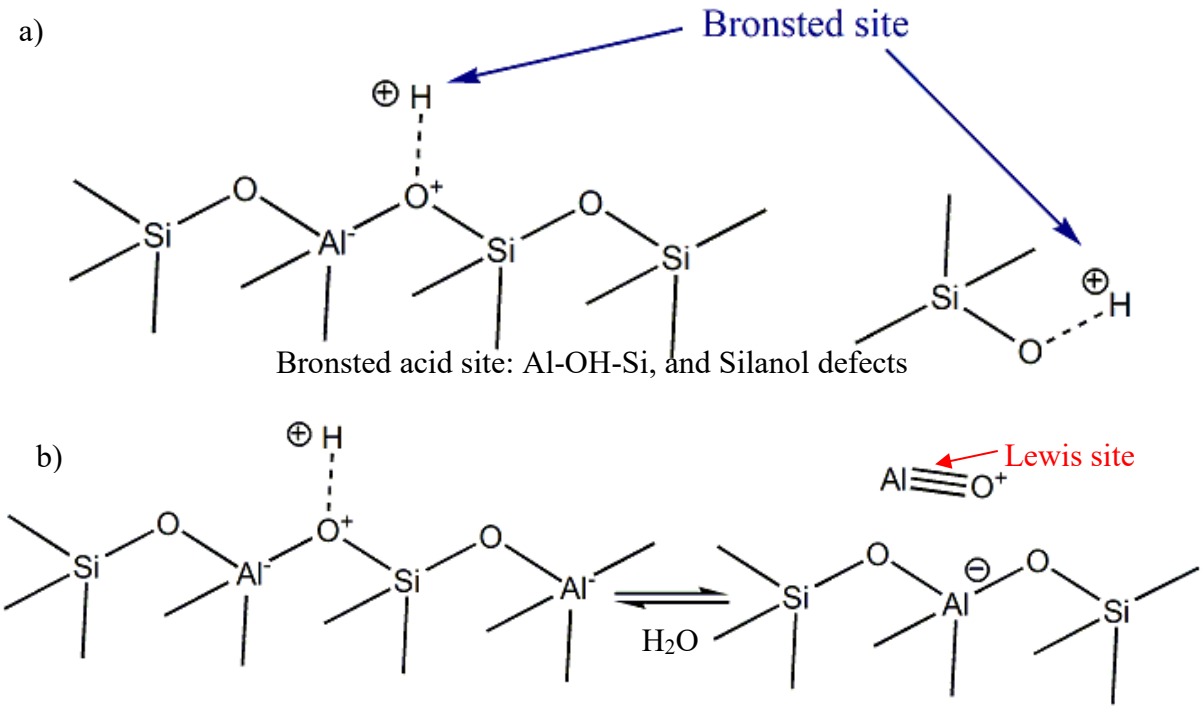

Bronsted acid site: Al-OH-Si, and Silanol defects

Lewis acid site: AlO^+, Al_xO_y, and Metal cations

Figure 2-8 Schematic representation of zeolites acidity a) Bronsted acid sites b) Lewis acid sites

Because Al atoms are the source negative changes, total acidity increase with deceasing of Si/Al ratio. Moreover, the acidity can be control with various method such as dealumination method which increase the silanol defect and acid strength (Bronsted acid) but decrease total acid site.

2.2.4 Hydrothermal stability of zeolites

Unlike vapor phase application that zeolites show the great performance and high stability under operating at high temperature (>500 °C) in various process, the stability of

zeolites in liquid water might curiously different from vapor phase. They may collapse and lose their crystallinity after only a couple hours in hot liquid water. In presence of water, dealumination might occur and create extra framework alumina (EFAl) which later can be removed from framework by dissolving in water, leading to a structural breakdown. In contrast to vapor phase reaction that EFAl is not detach from the framework, the presence of EFAl increase hydrothermal stability by encapsulating the zeolite structure with decreasing Bronsted site.

In this chapter, the previous studies of stability of zeolites are summarized in Table 2-3. However, the previous studies of stability of zeolite mostly limited only in closed system at temperature <= 200 ^{o}C. Only one researcher group (Mo & Savage, 2014) applied using H-ZSM-5 in supercritical water for hydrothermal catalytic cracking of fatty acids.

Table 2-3 Summary of hydrothermal stability of zeolites in various framework.

Zeolites (framework)-Si/Al	Reaction	System types	Temperature	Pressure	Time (h)	Stability	Ref.
Zeolite Y (FAU)-5, 14, 41; ZSM-5 (MFI)-15, 25, 40	Pure water	Closed system	150, 200 °C	Autogenic	6	All ZSM-5 are stable but Zeolite Y are completely transformed to amorphous.	(Ravenelle et al., 2010)
Zeolite Y (FAU)-2.7	Pure water	Closed system	130-200 °C	Autogenic	72	FAU → Kaolinite + Amorphous SiO_2 + metakaolinite	(Dimitrijevic, Lutz, & Ritzmann, 2006)
ZSM-5(MFI)-24-918; MOR-12, 20; β-zeolite (BEA) 21-200	Pure water	Closed system	200-240	Autogenic	72	ZSM-5 and MOR are stable but the others are decomposed (XRD).	(Lutz, Toufar, Kurzhals, & Suckow, 2005)
ZSM-5(MFI)- 11.5 Zeolite Y (FAU)-2.6 β-zeolite (BEA) -12.5	Pure water	Closed system	200 °C	Autogenic	6, 9	Stability of zeolites depend on terminal silanol defect. ↓Si-OH → ↑ Crystallinity	(Zhang, Chen, Chen, White, & Resasco, 2015)
ZSM-5(MFI)-30	Palmitic acid to aromatic compound	Closed system	400 °C	240 bars	3	XRD results maintain the identical result but reuse zeolite has lower yield.	(Mo & Savage, 2014)

Zeolite Y (FAU) and β-zeolite(BEA). Many researchers reported that zeolite Y has low stability under sub-critical water. Dimitrijevic et al. published that decomposition of zeolite Y (Si/Al = 2.7) increased with increasing of temperature. Zeolite Y structure was collapsed and changed to kaolinite, amorphous of SiO_2 and metakaolin at temperature 170 -200 ºC (Dimitrijevic et al., 2006). Ravenelle et al. also confirmed the support evidence of destructive structure by monitoring the changing of crystallinity in hot water (150-200 ºC)(Ravenelle et al., 2010). They found that zeolite Y completely transformed to amorphous phase during treatment in hot water for 6 hours. The main degradation mechanism was suggested to be hydrolysis of the siloxane bonds (Si-O-Si) as opposed to dealumination. In case of β-zeolite, it also found that has low stability in hot liquid water. Lutz et al. reported that β-zeolite decomposed in liquid water at 130-240 ºC in batch reactor over 72 hours (Lutz et al., 2005). Nevertheless, some researches stated that the stability of zeolites does not depend on the structures. Zapata et al. reported that the structural stability of H-Y zeolites can be improved by functionalization of terminal silanol with Organosilanes with varying alkyl chain length (Zapata, Huang, Gonzalez-Borja, & Resasco, 2013). This method greatly improved the stability of zeolites. Subsequently, another group researchers (Zhang et al., 2015) proposed that the stability of zeolites depend on the density of Si-OH terminal groups. The encapsulated silylation of the Si-OH with Organosilanes increased the hydrophobicity and the stability of zeolites.

ZSM-5 (MFI) and Mordenite (MOR). According to Lutz et al., Both zeolites exhibit high hydrothermal stability in batch reactor study for 72 hours up to temperature 240 ºC. They stated that hydrothermal treatment in ZSM-5 evoke a better structure by healing out the structure without significant damage of the framework, which leads to a product of increased hydrophobicity(Lutz et al., 2005). The high stability of ZSM-5 has also been confirmed by other researchers groups (Ravenelle et al., 2010; Zhang et al., 2015). Zhang et al. reported that the reason of high stability of ZSM-5 might from the low silanol defect (Si-OH). They examined that H-ZSM-5 has the density of defects only 0.04 mmol/g that is lower than zeolite Y and β-zeolites which has density of defects around 0.26 and 0.22 mmol/g, respectively.

In supercritical water, only one researcher group, P.E savage and Na Mo (Mo & Savage, 2014), applied using H-ZSM-5 in supercritical water for hydrothermal catalytic cracking of fatty acids. The result indicated that XRD result between fresh and regenerated ones were indistinguishable. However, further investigation such as %crystallinity change, and solubility of silica was unpublished in that report.

2.2.5 Dealumination and Desilication

It has been proposed that the presence of water in vapor phase or liquid water under acid condition lead to dealumination while liquid water under neutral or basic condition lead to desilication(Gounder, 2014). The detractive structure is occurred at Si-O-Al and Si-O-Si bonds by H+ and OH- that is dissociated from water, which causes dissolution of Si and Al, leading to the collapse of pores and the loss of surface area. During dealumination, Si-O-Al is broken and generate extra-framework alumina (EFAl) that deposit on framework. EFAL creates a net negative charge in the framework, which encapsulate four Si-OH groups. In case of desilication, the hydrolysis start at Si-O-Si bond is broken, and two silanol groups are formed. It has been suggested that this reaction accelerates upon formation of silanol groups because of their strong interaction with water molecules and hydroxyl ions. Byproducts of dealumination and desilication might include SiO_2, $Si(OH)_4$, $Al(OH)_3$, and aluminosilicate species. The detail of deactivation mechanisms is shown in Figure 2-9.

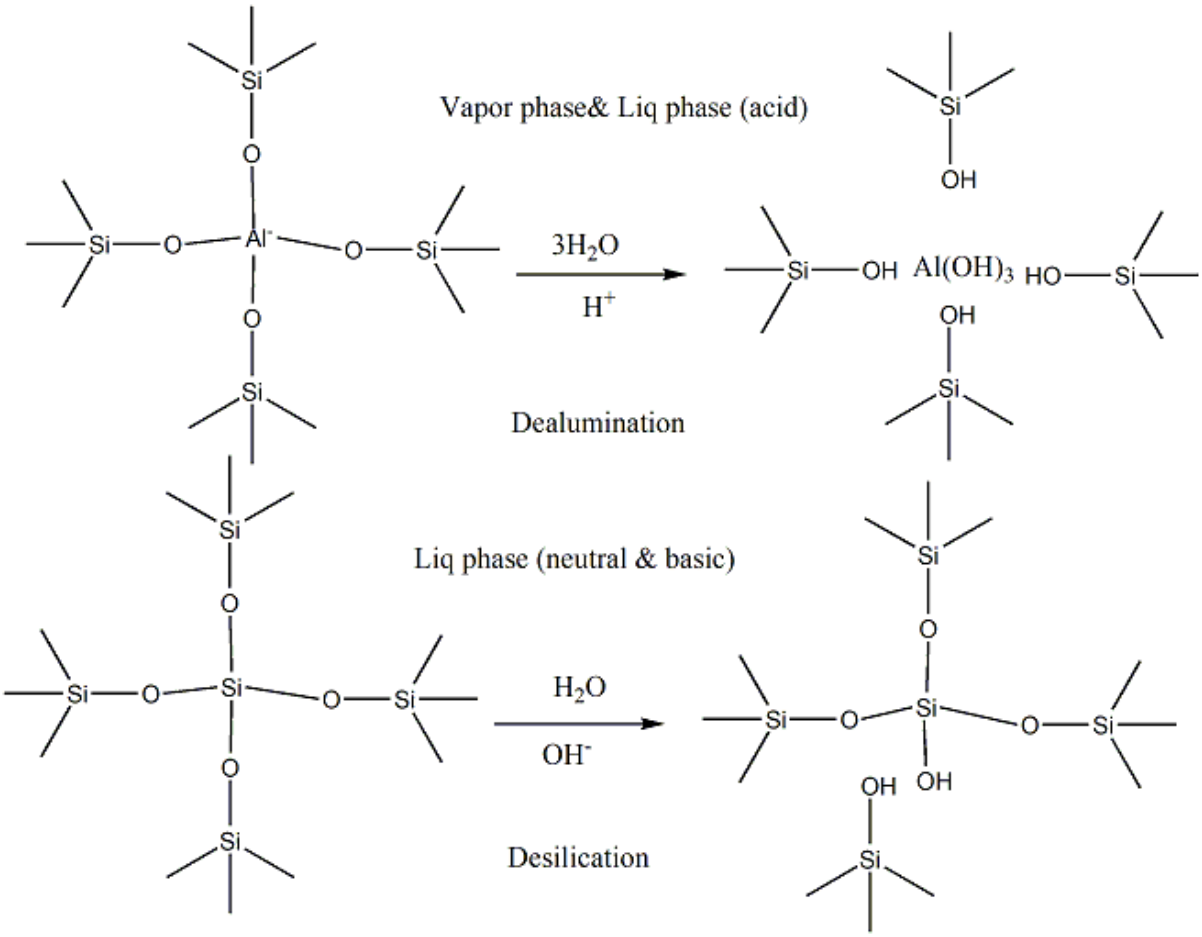

Figure 2-9 Mechanisms for dealumination and desilication reaction adapt from (Ravenelle et al., 2010) and (Gounder, 2014)

2.2.6 Thermodynamic stability of zeolites in various frameworks

In recent study (Zimmermann & Haranczyk, 2016), they proposed thermodynamic analysis stability by comparing formation energy of α-quartz with target frameworks (see

Equation 2)

Equation 2 thermodynamic analysis of zeolites

$$\Delta E_i = \frac{E_i}{N_{SiO_{2,i}}} - \frac{E_{qtz}}{N_{SiO_{2,qtz}}}$$

where E_i denotes the structural framework energy from the relaxation state to zeolites framework species i, $N_{SiO2,i}$ is the number of SiO_2 units in the unit cell in species i, and subscript "qtz" indicates α-quartz. The relative structural framework energy (ΔE_i) is a standard thermodynamic descriptor to make predictions about zeolite feasibility of target zeolites comparing with α-quartz. (α-quartz is believed to be the most stable form of silica structure which has the lowest structural framework energy.)

Moreover, they also develop method to compare the angles of SiO_4 in zeolites framework with the perfect tetrahedral angle of $\theta_{tet} = 109.47°$ and convert into dimensionless and normalized (θ_i) to values between 0 and 1, where 1 indicates a perfect tetrahedral coordination environment and 0 indicates an extremely distorted surrounding.

As a result, they summarize the differential heat of formation energy of α-quartz and perfect tetrahedral angle among of 217 various structure of zeolites presented in their publication. Particularly, the summarize industrial zeolite frameworks that usually applied in industrial process was shown in Table 2-4.

According to Table 2-4, ZSM-5 or MFI framework demonstrated the high thermal stability among of all commercial zeolites due to highest tetrahedrality (θ_{tet}) and lowest relative structural framework energy (ΔE_j).

Table 2-4 Structural and thermodynamic of industrial zeolite frameworks and averages value*.

Zeolites (Framework)	Tetrahedrality(θ_{tet})	Relative energy ΔE_i (kJ/mol)
ZSM-5 (MFI)	0.979	10
Zeolite Y (FAU)	0.979	20
β-zeolite (BEA)	0.976	14
Mordenite (MOR)	0.971	12
Chabazite (CHA)	0.977	16
Average all framework**	0.976	17

* Adapted from (Zimmermann & Haranczyk, 2016) data, ** Average from 217 structure zeolites.

2.2.7 Commercial zeolites

The first synthetic zeolite to be used in commercial application was zeolite A (LTA) as the adsorbent in the 1950s. After that around 10 years, Y-type zeolite faujasite (FAU) and mordenite (MOR) was successful to synthesis for commercial catalytic applications. In the 1970s the Mobil discovery of ZSM-5 (MFI) led to many catalytic uses. Ten year later, the applications develop for Rho (RHO) and L-zeolite (LTL) was successful as use as catalyst. In the 1990s, SAPO-11 (AEL), SAPO-34 (CHA), Beta zeolite (BEA), Ferrierite (FER) and MCM-22 (MWW) was the latest catalyst that success to apply in catalytic applications of petrochemical process. The summary of zeolites using as commercial catalyst in various refining and petrochemicals was shown in Table 2-5. As a result, ZSM-5 or MFI is frequently used in various petrochemical processes as the most popular and general structure of zeolites.

According to various studies including stability of zeolites at 200 ^{o}C, structural and thermodynamic analysis, and general commercial zeolites in various structures, it found that MFI structure or ZSM-5 has the highest possible to be stable in sub- and supercritical water due to lowest appearing of defects in structure framework, lowest relative structural framework energy, and having SiO_4 closest to perfect tetrahedral angle. Moreover, this structure has already been completely developed to produce in commercial scale, so ZSM-5 was selected as the representative structure of zeolites in this study.

Table 2-5 Commercial zeolites using in refinery and petrochemical process adapted from(Tanabe, 1999).

Zeolites	**Y**	**L**	**MOR**	**BETA**	**MCM-22**	**ZSM-5**	**SAPO-11**	**Ferrierite**	**Rho**	**SAPO-34**
IZA code	**FAU**	**LTL**	**MOR**	**BEA**	**MWW**	**MFI**	**AEL**	**FER**	**RHO**	**CHA**
Process										
Ethylbenzene					✓	✓				
Cumene	✓		✓	✓	✓	✓				
Other aromatics						✓				
Xylene isomer						✓				
C4 isomer			✓							
C_4^{2-} isomer						✓		✓		
C_5^{2-} isomer						✓				
Iso-dewaxing							✓			
Amination			✓			✓			✓	✓
C_3, C_4/aromatic						✓				
Naphtha aromatic		✓								
FCC	✓					✓				
Dewaxing						✓				
Hydrocracking	✓					✓				
MTG						✓				
MTO						✓				
Toluene						✓				
Trans-alkylation						✓				

CHAPTER 3 EXPERIMENTAL

This chapter describes the preparation of methods and experimental conditions that used in this study for investigating the stability of zeolites under sub- and supercritical water. In addition, the various analytical techniques used to investigate morphology, Si/Al ratio, activity, acidity, and solubility are presented and discussed in this chapter.

3.1 Catalyst preparation

There are two kind of zeolite structures used in this study; ZSM-5 and β zeolite were used to test the stability. However, β zeolite was tested only in powdered form under supercritical water due to the preliminary result of structures analysis indicated that it completely converted to amorphous phase. For ZSM-5, it was intensively investigated in both powdered and pellet form with various Si/Al ratio.

3.1.1 Preparation of powdered forms ZSM-5 and β zeolite

All powdered forms ZSM-5 and β zeolite were supplied from TOSOH Corporation based on commercial H- β zeolite with Si/Al (mol/mol) = 40, H-ZSM-5 with Si/Al (mol/mol) = 1500, and NH_4- ZSM-5 with Si/Al ratio (mol/mol) = 24 and 40. Both NH_4- ZSM-5 were calcined in air atmosphere in muffle furnace at temperature 600 ºC. The temperature was ramped from room temperature to 600 °C (10 ºC/ min) and then held for 8 h. After that, cool down with cooling rate 10 ºC/min. During this treatment, the ammonium form of zeolite was converted into the proton form. All zeolites are kept in Laboratory desiccator to control humidity. The material specifications and sample codes are shown in Table 3-1.

3.1.2 Preparation of pellet forms ZSM-5

The powered forms of ZSM-5 were manufactured into pellet forms by TOSOH Corporation. According to company information, the powered forms of ZSM-5 was mixed with boehmite (aluminum oxide hydroxide) around 20% by volume. Boehmite was used as binders to improve the rheology of the paste such that it could be extruded into rods of 1.5 mm. in diameter. The receiving pellet form of zeolites from TOSOH were ground and sieved to 0.300-0.500 mm.; then were rinsed with ultra-pure water and dried in vacuum oven at room temperature for 24 hours. The grounded zeolites were stored in desiccators. Samples are

named according to the Si/Al ratio (mol/mol) before mixed with boehmite as P-H-ZSM-5(24), P-H-ZSM-5(40), and P-H-ZSM-5(1500).

Table 3-1 Material Specifications and codes

Code name (Si/Al)	Pore size	Si/Al (mol/mol)	BET (m^2/g)	Crystal size (μm)	Particle size (μm)	NH3-TPD (mmol/g)
β zeolite (40)	6.5 A	40	530	0.5~1.0	4	0.5
H-ZSM-5(24)	5.8 A	24	330	0.1 x 0.5	5	1.8
H-ZSM-5(40)	5.8 A	40	330	2.0 x 4.0	10	1.3
H-ZSM-5(1500)	5.8 A	1500	310	2.0 x 5.0	4	-

3.2 Characterization techniques

3.2.1 Determination of Si/Al ratio of zeolites (EDX)

The Si and Al composition were analyzed by Scanning Electron Microscope (SEM) equipped with EDX detector. Energy-dispersive X-ray spectroscopy (EDX) is a spectroscopy technique used in conjunction with SEM. This analytical technique was used for elemental analysis by relieving electron beam to excite election in ground state. An EDX spectrometer detector measures the relative abundance of emitted x-rays versus their energy. The spectrum of X-ray energy versus counts was evaluated to determine the elemental composition of the samples. With different elemental composition, it will provide the different spectrum position of energy releasing. The SEM model that used in this report is JSM-5600 with EDX

3.2.2 Morphology of zeolites (SEM)

The morphology of zeolites was investigated by scanning electron microscopy (SEM) technique using JSM-5600 operating at 20 keV. The powder samples were mounted in a silver sample holder on double-side adhesive carbon tape and coating with carbon in vacuum auto carbon coater (108 Auto/SE model) setting at 3 seconds

3.2.3 X-ray diffraction pattern (XRD) and %Crystallinity

X-ray diffraction spectroscopy (XRD) is a general instrumental technique used for identification the different type of crystalline structures since it is fast, not destructive sample, and cheap. The basic principle of X-ray diffraction analysis is the crystalline atoms cause an

injecting beam of monochromatic X-rays to diffract with different angles that corresponding to the distance of lattice planes in their structure, and the wavelength of radiation, see Equation 3

Equation 3 Bragg's law

$$n\lambda = 2d \sin \theta$$

Where:

n is an integer,

λ is the wavelength of the incident X-ray radiation,

d is the distance between atomic layers in a crystal (d-spacing), and

θ is the angle of incidence between the X-ray beam and the diffraction planes.

Moreover, by measuring the angles and intensities of these diffracted beams, a three-dimensional picture of the density of electrons within the crystal can be calculated. Furthermore, from this electron density, the mean positions of the atoms in the crystal can be determined, as well as their chemical bonds, and their disorder. For example, the estimation of particle size can be calculated from Scherrer equation, see Equation 4

Equation 4 Scherrer equation

$$T = \frac{K\lambda}{\beta \cos\theta}$$

Where:

T is the particle size

K is the Scherrer constant typically ranging from 0.9 to 1.0 (0.9 in this work)

λ is the X-ray wavelength (α = 1.54 A°),

β is the instrument broadening described by the full width at half maximum (FWHM, in radians) of the relevant peaks

θ is the Bragg angle (in degrees).

In this study, the XRD pattern of all samples were obtained on a Rigaku SmartLab Diffractometer using 40 kV and 35 mA CuK_{α} radiation (α = 1.5404 A°), in-plan arm for the detector with nickel filter and SAXS slit systems. All measurements were carried out at

temperature control room at 22 ºC. Diffractograms were obtained from 2θ = 4º to 50º with step size of 0.02º

The relative crystallinity of ZSM-5 samples was determined based on comparing the integrated areas of five strong peak in 2θ range of 22.5 to 25.0 base on standard ASTM method (Astmd5758-01, 2011), where the untreated samples were assumed to the reference samples, see Equation 5

Equation 5 % Crystallinity

$$\% \text{ Xrd relative crystallinity ZSM-5} = S_x/S_r \times 100$$

Where:

S_x = integrated peak area for the sample ZSM-5, and

S_r = integrated peak area for the reference ZSM-5.

3.2.4 Brunauer–Emmett–Teller (BET) analysis

BET analysis is an instrumental technique used to explain the physical adsorption of gas molecules on a solid surface to estimate the surface area. This technique is commonly used to determine the specific surface area of zeolites and other microporous solid catalysts. Nitrogen is the most commonly employed as representative gas for surface probing by BET method. The concept of BET method was developed by Stephen Brunauer, Paul Emmett and Edward Teller in 1938 to describe the phenomenon of multilayer adsorption that extend from Langmuir theory, which is a theory for monolayer molecular adsorption.

BET analysis was developed base on the three major hypotheses: 1. gas molecules physically adsorb on a solid in layers infinitely; 2. gas molecules only interact with adjacent layers; and 3. the Langmuir theory can be applied to each layer. BET adsorption isotherms equation is shown in Equation 6.

Equation 6 BET adsorption isotherm equation

$$\frac{1}{V_a(\frac{P_0}{P}-1)} = \frac{C-1}{V_m C}\ x\ \frac{P}{P_0} + \frac{1}{V_m C}$$

Where;

P, P_0 are the equilibrium and the saturation pressure of adsorbates at the temperature of adsorption which is -195.8 ^oC for the boiling point of nitrogen. (Pa).

V_a is the adsorbed gas quantity at standard temperature and pressure. (ml)

V_m is the monolayer adsorbed gas quantity. (ml)

C is the BET constant which is calculated from Equation 7 or approximation method by Equation 8.

Equation 7 BET constant and heat of adsorption equation.

$$C = e^{\frac{E_1 - E_2}{RT}}$$

Where;

E_1 is the heat of adsorption for the first layer

E_2 is that for the second and higher layers and is equal to the heat of liquefaction.

R is gas constant 8.314 J/ (K x mol)

T is Temperature of gas adsorption (K)

By plotting $\frac{1}{V_a(\frac{P_0}{P}-1)}$ as y-parameter VS $\frac{P}{P_0}$ as x-parameter in linear equation of Equation 6 (x-parameter usually estimate from $0.05 < \frac{P}{P_0} < 0.35$). From the resulting linear plot of the slope $\frac{C-1}{V_m C}$ and the intercept $\frac{1}{V_m C}$ are obtained from the linear regression analysis, so BET constant (C), V_m, and BET specific area (S_{BET}) can be calculated by Equation 8, Equation 9, and Equation 10

Equation 8 BET constant (C)

$$C = \frac{Slope}{Intercept} + 1$$

Equation 9 The formula for the monolayer adsorbed gas quantity; V_m (ml)

$$V_m = \frac{1}{(Slope + Intercept)}$$

Equation 10 The formula for BET specific surface area; S_{BET} (m^2/g)

$$S_{BET} = \frac{V_m \times N \times s}{V \times m}$$

Where;

V_m is in units of volume which are also the units of the monolayer volume of the adsorbate gas.

N is Avogadro's number (6.02×10^{23} mol^{-1}).

s is the adsorption cross section of the adsorbing species (N_2 = 0.162 nm^2).

V is the molar volume of the adsorbate gas at STP (22400 ml).

m is the mass of the solid sample or adsorbent (g).

In this study, BET adsorption isotherms of samples were obtained by using liquid nitrogen as a molecular probe from relative pressure (P/P_0) 0.05 to 0.20, using Nova e-series model 2200 (Quantachrome Instruments) analyzer. All samples were fill in 9mm large bulb cell equipped rod approximately 50 mg to degassed in a flowing nitrogen gas at 200 ºC for 2 h. The adsorption-desorption was conducted by passing nitrogen through the sample cell which was immerged into liquid nitrogen. Micropore area, micropore volume and average pore diameter were calculated from the adsorption branch of the isotherms using Barrett-Joyner-Halenda (BJH) method.

3.2.5 Acidity of zeolites (NH_3-TPD)

The acidity of zeolites was determined by NH_3 adsorption capacity as the function of temperature detected by a thermal conductivity detector(TCD). This method is known as Ammonium-temperature programmed desorption or NH_3-TPD. NH_3TPD is one of the most common methods for studying the total surface acidity of zeolites or mesoporous structure due to the simplicity and relatively low cost. However, this method cannot separate between Brønsted and Lewis acid sites.

In this study, NH_3-TPD systems was constructed and designed by another researcher in our group members(Akizuki & Oshima, 2017). The schematic diagram of NH_3-TPD systems was shown in Figure 3-1.

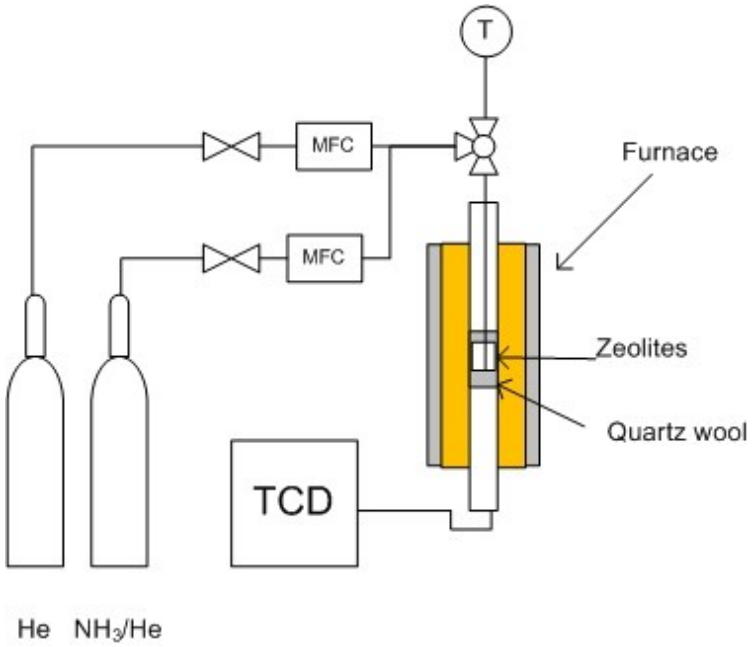

Figure 3-1 Schematic diagram of NH_3-TPD analysis. Note MFC is mass flow controller.

Approximately 100 mg of zeolite was placed between quartz wool into quartz tube reactor heated by electric furnace. Zeolite was pre-heated to remove water contain by adding helium flow (Nihon Helium Corp., Japan, 55 ml/min), and setting electric furnace with heating rate 10 ºC/min until the temperature reach 650 ºC, hold the temperature for 1 hour, and then cooled down to 100 ºC. After the temperature was stable, 5.21 vol. % NH_3/He (Japan Fine Products Corp., Japan) was flowed at flow rate 20 ml/min for 30 minutes, and then rinsed with pure He again at the same temperature for 30 minutes to remove excess physical adsorption of NH_3 on zeolites surface. The desorption of ammonia was measured by thermal conductivity detector (TCD, GC-8A, Shimadzu Corp., Japan) starting by increasing the temperature to 650 ºC at heating rate 10 ºC/min with pure helium flow at 55 ml/min. NH_3 desorption profiles was recorded to determine the areas of fitting cures using Multipeak fitting package of Igor Pro 6.36 (WaveMetrics, Inc., USA). By comparing NH_3 desorption profile of standard sample and zeolites, the total acidity can be obtained.

3.2.6 Coking analysis (TGA)

The amount of coke deposited on zeolites was determined by comparing the weight change of fresh and spent zeolites performed in Thermogravimetric analysis (TGA). This method is measurement the mass of a sample over time as the temperature increasing. Thermogravimetric analysis data were measured using a Rigaku TG 8210 plus. Around 10 mg of zeolites was placed in a flowing N_2 at 200.0 ml/min and air at 200 ml/min. Temperature

profile start from raising the sample from room temperature to 200 ºC with heating rate 10 ºC/min to remove moisture content in the sample, hold the sample at this temperature for 30 mins. After that, increase temperature to 800 ºC with heating rate 10 ºC/min. The weight loss between 200 ºC to 800 ºC was attributed to coking. The weight percentage of coke content was calculated as shown in Equation 11

Equation 11 % coking content

$$\%Coking = \frac{(w_{200} - w_{800})}{w_{800}} - (\frac{w_{200}^{Std} - w_{800}^{Std}}{w_{800}^{Std}}) \times 100\%$$

Where;

w_{200} is the weight of spent zeolite heating at Temperature 200 ºC.

w_{800} is the weight of spent zeolite heating at Temperature 800 ºC.

w_{200}^{Std} is the weight of fresh zeolite heating at Temperature 200 ºC.

w_{800}^{Std} is the weight of fresh zeolite heating at Temperature 800 ºC.

Note The weight loss of fresh zeolite come from organic structure-directing agent(OSDA) which was used during create zeolites structure.

3.2.7 Solubility of zeolites (ICP-AES)

The dissolved Si and Al from zeolites were investigated by inductively couple plasmas with atomic emission spectroscopy (ICP-AES). This analytical technique is used for detection of widely elements in liquid phase solution. The analysis start from solution becomes atomized into a mist-like cloud. This mist is carried into the argon plasma with a stream of argon gas. The plasma produces temperatures around 7,000°C, which thermally excites the outer-shell electrons of the elements in the sample. The relaxation of the excited electrons as they return to the ground state is accompanied by the emission of photons. These emit electromagnetic radiation at wavelengths characteristic of element.

In this study, the effluent recovered from the reactors were diluted five times with ultra-pure water, and it was analyzed for detecting Al and Si using ICP-AES HORIBA JY138KH ULTRACE (Horiba, Ltd., Japan). The standard solutions of Si and Al were prepared by stock samples methods with concentration 0.5, 1, 5, 10, 20, and 40 ppm.

3.2.8 Activity of zeolites (GC-FID)

The activity of zeolites was investigated in various reaction model by monitoring the conversion and selectivity of target product. All liquid phase samples were analyzed by gas chromatograph (GC) equipped with a Flame ionization detector (FID) and capillary column. Gas chromatograph is a chemical analysis instrument for separating chemicals in a complex sample using solid as stationary phase and gas as mobile phase. With increasing the temperature, the mixture will be separated because each compound has the boiling point differences. In this report, the operating conditions of GC-FID are listed in Table 3-2

Table 3-2 Operating conditions of GC-FID

Gas chromatography	Shimadzu GC-2014
Detector	FID
Capillary column (Diameter x Length)	TC-1701 (0.25 mm x 30.0m)
Carrier gas	He
Linear Velocity	Constant at 30.0 cm/sec
Make up gas	N_2
Injector volume	1 mL
Split Ratio	50
Injector temperature	250 ºC
Detector temperature	250 ºC
Initial column temperature	60 ºC (hold time 10 min before heating it up)
Heating rate	10 ºC/min
Final column temperature	240 ºC (hold time 10 min)

3.2.9 Qualitative chemical analysis (GC-MS)

Qualitative chemical analysis of unknown compound mixtures was performed on gas chromatography-mass spectrometry (GC-MS). GC-MS is an analytical technique that combines the features of gas chromatography which has ability to separate mixtures as explain in section 3.2.8 and mass spectrometry which can identify the different substances. Mass spectrometry analysis is started by ionization of the atom or molecule into ionized fragments, and detecting these fragments using their mass-to-charge ratio. (m/z), where m is the mass number of the ion in atomic mass units and z is the number of fundamental charges

that it bears. A mass spectrum is defined as a plot of the ion signal intensity as a function of the mass-to-charge ratio. By comparing this spectrum with a spectrum library, it can identify chemical compound in target samples. In this study, the operating conditions of GC-MS are listed in Table 3-3

Table 3-3 Operating conditions of GC-MS

Gas chromatography	Shimadzu GCMS-QP2010
Detector	MS
Capillary column (Diameter x Length)	TC-1701 (0.25 mm x 30.0m)
Carrier gas	He
Linear Velocity	Constant at 30.0 cm/sec
Split Ratio	50
Injector volume	1 mL
Injector temperature	200 ºC
Ion source temperature	200 ºC
Interface temperature	200 ºC
Initial column temperature	40 ºC (hold time 10 min before heating it up)
Heating rate	10 ºC/min
Final column temperature	200 ºC (hold time 1 hour)

3.3 Apparatus and procedure.

The apparatus was mainly separated in two sections. 1) Closed system which operate in batch reactor to investigate the structure stability of zeolites in pure water. 2) Open system which operate in plug flow reactor to investigate the activity of zeolites. The details of each equipment including operation procedure are explained as following

3.3.1 Closed system (Batch reactor)

The structure stability test was performed using batch reactor as shown in Figure 3-2. Batch reactor was created from nominal ½-inches diameter thickness 1.24 mm. Stainless steel Swagelok tube fittings covered by two Swagelok caps. This reactor had volume around 10.0 cm^3, and it was place in fluidized sand bath connected with temperature controller unit, heating coil, and suction air pump to operate isothermal condition in sub- and supercritical water.

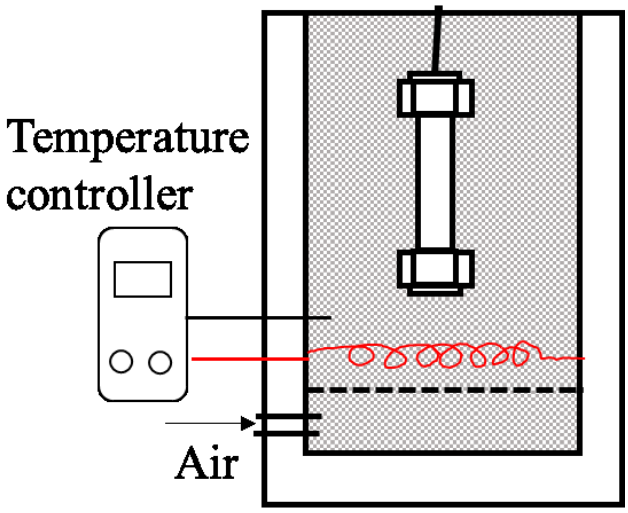

Figure 3-2 Schematic drawing batch reactor

3.3.1.1Pre-aging reactor

All new batch reactor tube was pre-aging to remove the impurity metal oxide in stainless steel since preliminary experiments indicated that new reactors generated the reaction difference from the reactors that have been used at least once. The operating sequences is exactly same as the normal procedure excluding pre-aging method does not fill any zeolite in the reactor. The detail preparation was described by step-by-step as following

- Ultra-pure water was filled around 1 ml in new Swagelok tube reactor.
- Tube reactor was placed in fluidized sand bath which already pre-heated at 400 ºC for 1 hour.
- Tube reactor was removed from sand bath and immediately quenched by submersion in cold water bath.
- Cap of tube reactor was removed and washed with ultra-pure water.
- Reactor was dried in electric oven at 120 ºC to remove water content.

3.3.1.2 Structure stability test

All structure stability was tested in aging tube reactor that was explained in section 3.3.1.1. The investigation was described by step-by-step as following

- Aging tube reactor was filled with ultra-pure water or Si/Al solution at desirable condition. For subcritical water, water was loaded at nearly filled at single liquid phase of water condition (97.5% single liquid phase) which is calculated from water

density published by(Wagner & Pruß, 2002). Amount of water that fill in water was shown in Table 3-4. For supercritical water, Filling water was also calculated from the literature (Wagner & Pruß, 2002) at selected condition temperature 400 ºC, pressure 24.13 MPa (1.5 ml), and 30.6 MPa (2.14 ml).

- Filling zeolites around 0.2 g in aging tube reactor (β zeolite (40), H-ZSM-5(24), H-ZSM-5(40), and H-ZSM-5(1500)).
- Fluidized sand bath was pre-heated at selected temperature (200-400 ºC).
- Aging tube reactor was placed in fluidized sand bath for 1 or 6 hours.
- Tube reactor was removed from sand bath and immediately quenched by submersion in cold water bath.
- Water effluent and powder zeolites were collected, and separated by laboratory centrifuge (Kubota model 2420) at 4000 rpm for 10 min.
- Water effluent was further analyzed the solubility of Si and Al by ICP-AES (Section 3.2.8)
- Zeolites were washed with ultra-pure water and centrifuged at 4000 rpm for 10 min, and then repeat this step two times.
- Zeolites were dried in vacuum oven for 12 hours to remove moisture.
- Aging reactor tube was re-used to test the structure stability in a couple times before disposal.
- The dried zeolite was further analyzed the structure stability by SEM, XRD, NH_3-TPD, and BET.

Table 3-4 Filling water in batch reactor at subcritical water

Temp(ºC)	200	225	250	275	300	325	350
water fill (ml)	7.11	6.87	6.60	6.29	5.94	5.51	4.95

3.3.2 Open system (fixed-bed flow reactor)

The activity of zeolites was investigated by fixed-bed flow systems, as shown in Figure 3-3. This systems (except pack bed reactor) was designed and constructed by another researchers in our group study (Akizuki, Tomita, & Oshima, 2011). Cyclohexene or mixture of 3%Cyclohexene with water was pumped using a syringe pump (260D; Teledyne Isco, Inc., Lincoln, NE). Ultra-pure water was pumped using a plunger pump (PU-2080; JASCO Corp.,

Tokyo, Japan) and preheated by heating coil before mixing with organic line. The mixing line was measurement by temperature probe before fed into pack-bed reactor, which was filled with zeolites. The stream outlet from reactor was cooled by a water-cooled heat exchanger and depressurized by back-pressure regulator (SCF-Bpg; JASCO Corp., Tokyo, Japan). Finally, product was collected using glass vial to further analyze by gas chromatograph (GC-FID) and plastic vial for analysis the solubility of Si and Al (ICP-AES). All tube line in this system was 1/16-inches diameter thickness 1.24 mm. (stainless steel Swagelok) to minimize the residence time.

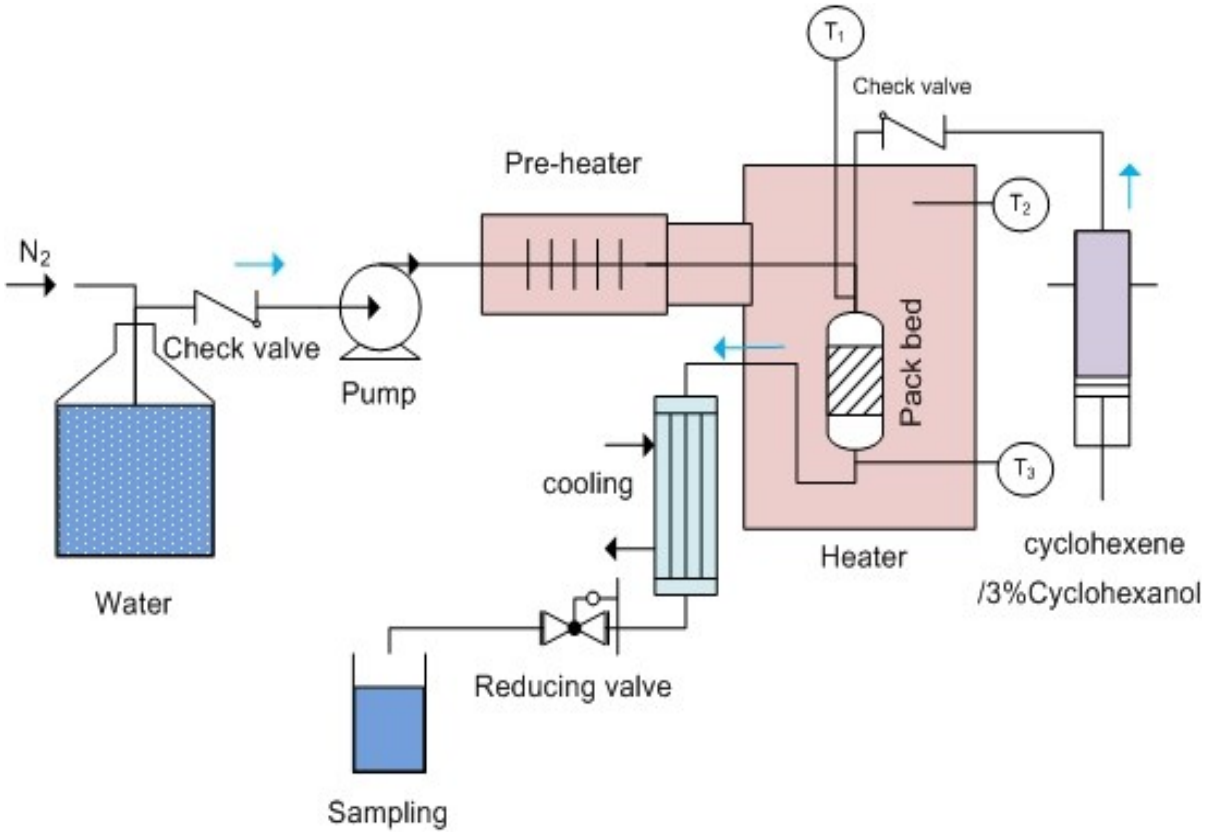

Figure 3-3 Schematic diagram of fixed-bed flow system

3.3.2.1 Sub-critical water

Hydration of cyclohexene was selected as the reaction model to test the stability of zeolites in sub-critical water since cyclohexene hydration is exothermic reaction. In the theory, low temperature is preferable for product side of exothermic reaction. However, rate of reaction and solubility of water and cyclohexene decrease at lower temperature, so intermedia temperature and high pressure, sub-critical water, is the most suitable condition

for cyclohexene hydration. By applied zeolites as the catalyst of cyclohexene hydration, it also provides high selectivity due to porous structure of zeolites has the pore diameter as same as the average kinetic diameter of cyclohexene which can prevent larger average kinetic diameter by-product such as dicyclohexyl ether. The detail procedure of this reaction was described by step-by-step as following

- Pack bed reactor was created from nominal 3/8-inches diameter thickness 1.24 mm., length 12.5 cm (stainless steel Swagelok tube fittings) covered by reducing fitting Swagelok 3/8 to 1/16-inches for both side.
- Zeolites (P-H-ZSM-5(24), P-H-ZSM-5(40), and P-H-ZSM-5(1500)) was loaded in reactor around 3 grams. covered with stainless steel filter (Valco instruments, thickness 0.5-micron 316SS) in both side of reactor. After that, Pack bed reactor was connected to perform leak test with ultra-pure water at pressure 25 MPa.
- Syringe pump (260D; Teledyne Isco, Inc., Lincoln, NE) was washed by acetone two times and leached with cyclohexene 99.0% (KANTO Chemical, Japan).
- Stability investigation was started from set up flow rate of ultra-pure water and cyclohexene (constant flow mode) at 4.34 and 0.868 mL/min, respectively to keep flow ratio (water/cyclohexene) at 5 following by slowly increasing pressure to 25 MPa and temperature at selected conditions (200, 225, 250, 300 ^{o}C)
- Samples were collected every 0.5 hours for 6 hours in plastic and glass vials. Each glass vial was leaved at room temperature for 1 hour to separate water and organic phases. For plastic vial, it leaved over night before collecting only water phase to analyze in ICP-AES to check solubility of Si/Al.
- Water and organic phases from glass vial were analyzed in GC-FID to investigate conversion and selectivity of product. Water phase was analyzed by external standard method ("external standard in chromatography," n.d.), and organic phase was analyzed by internal standard method ("internal standard in chromatography," n.d.) selected pentane as solvent, and methylcyclohexane as internal standard. The details preparing of standard solution in both external and internal standard was explained in another section.
- Spent zeolites were retrieved from pack bed, and washed with ultra-pure water twice before centrifuged at 4000 rpm for 10 min. After that, Zeolites were dried in vacuum oven for 12 hours to remove moisture.

- Spent zeolite were investigated by various characterization such as SEM, XRD, NH_3-TPD, TGA, and BET to check the stability.

3.3.2.2 Supercritical water

For stability of zeolites in supercritical water, Dehydration of cyclohexanol was selected as the reaction model. This reaction is endothermic reaction which prefer at high temperature. Without catalyst, previous study (Akiya & Savage, 2001) of cyclohexanol dehydration in supercritical water indicated that the reaction is slow, and cyclohexene is only product at low water densities. By applied zeolites as the catalyst, it might promote the activity and improve selectivity due to porous structure of zeolites has the pore diameter as same as the average kinetic diameter of cyclohexanol which can prevent larger average kinetic diameter by-product such as Dicyclohexyl ether. The detail procedure was described by step-by-step as following

- Pack bed reactor was created in three reactor sizes to achieve different target residence time (RT) of reaction as the following.
    - 3/8-inches diameter thickness 1.24 mm., length 12.5 cm (stainless steel Swagelok tube fittings) for WHSV = 100 h^{-1}
    - 1/4-inches diameter thickness 1.24 mm., length 12.5 cm (stainless steel Swagelok tube fittings) for WHSV = 300 h^{-1}
    - 1/4-inches diameter thickness 1.24 mm., length 2.5 cm (stainless steel Swagelok tube fittings) for WHSV = 1500 h^{-1}
- Zeolites (P-H-ZSM-5(24), P-H-ZSM-5(40), and P-H-ZSM-5(1500)) was loaded in reactor (0.2, 1.0, and 3.0 grams for WHSV =100 h^{-1}, 300 h^{-1}, 1500 h^{-1}, respectively) covered with stainless steel filter (Valco instruments, thickness 0.5-micron 316SS) in both side of reactor. After that, Pack bed reactor was connected to perform leak test with ultra-pure water at pressure 25 MPa.
- Cyclohexanol 99.0% (Commercial grade, Wako Chemical, Japan) was mixed with ultra-pure water to receive 3 %wt. Cyclohexanol in water solution (Note solubility of Cyclohexanol in water is 4.3 %wt. at temperature 30 ^oC)
- Syringe pump (260D; Teledyne Isco, Inc., Lincoln, NE) was washed by ultra-pure water and leached with 3 %wt. Cyclohexanol solution.
- Stability investigation was started from set up flow rate of ultra-pure water and 3% wt. Cyclohexanol (constant flow mode) at 4.689 and 0.521 mL/min, respectively to

keep flow ratio (water/3% cyclohexene) at 10 following by slowly increasing pressure to 25 MPa and temperature to 400 ºC.

- 4.7 mL of samples were collected every 0.5 hours for 6 hours in plastic and glass vials. For glass vials, the effluent of the reactor including both the organic phase and water phase was extracted with 4.7mL methyl acetate to collect all the organics into one liquid phase, then this extraction samples were further analyzed in GC-FID by external standard method ("external standard in chromatography," n.d.) to check conversion and selectivity of product. To identify the chemical compound in extraction samples, qualitative analysis was performed on GC-MS (details see section 3.2.9)
- For plastic vial, it leaved over night before collecting only water phase to analyze in ICP-AES to check solubility of Si/Al.
- Spent zeolites were retrieved from pack bed, and washed with ultra-pure water twice before centrifuged at 4000 rpm for 10 min. After that, Zeolites were dried in vacuum oven for 12 hours to remove moisture.
- Spent zeolites were investigated by various characterization techniques such as SEM, XRD, NH_3-TPD, TGA, and BET to check the stability.

CHAPTER 4 RESULTS AND DISCUSSION

The investigation of stability of zeolites was divided in four parts including closed system operated in batch reactor mainly focusing on investigating structure stability in both sub- and supercritical water, and open system operated in plug flow reactor focusing on activity of zeolites (H-ZSM-5) over cyclohexene hydration (sub-critical water) and cyclohexanol dehydration. The variation of conditions such as temperature, pressure, residence times, and Si/Al ratio in zeolites structure were investigated in this study.

4.1 Structure stability of zeolites in supercritical water (closed system).

4.1.1 Effect of zeolites structures

H-ZSM-5 and β zeolite having silica per alumina ratio 40 performed at supercritical water (400 ºC), pressure 24.13 MPa, and residence time 1 hour was investigated the structure stability (XRD, SEM, and EDX) before and after reaction with ultra-pure water.

4.1.1.1 β zeolite

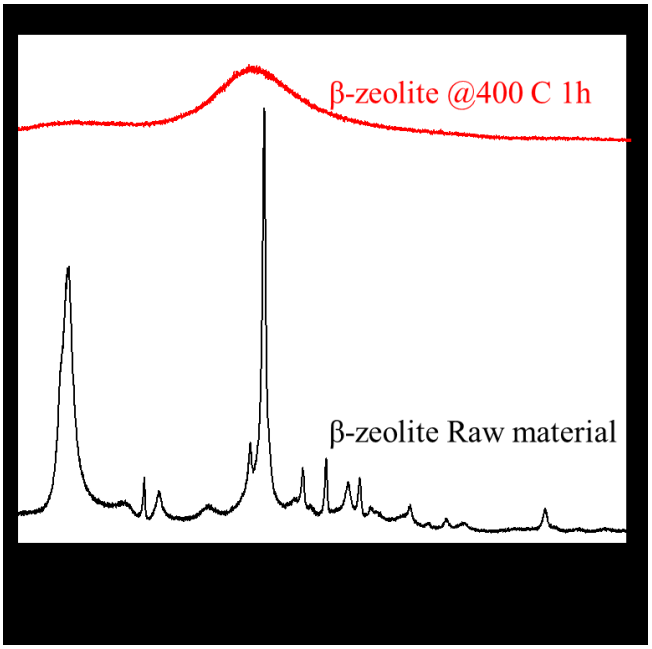

Figure 4-1 X-ray diffractograms of β zeolite before(bottom) and after (top) treatment with ultra-pure water for 1 h.

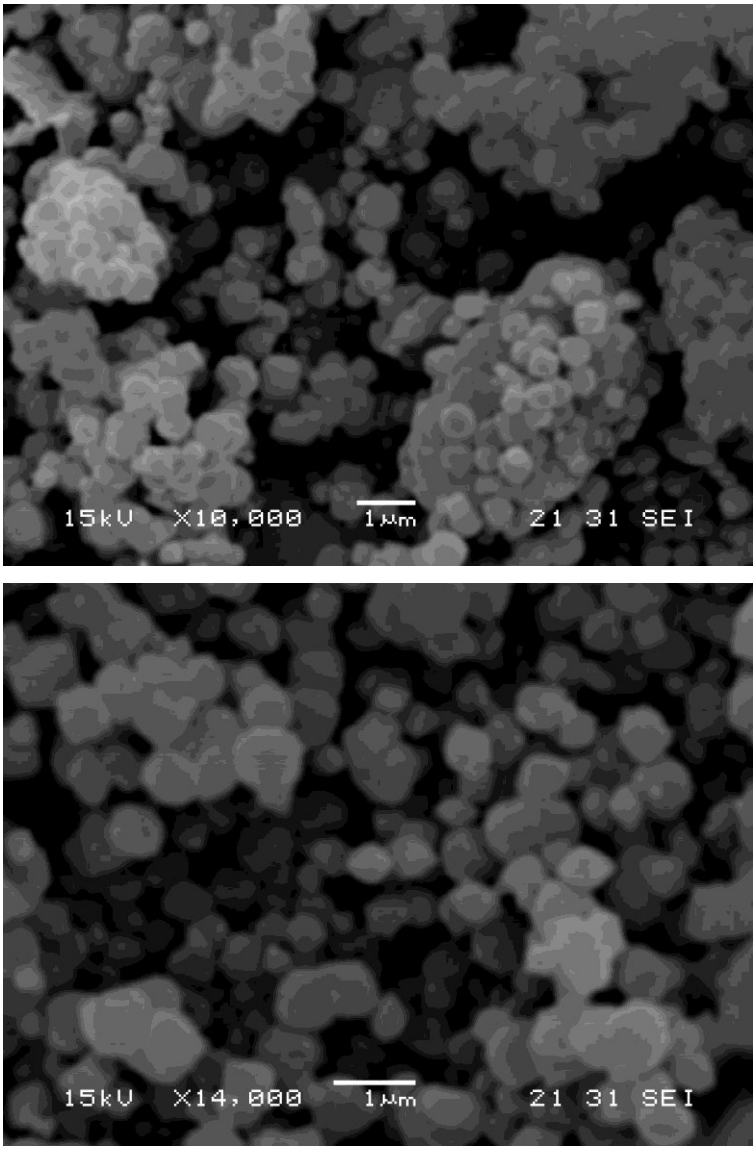

Figure 4-2 Scanning electron microscope of β zeolite before(bottom) and after (top) treatment with ultra-pure water for 1 h.

The X-ray diffractograms (XRD) of β zeolite before treatment with water were shown x-ray pattern as expected, with major peaks located at 2θ = 7.74º, 21.9º, and 22.1º corresponding to the (101), (205), and (302) lattice planes, respectively (Camblor & Pérez-Pariente, 1991). After operating in supercritical water, XRD pattern (see Figure 4-1) completely changed by degradation to one single broad peak, which indicated that the crystallinity of β zeolite change into amorphous structure. However, the morphology of β zeolite (see Figure 4-2) did not show any sign of degradation of the crystal structure and no noticeable change in the particle size as compared to before treatment in supercritical water. In conclusion, the structure collapsed due to high pressure and temperature might be the reason of crystallinity loss in their structure.

4.1.1.2 H-ZSM-5

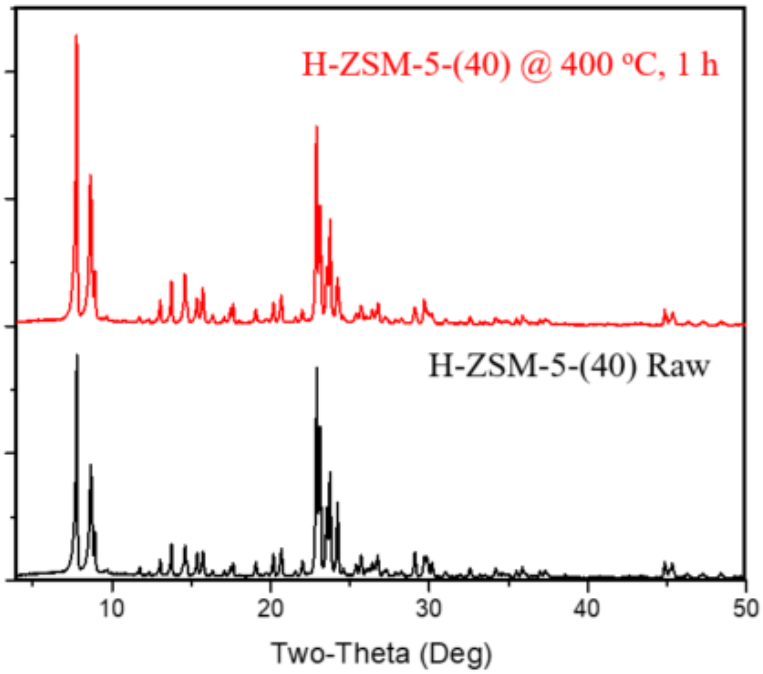

Figure 4-3 X-ray diffractograms of H-ZSM-5 before(bottom) and after (top) treatment with ultra-pure water for 1 h.

The X-ray diffractograms (XRD) of H-ZSM-5 before treatment with water were shown x-ray pattern as expected, with major peaks located at $2\theta = 7.9^{o}$, 8.9^{o}, and 23.1^{o} corresponding to the (011), (200), and (051) lattice planes, respectively (Kokotailo, Lawton, Olson, & Meier, 1978). After operating in supercritical water, XRD pattern (see Figure 4-3) surprisingly showed no appreciable change in all signature peaks. Moreover, broad signal (inferred to amorphous phase) and additional peaks did not appear in this experiment. However, the relative intensity of XRD pattern slightly changed. The intensity of low angle ($2\theta = 4^{o}$-15^{o}) of after experiment increased. In contrast, the in intensity of mid-high angle ($2\theta = 20^{o}$-50^{o}) decreased after treatment with water. This result indicated that the minor structure of H-ZSM-5 might change during water attack, but the major structure of H-ZSM-5 can retain under high temperature and high pressure of supercritical condition. The scanning electron microscope (SEM) result of H-ZSM-5 (see Figure 4-4) also support this hypothesis. The morphology of H-ZSM-5 after operating in supercritical water showed sign of degradation of the crystal structure starting at the outer boundary which directly contact with the water.

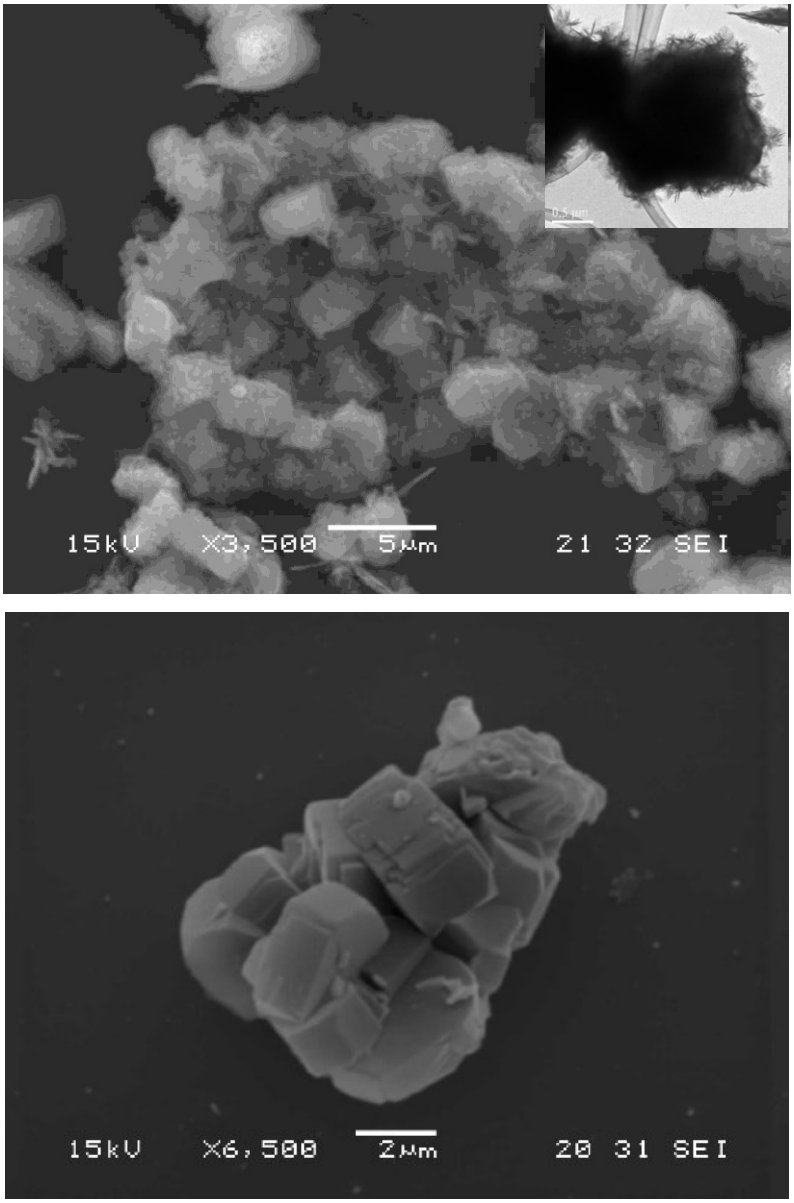

Figure 4-4 Scanning electron microscope of H-ZSM-5 before(bottom) and after (top, including sub-figure from TEM) treatment with ultra-pure water for 1 h.

In summary, the stability of zeolites strongly depends on their structure. H-ZSM-5, which has report to be stable at temperature 150-200 ºC in previous study (Ravenelle et al., 2010), also has highly structure stability in supercritical water but long term stability and open system should be concerned due to intensity change in XRD, and water attack at boundary observing by SEM and TEM. In contrast, β zeolite cannot maintain their structure in supercritical water. The structure completely changed to amorphous phase which correspond to the previous study of stability of β zeolite at 200 ºC (Zhang et al., 2015) that they found β zeolite has decreasing of crystallinity. (Note The details explanation of previous study of H-ZSM-5 and β zeolite at 200 ºC is presented in section 2.2.4).

The reason of higher stability of H-ZSM-5 than β zeolite structure was already predicted by lower appearing of defects in structure framework, lower heat of formation, and having SiO_4 closest to perfect tetrahedral angle (see section 2.2.6).

4.1.2 Effect of residence time

Since previous study of H-ZSM-5 (section 4.1.1.2) show high stability in supercritical water (T= 400 °C, P= 24.13 MPa) for 1-hour operation. Longer time operation is requested for testing the stability of H-ZSM-5 to confirm that H-ZSM-5 is truly stable in supercritical water. In this section, H-ZSM-5 with Si/Al ratio 24 and 40 (code name H-ZSM-5(24) and H-ZSM-5(40)) were investigated by XRD and SEM under supercritical water for 1 and 6-hours operation.

4.1.2.1 H-ZSM-5(24)

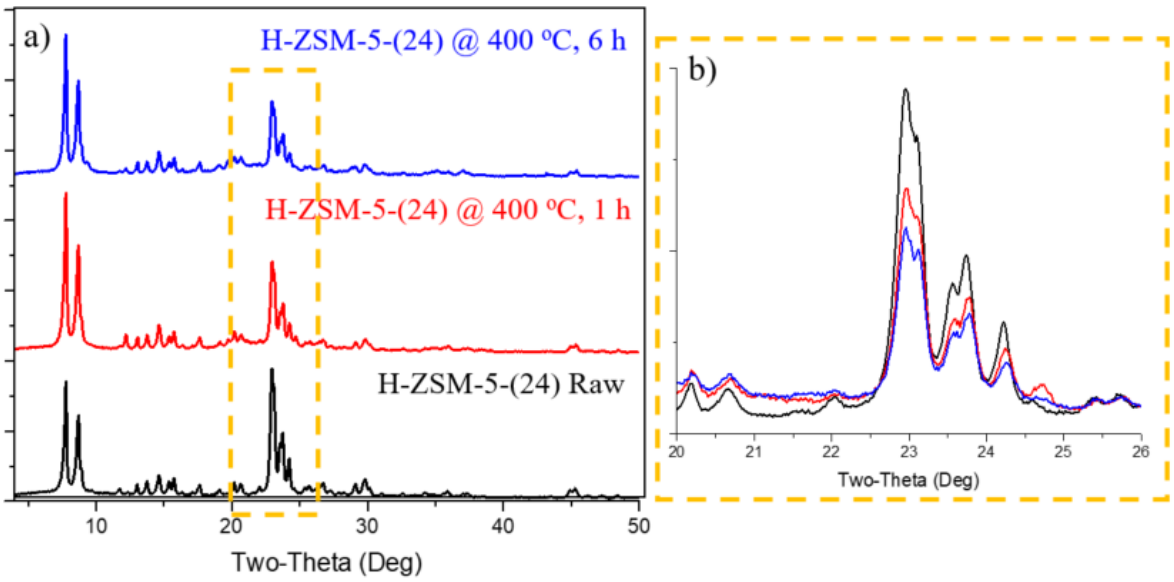

Figure 4-5 a) X-ray pattern (2θ =4°-50°) of H-ZSM-5(24) before operating in supercritical water (bottom), after operating in supercritical water for 1 h. (middle), and 6 h. (top) b) X-ray pattern focusing in middle angle (2θ =20°-26°) of H-ZSM-5(24) in supercritical water.

After H-ZSM-5(24) was treated at supercritical water, the XRD intensity of middle angle pattern decreased over the time, indicating a decreasing in crystallinity (see Figure 4-5). However, broad amorphous signal and additional peak did not appear in this experiment. The morphology of H-ZSM-5(24) also confirmed the water attack in both 1 and 6 hours operation. However, the longer operation trend to have higher

degradation (see Figure 4-6). The shape of H-ZSM-5(24) was changed from rectangular prism to needle shape formation.

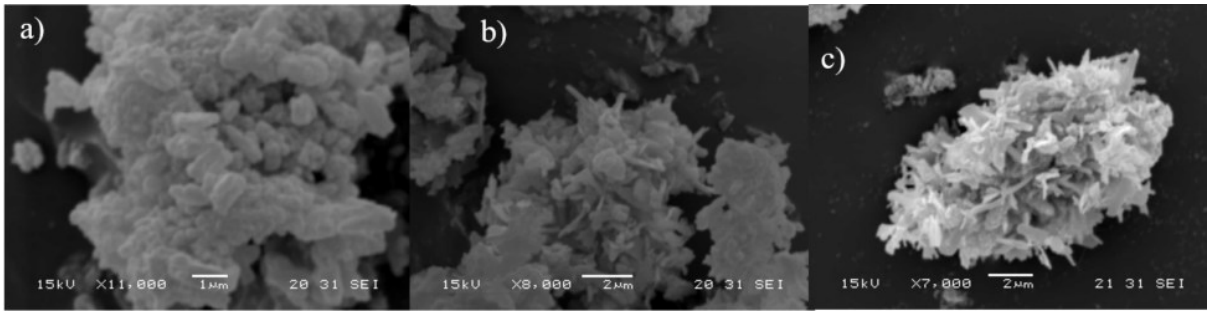

Figure 4-6 Scanning electron microscope of H-ZSM-5(24) a) Raw material b) supercritical water (400 ºC) for 1 h. c) supercritical water (400 ºC) for 6 h

4.1.2.2 H-ZSM-5(40)

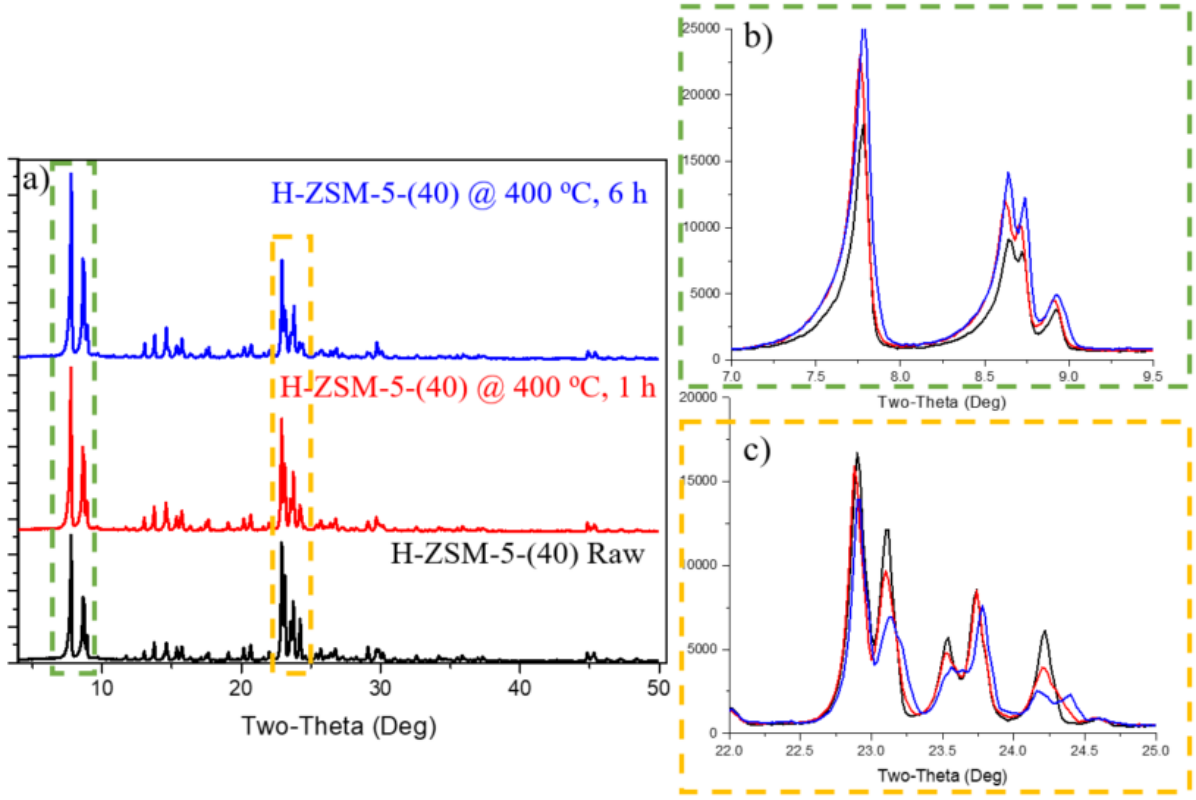

Figure 4-7 a) X-ray pattern (2θ =4º-50º) of H-ZSM-5(40) before operating in supercritical water (bottom), after operating in supercritical water for 1 h. (middle), and 6 h. (top) b) X-ray pattern in low angles (2θ =7º-9.5º) c) X-ray pattern in middle angles (2θ =22º-25º).

After H-ZSM-5(40) was treated at supercritical water, the XRD intensity of low angle pattern increased but middle angle pattern decreased over the time (see Figure 4-7), indicating a decreasing in crystallinity which calculated based on ASTM crystallinity definition (Astmd5758-01, 2011)(see section 3.2.3). The calculation of standard ASTM method mainly calculated by integration of only five strong peak in middle angles ($2\theta = 22^{o}$-25^{o}) due to at low angles, the sample intercepts only part of the beam resulting in reduced beam intensity per unit area sample which is not appropriate for quantitative analysis (McCusker, 1998), However, some researchers (Viswanadham, Gupta, Dhar, & Garg, 2006) also reported that the intensity of low-angle peak related with dealumination reaction (see section 2.2.5). The intensity of XRD increased after dealumination reaction occurred. The increased intensity at low angles also inferred to the increased hydrophobic property of ZSM-5(40). The morphology of H-ZSM-5(40) also confirmed the water attack in both 1 and 6 hours operation (see Figure 4-8). However, the longer operation trend to have higher degradation. Unlike H-ZSM-5(24) that the shape of structure change to needle form, H-ZSM-5(40) remained the major shape with severe destruction at the boundary surface.

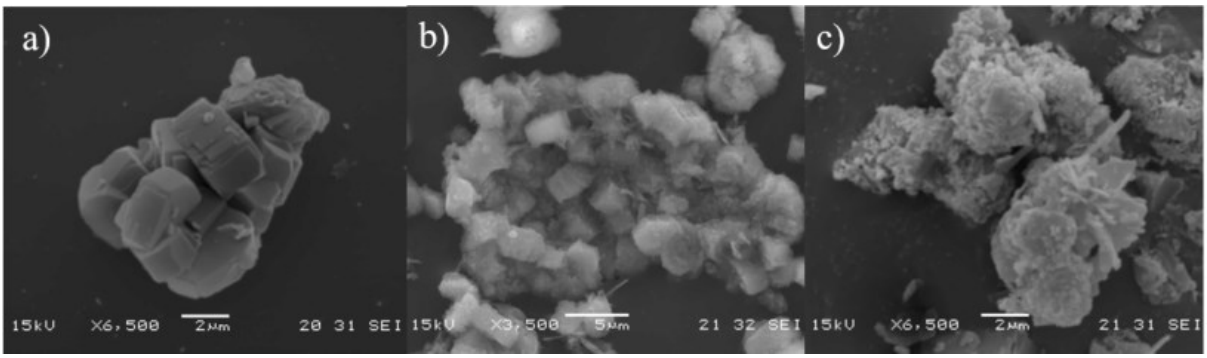

Figure 4-8 Scanning electron microscope of H-ZSM-5(40) a) Raw material b) supercritical water (400 ^{o}C) for 1 h. c) supercritical water (400 ^{o}C) for 6 h

In conclusion, at longer operation, both H-ZSM-5(24) and H-ZSM-5(40) have higher destructive structure. However, the rate of destruction from 1 h to 6 h is slower comparing with destruction from 0 h to 1 h. It seems that the destruction of the structure might reach the equilibrium leading to low rate of destruction. Subsequently, this hypothesis was confirmed in another experiment (section 4.1.5).

4.1.3 Effect of pressure

The stability of H-ZSM-5 was investigated the effect of pressure in three Si/Al ratio; H-ZSM-5(24), H-ZSM-5(40), H-ZSM-5(1500) at pressure 24.1 and 26.9 MPa with control parameters: temperature 400 ºC, and residence time 1 h.

4.1.3.1 H-ZSM-5(24)

In case of H-ZSM-5(24), pressure slightly effect on the intensity of H-ZSM-5(24). At low angle of 2θ, the intensity of H-ZSM-5(24) at different pressure (24.1, and 26.9 MPa.) are identical (see Figure 4-9). However, the crystallinity of H-ZSM-5(24) which calculate from the integrated area of five strong peak in middle angle (22º-25º) are slightly different. In other words, the crystallinity at pressure 24.1 MPa is higher than pressure 26.9 MPa. (Crystallinity are 72.6% and 71.4%, respectively). The morphology of H-ZSM-5(24) also found the structure transformation from rectangular prism to needle shape formation in both condition. The decreasing of low angle and increasing of middle angle were already explained in section 4.1.2.

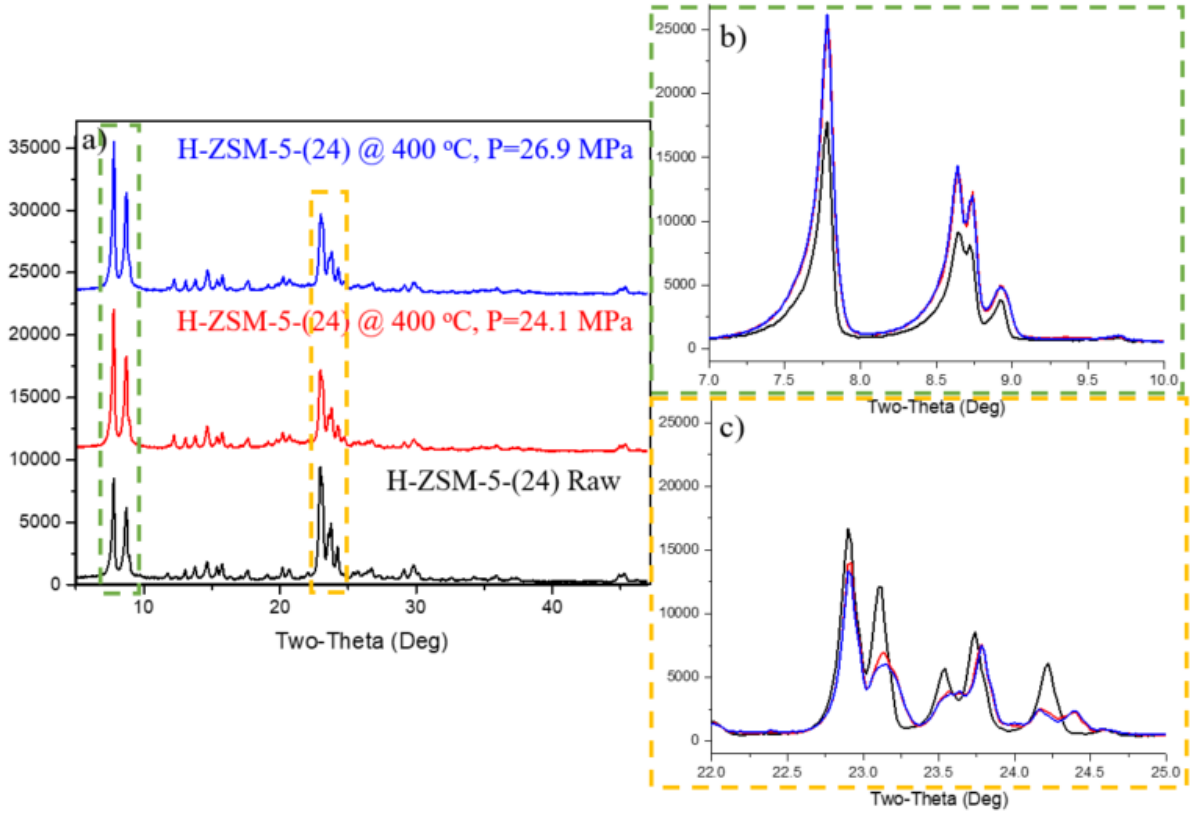

Figure 4-9 a) X-ray pattern (2θ =4°-50°) of H-ZSM-5(24) before operating in supercritical water (bottom), after operating in supercritical water at pressure 24.1 MPa (middle), and 26.9 MPa. (top) b) X-ray pattern in low angles (2θ =7°-9.5°) c) X-ray pattern in middle angles (2θ =22°-25°).

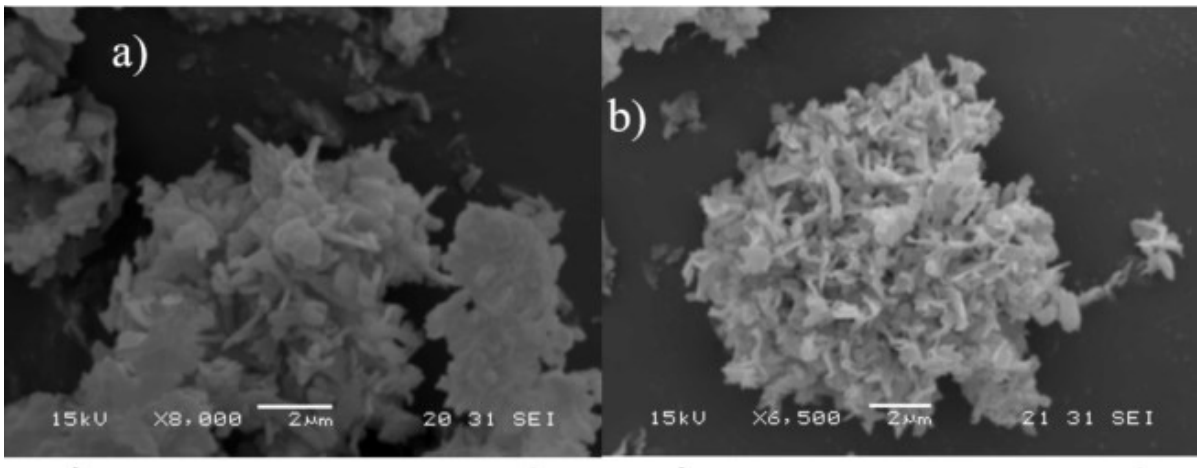

Figure 4-10 Scanning electron microscope of H-ZSM-5(24) after operating in supercritical water at pressure a) 24.1 MPa b) 26.9 MPa

4.1.3.2 H-ZSM-5(40)

Unlike H-ZSM-5(24) which has the identical result in both pressure of XRD in low angles, XRD intensity of H-ZSM-5(24) (see Figure 4-11) at high pressure has slightly increasing in low angles area and decreasing in middle angles area. The Crystallinity are 93.0% and 87.5% at pressure 24.1 MPa, and 26.9 MPa, respectively.

The morphology of H-ZSM-5(24) was investigated by scanning electron microscope (SEM) and transmission electron microscope (TEM) (see Figure 4-12). The destructive structure by water attack was appeared in both different pressure conditions. However, surprisingly the destructive structures are different based on morphology observation. At low pressure (24.1 MPa) supercritical water which has lower water disassociation (K_w) than high pressure (26.9 MPa) supercritical water (see Figure 2-3 and detail in section 2.1.1), severe destruction at the boundary surface can be observed in TEM analysis which might cause from desilication reaction. However, the destruction at the boundary surface did not present in high pressure (26.9 MPa) case. Instead of boundary destruction, it presented the extra-framework species, which was predicted to be Alumina or extra framework alumina (EFAl) because of dealumination (see section2.2.5).

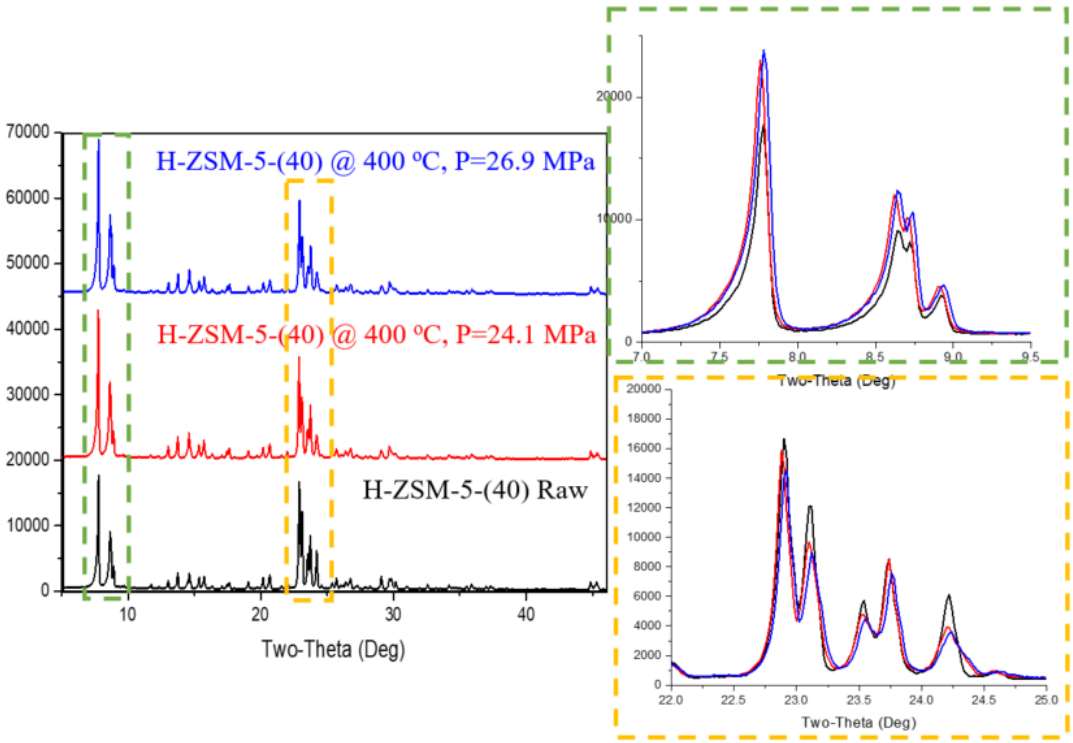

Figure 4-11 a) X-ray pattern (2θ =4°-50°) of H-ZSM-5(40) before operating in supercritical water (bottom), after operating in supercritical water at pressure 24.1 MPa (middle), and 26.9 MPa. (top) b) X-ray pattern in low angles (2θ =7°-9.5°) c) X-ray pattern in middle angles (2θ =22°-25°).

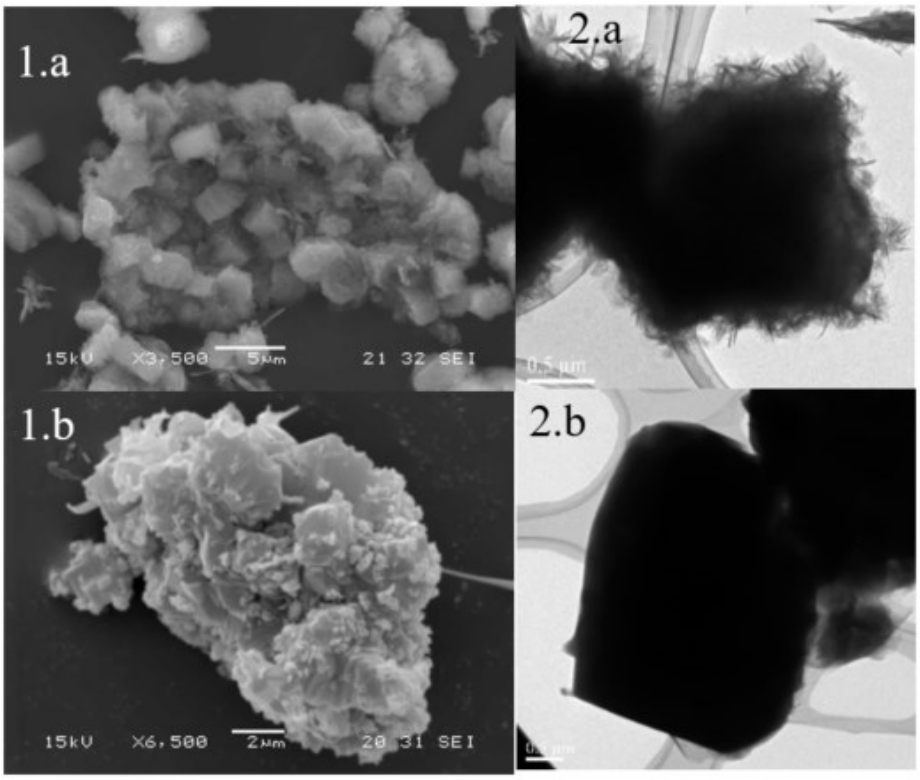

Figure 4-12 1) Scanning electron microscope (SEM) and 2) transmission electron microscope (TEM) of H-ZSM-5(40) after operating in supercritical water at pressure a) 24.1 MPa b) 26.9 MPa

4.1.3.3 H-ZSM-5(1500)

Unlike other H-ZSM-5 with silica per alumina ratio 24 and 40, the morphology of H-ZSM-5(1500) in both operating pressure does not show any sign of degradation on the boundary or surface of zeolite structure. Crystallinity which defined as the integration of XRD pattern between 2θ = 22.5°-25° are also identical in both pressure. However, the crystallinity values are slightly higher than 100% due to split peak occurred at 2θ =23.4° and 23.8°. These phenomena indicated that the minor conformation is changed. By reconstruction of structure unit molecule of the structure using XRD information, the split peaks from doublet to triplet peaks are the result from changing orthorhombic to monoclinic structure (see) which occurred in high silica per alumina ratio of zeolite starting at temperature 178 °C(Ardit, Martucci, & Cruciani, 2015). Both minor structure

still defined as H-ZSM-5, since ZSM-5 can exist with either orthorhombic or monoclinic symmetry according to ASTM definition(Astmd5758-01, 2011).

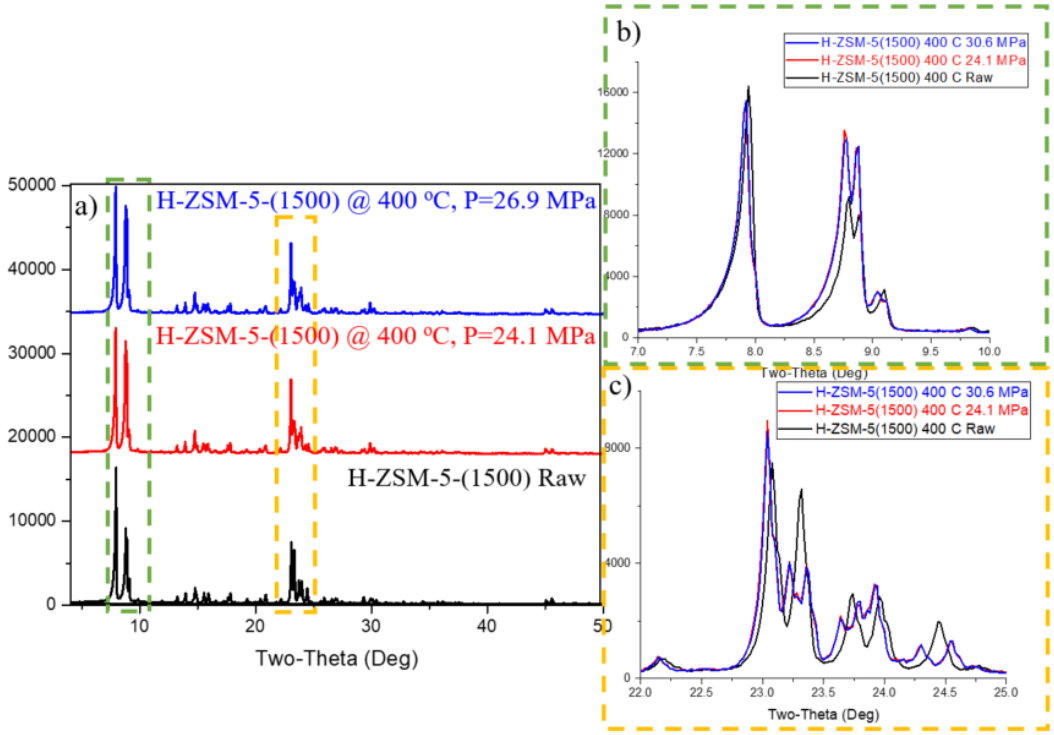

Figure 4-13 a) X-ray pattern (2θ =4º-50º) of H-ZSM-5(1500) before operating in supercritical water (bottom), after operating in supercritical water at pressure 24.1 MPa (middle), and 26.9 MPa. (top) b) X-ray pattern in low angles (2θ =7º-9.5º) c) X-ray pattern in middle angles (2θ =22º-25º).

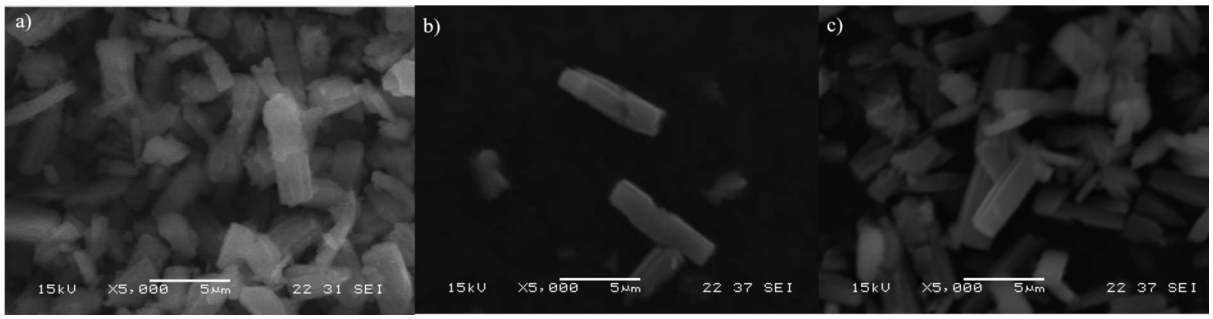

Figure 4-14 Scanning electron microscope of H-ZSM-5(1500) a) fresh zeolite before operating in supercritical water, and after at pressure b) 24.1 MPa c) 26.9 MPa.

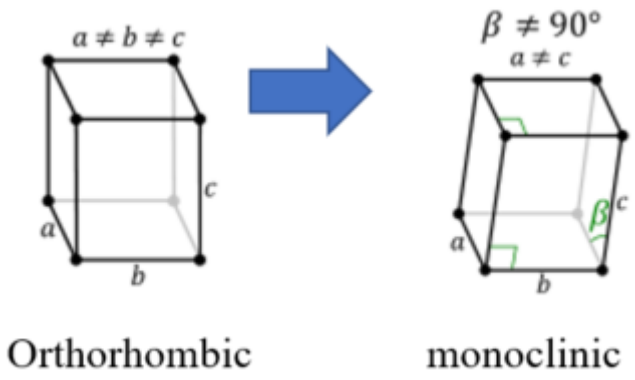

Figure 4-15 Monoclinic–Orthorhombic phase transition in H-ZSM-5 (1500)

In summary, the different pressure in supercritical water effect to the destruction degree of H-ZSM-5. Even all major characteristic peak of XRD maintain in all condition at various Si/Al of H-ZSM-5 structure, the intensity of XRD peak decreased, which implied that the decreasing of crystallinity except in the case of H-ZSM-5 with low Al content that has crystallinity over 100%. The main destructive mechanism was proposed by dealumination and desilication which dominate at different pressure which indirectly demonstrated by Si/Al ratio detected by SEM-EDX in Table 4-1.

4.1.4 Effect of Temperature

The stability of H-ZSM-5 was investigated the effect of temperature in both H-ZSM-5(24) and H-ZSM-5(40) at temperature 400 ºC (pressure 24.13MPa) and 450 ºC (pressure 30.6 MPa) with control parameters: residence time 6 h.

4.1.4.1H-ZSM-5(24)

In case of H-ZSM-5(24), temperature has strongly affected on the intensity of XRD and crystallinity (see Figure 4-16). At high temperature (450 ºC), the XRD intensity shapely drop to 34.5 % crystallinity remaining (comparing with 60.3% crystallinity remaining at temperature 400 ºC). The broad peak intensity, which referred to amorphous phase, also appeared at operating at 450 ºC but it slightly appeared in 400 ºC. the destructive structures at the boundary were observed by SEM analysis (see Figure 4-17) in both temperature cases. According to EDX analysis, Si/Al ratio in both different temperature conditions were decreased. It means that silica was decreased from the structure which inferred desilication reaction occurred. At higher temperature (400 ºC), the destruction by desilication is higher based on decreasing XRD intensity and Si/Al ratio in EDX analysis.

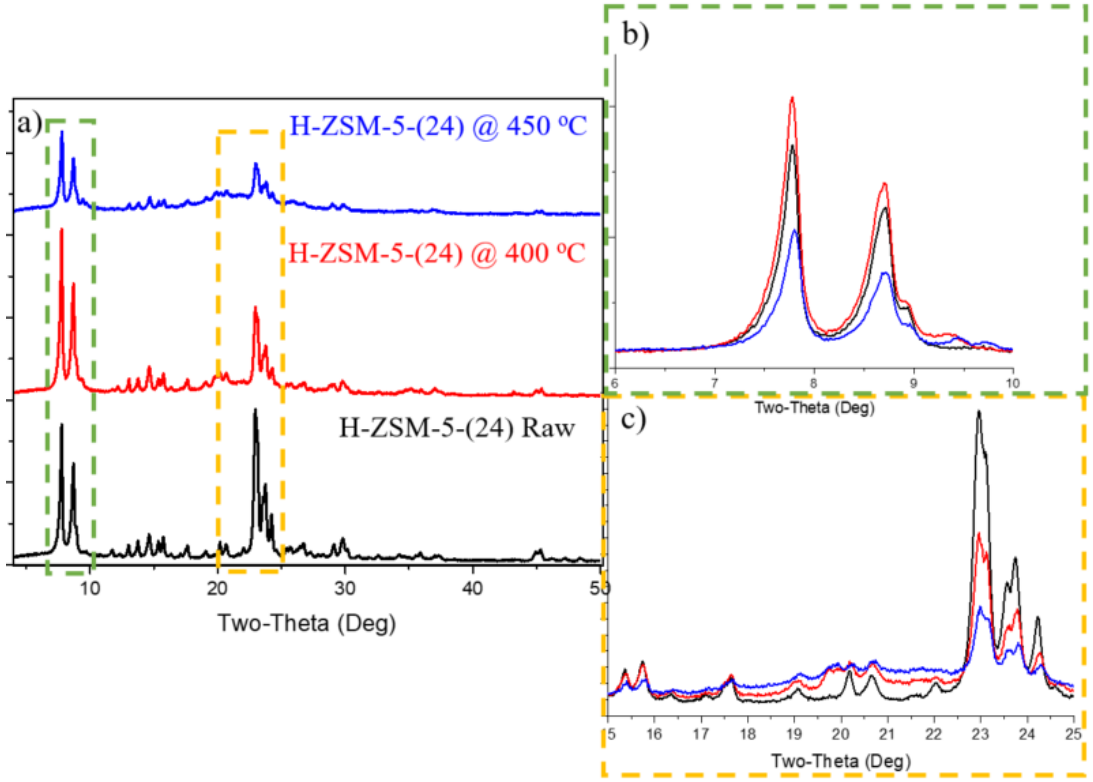

Figure 4-16 a) X-ray pattern (2θ =4º-50º) of H-ZSM-5(24) before operating in supercritical water (bottom), after operating in supercritical water at Temperature 400 ºC (middle), and 450 ºC (top) b) X-ray pattern in low angles (2θ =7º-9.5º) c) X-ray pattern in middle angles (2θ =22º-25º).

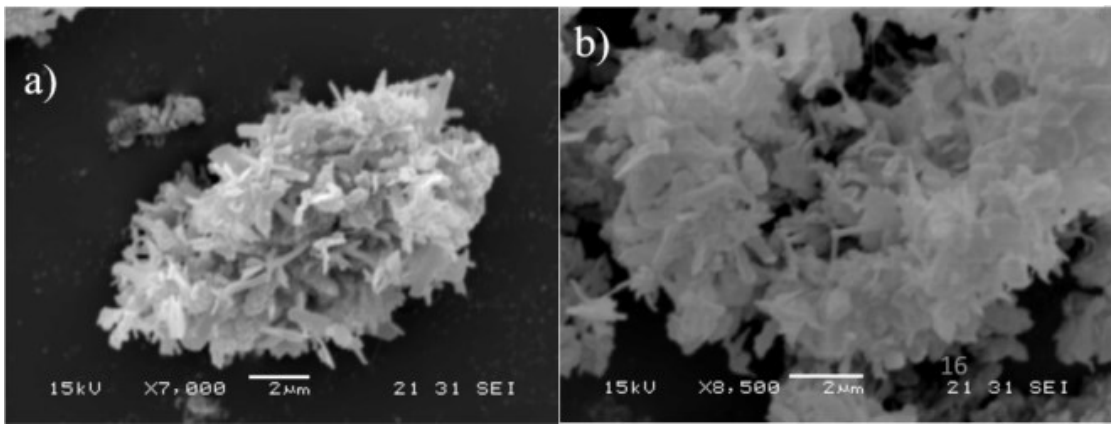

Figure 4-17 Scanning electron microscope of H-ZSM-5(24) after operating 6 hours in supercritical water at temperature a) 400 ºC b) 450 ºC

4.1.4.2 H-ZSM-5(40)

Unlike H-ZSM-5(24) which temperature has strongly affected on the intensity of XRD and crystallinity. H-ZSM-5(40) has lower affected on the increasing temperature. At

temperature 450 ºC, the remaining crystallinity of H-ZSM-5(40) decreased to 81.0 % (comparing with 85.6 at temperature 400 ºC). In detail, the XRD intensities of H-ZSM-5(40) at temperature 400 ºC and 450 ºC are completely matched in low angle and only one difference of intensity peak at 2θ= 23.1º corresponding to (051) lattice plane (see Figure 4-18). The destructive structures and EFAl were observed by SEM analysis in both temperature (see Figure 4-19). However, both temperatures have the identical destructive structure. According to EDX analysis, Si/Al ratio in both different temperature conditions were decreased. It means that silica was decreased from the structure which inferred desilication reaction dominated.

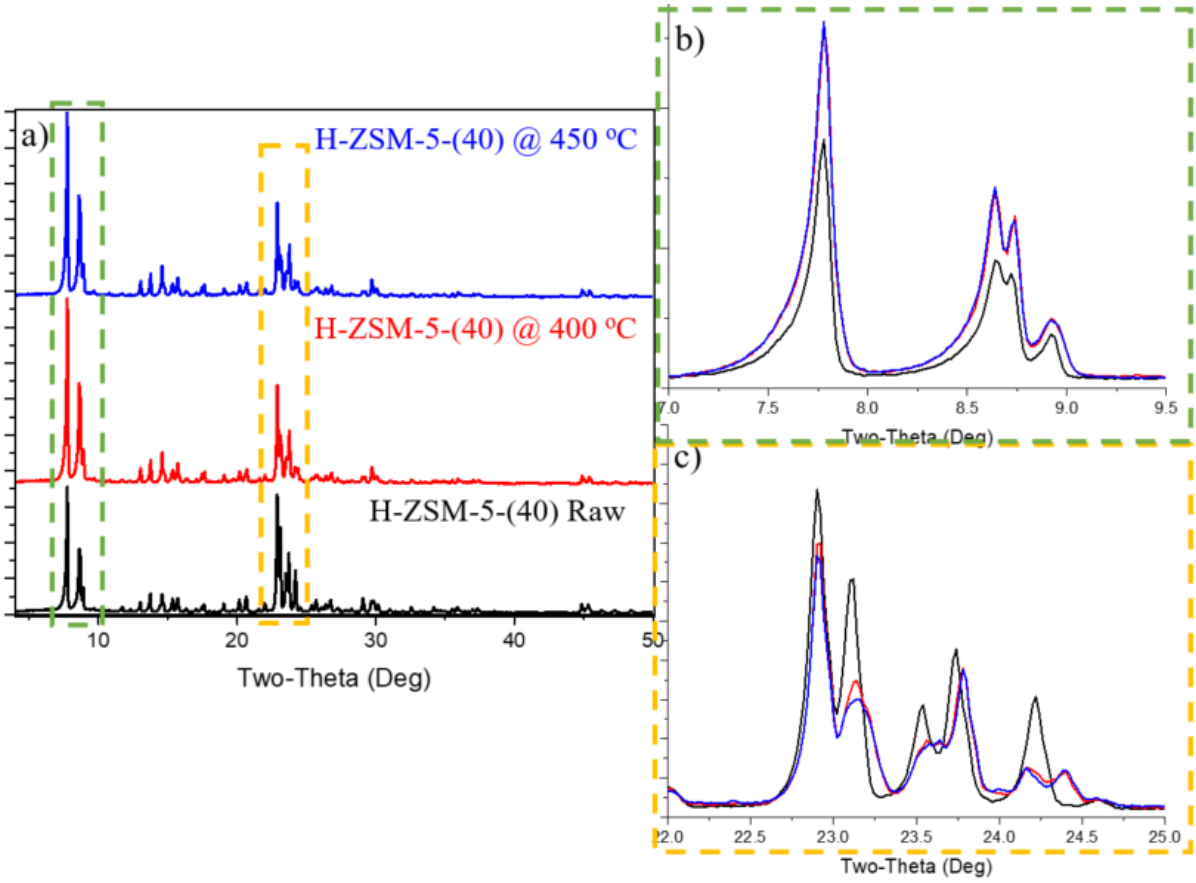

Figure 4-18 a) X-ray pattern (2θ =4º-50º) of H-ZSM-5(40) before operating in supercritical water (bottom), after operating in supercritical water at temperature 400 ºC (middle), and 450 ºC (top) b) X-ray pattern in low angles (2θ =7º-9.5º) c) X-ray pattern in middle angles (2θ =22º-25º).

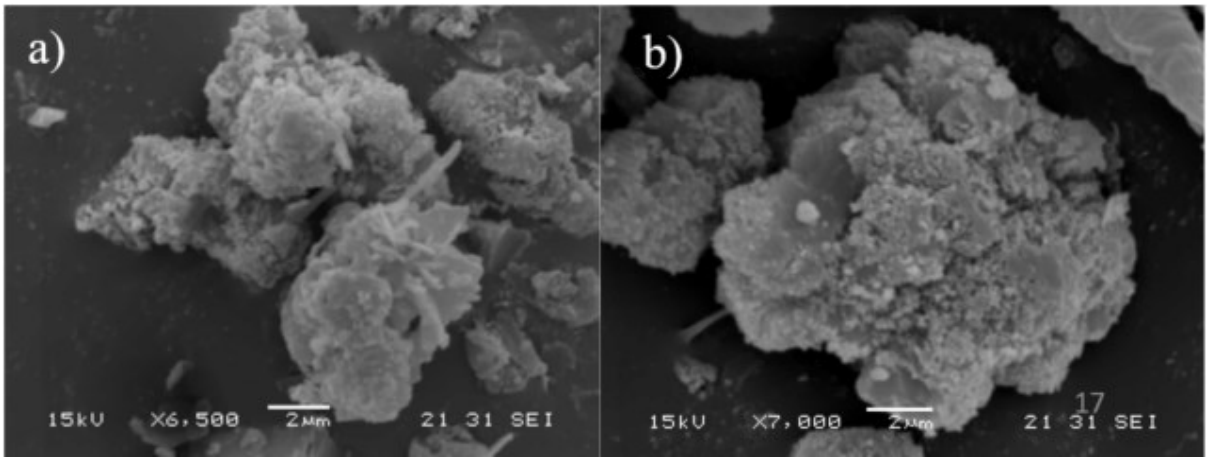

Figure 4-19 Scanning electron microscope of H-ZSM-5(40) after operating 6 hours in supercritical water at temperature a) 400 ºC b) 450 ºC

In conclusion, the investigation of destructive structure by increasing temperature in supercritical water region found that it strongly depended on the Si/Al of H-ZSM-5. In low Si/Al ratio case (H-ZSM-5(24)), the destructive structure increased shapely with temperature increasing. However, it has low affect in the case of high Si/Al ratio (H-ZSM-5(40)).

4.1.5 Effect of Si and Al solution

Since the experiments in open system (section 4.3 and 4.4) indicated that Si and Al dissolved in water in all condition without the decreasing tendency, even though XRD analysis result in all experiment still showed the high crystallinity which indicated that it has high structure stability. Si and Al solution (125 ppm, and 0.1 ppm, respectively) were used instead of pure water to prove that the destructive structure was limited by the saturation of Si and Al in close system on H-ZSM-5(24) and H-ZSM-5(1500).

4.1.5.1 H-ZSM-5(24)

H-ZSM-5(24) with Si and Al solution has the remaining crystallinity 87.7% higher than pure water which has only 60.3% as shown in XRD analysis result (see Figure 4-20). XRD pattern of H-ZSM-5(24) with Si and Al solution also did not appear of additional peak

or amorphous phase.

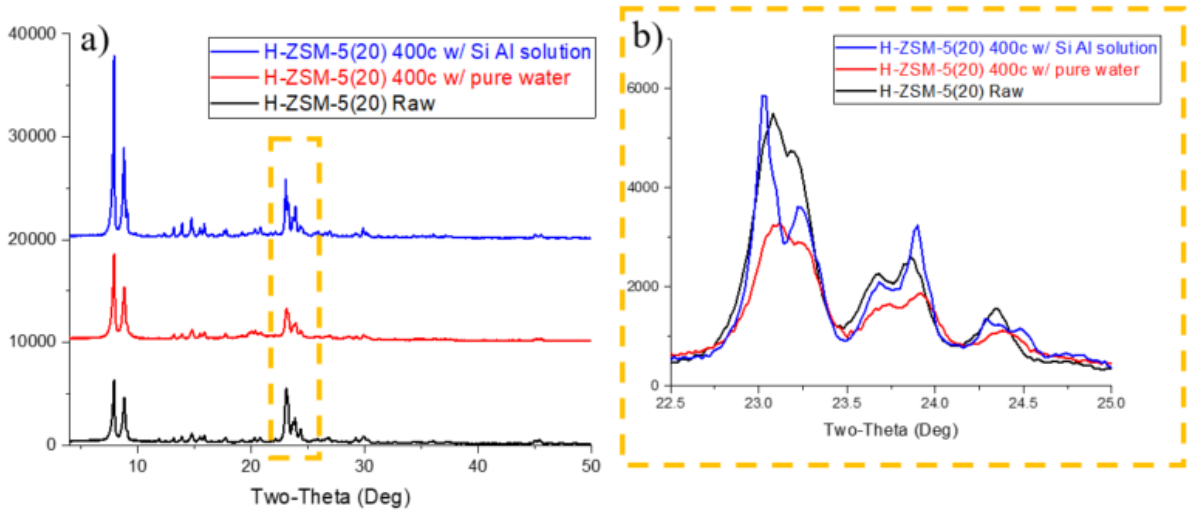

Figure 4-20 a) X-ray pattern (2θ =4°-50°) of H-ZSM-5(24) before operating in supercritical water (bottom), after operating in supercritical water at temperature 400 °C (middle), and with Si Al solution (top) b) X-ray pattern in middle angles (2θ =22°-25°).

Morphology of H-ZSM-5(24) with Si Al solution observed by SEM also show undistinguishable with before treatment with water unlike the pure water case that show sign of water and changing of crystal shape (see Figure 4-21).

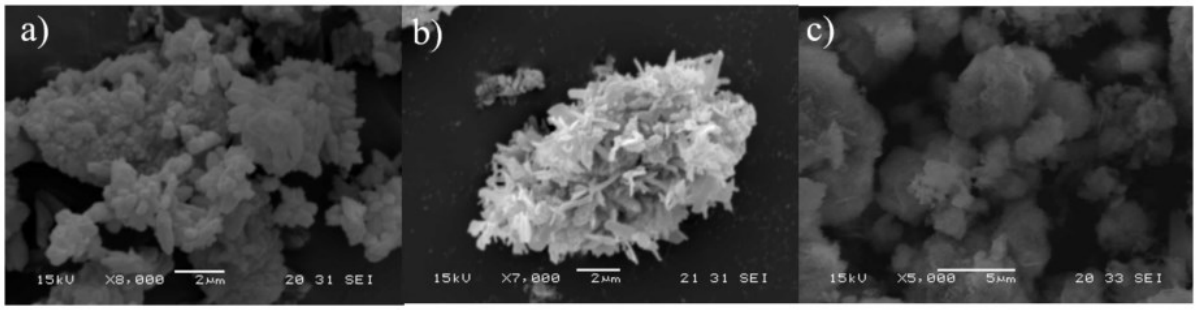

Figure 4-21 Scanning electron microscope of H-ZSM-5(24) a) before reaction b) after operating 6 hours in supercritical water at temperature 400 °C with pure water and c) with Si Al solution

4.1.5.2 H-ZSM-5(1500)

For H-ZSM-5(1500), the crystallinity of pure water and Si and Al solution are nearly identical due to usual low Al content. However, peak split from doublet to triplet in XRD pattern of middle angle (2θ = 22.5°-25°) which indicated shape of crystal change from

orthorhombic to monoclinic still also appear in case filing with Si and Al solution.

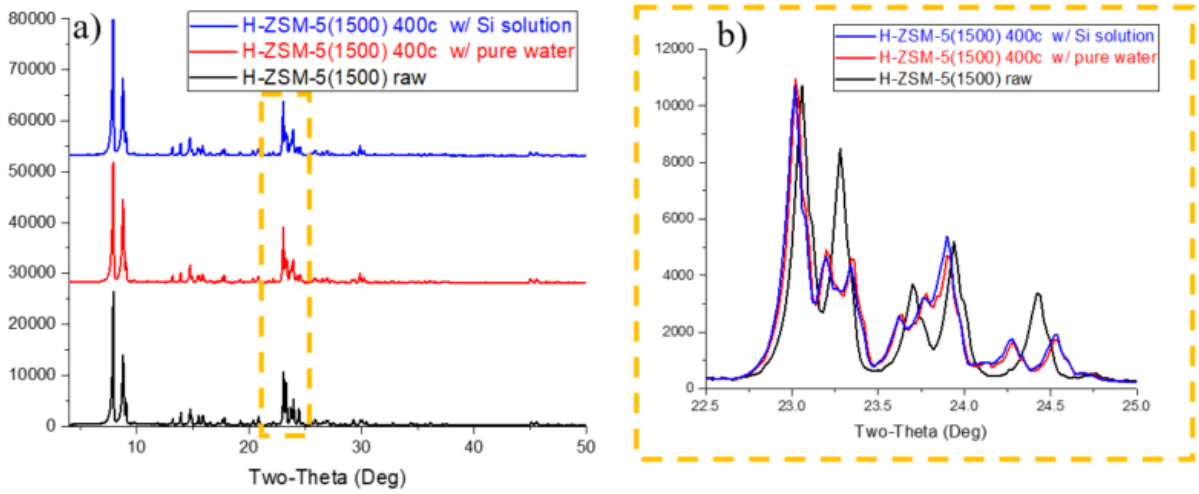

Figure 4-22 a) X-ray pattern (2θ =4°-50°) of H-ZSM-5(1500) before operating in supercritical water (bottom), after operating in supercritical water at Temperature 400 °C (middle), and with Si Al solution (top) b) X-ray pattern in middle angles (2θ =22°-25°).

Morphology of H-ZSM-5(1500) with Si Al solution observed by SEM also show undistinguishable with before and after treatment with water as shown in Figure 4-23.

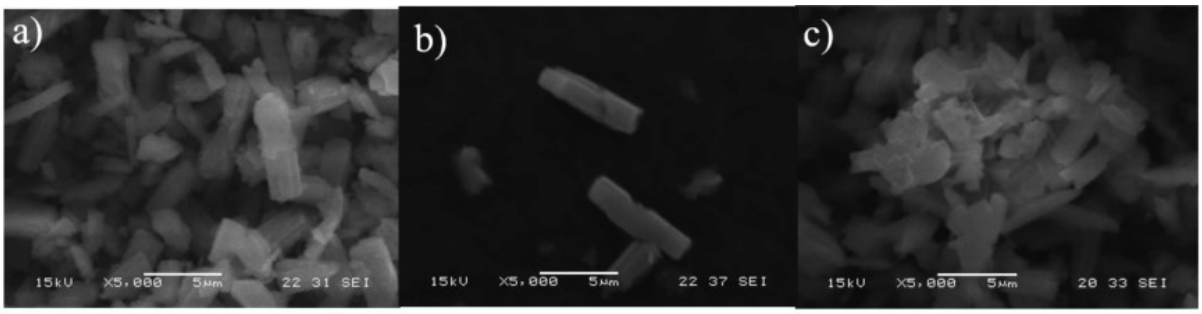

Figure 4-23 Scanning electron microscope of H-ZSM-5(1500) a) before reaction b) after operating 6 hours in supercritical water at temperature 400 °C with pure water and c) with Si Al solution

In conclusion, filling Si and Al solution instead of water can improve the stability of zeolite by water attack, which occurred staring at Al framework as dealumination to create extra alumina framework, dissociation and desilication. Pre-filling with Si and Al prevent dealumination and desilication since it already reached the equilibrium between Si Al solid framework and solution (see Figure 4-24).

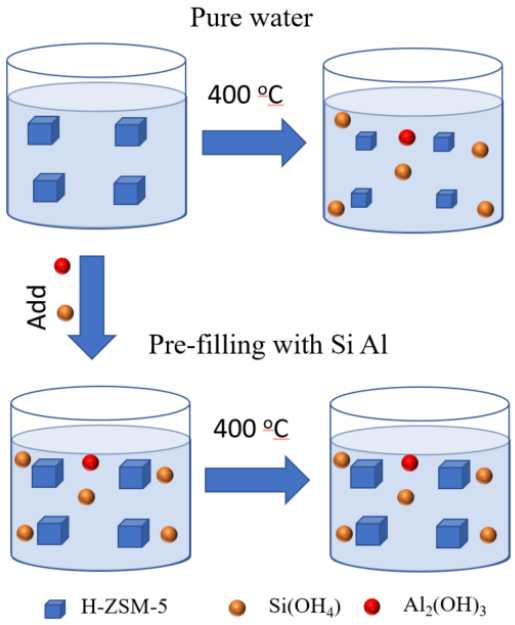

Figure 4-24 schematic diagram of stability of zeolites in batch rector with filling with pure water and Si Al solution

Crystallinity, Si/Al ratio detected by SEM-EDX, amorphous phase determined by XRD, and changing of morphology investigated by SEM are summarized in Table 4-1. In conclusion from study stability of zeolite in supercritical water, H-ZSM-5 framework maintain their framework. However, β-zeolite cannot maintain their structure in high pressure and temperature. It was corrupted and change to amorphous. Even though H-ZSM-5 framework maintain the major framework in this condition, it was distorted by water attack, and the degree of water attack was related with the disassociation of water.

Table 4-1 summarize various evaluating parameters of stability of zeolites in supercritical water

Samples	Time (h)	Temperature (°C)	Pressure (MPa)	Crystallinity (%)	SiO_2/Al_2O_3 (EDX)	Amorphous phase (Y/N)	Morphology change (Y/N)
β- zeolite	1	400	24.13	0.0	42	Y	N
H-ZSM-5(24)	1	400	24.13	72.6	21.4	N	Y
H-ZSM-5(24)	1	400	26.85	71.4	18.5	N	Y
H-ZSM-5(24)	6	400	24.13	60.3	20.7	Y	Y
H-ZSM-5(24)	6	450	30.6	34.5	20.1	Y	Y
H-ZSM-5(24) w/ Si Al	6	400	24.13	87.7	22.1	N	N
H-ZSM-5(40)	1	400	24.13	93.0	36.6	N	Y
H-ZSM-5(40)	1	400	26.85	87.5	39.6	N	Y
H-ZSM-5(40)	6	400	24.13	85.6	24.8	N	Y
H-ZSM-5(40)	6	450	30.6	81.0	35.7	N	Y
H-ZSM-5(1500)	6	400	24.13	104.3	-	N	N
H-ZSM-5(1500) w/ Si Al	6	400	24.13	106.2	-	N	N

4.2 Structure stability of zeolites in sub-water (closed system).

Structure stability of zeolites was investigated in sub-critical water at temperature 200-350 °C, saturated pressure condition for 6 hours. β-zeolite and H-ZSM-5 at various Si/Al were selected as the representative zeolite structure to investigate stability. Crystallinity, Si/Al ratio detected by SEM-EDX, amorphous phase determined by XRD, and changing of morphology investigated by SEM are summarized in Table 4-2. and the effect of temperature was separately explained on each type of zeolites and Si/Al ratio as the following.

Table 4-2 summarize various evaluating parameters of stability of zeolites in sub-critical water

Samples	Temperature (°C)	Pressure (MPa)	Crystallinity (%)	SiO_2/Al_2O_3 (EDX)	Amorphous phase (Y/N)	Morphology change (Y/N)
β- zeolite	200	1.55	82.5	40.1	N	N
H-ZSM-5(24)	200	1.55	100.3	24.3	N	N
H-ZSM-5(24)	250	3.97	102.5	25.0	N	N
H-ZSM-5(24)	300	8.59	101.1	25.5	N	N
H-ZSM-5(24)	350	16.53	93.4	24.8	N	N
H-ZSM-5(40)	200	1.55	97.4	40.2	N	N
H-ZSM-5(40)	250	3.97	97.2	40.2	N	N
H-ZSM-5(40)	300	8.59	95.0	39.2	N	N
H-ZSM-5(40)	350	16.53	99.5	46.2	N	N
H-ZSM-5(1500)	250	3.97	105.0	-	N	N
H-ZSM-5(1500)	300	8.59	105.2	-	N	N
H-ZSM-5(1500)	350	16.53	103.3	-	N	N

4.2.1 β-zeolite

Unlike operating in supercritical water, β-zeolite can maintain major structure at sub-critical water and remaining the crystallinity around 82.5% without appearing of amorphous phase in XRD pattern (see Figure 4-25). However, the intensity peak of β-zeolite was decreased in all 2θ range which is different from H-ZSM-5 that has increasing of peak intensity in low angle (2θ = 5-10°). The decreasing of intensity indicated that particle size is smaller based on Scherrer's equation (see section 3.2.3)

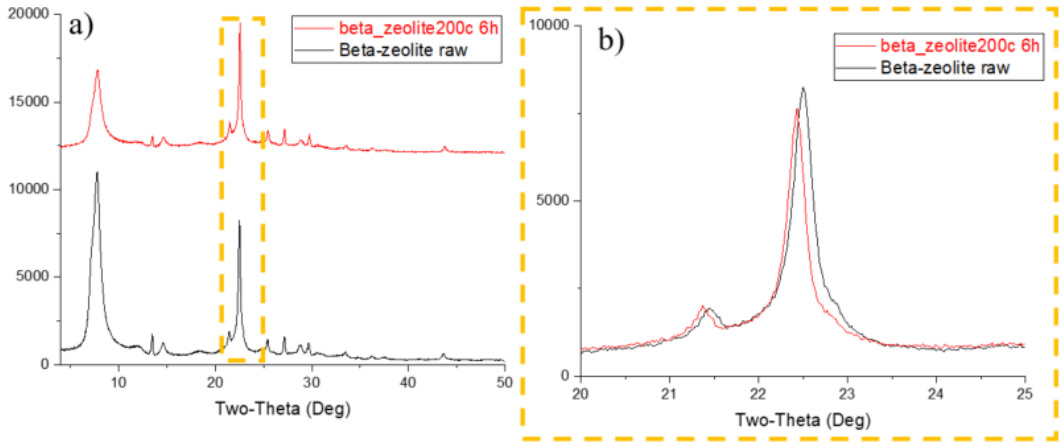

Figure 4-25 a) X-ray pattern (2θ =4°-50°) of β-zeolite before operating in sub-critical water (bottom), after operating in sub-critical water at Temperature 200 °C (top) b) X-ray pattern in middle angles (2θ =22°-25°).

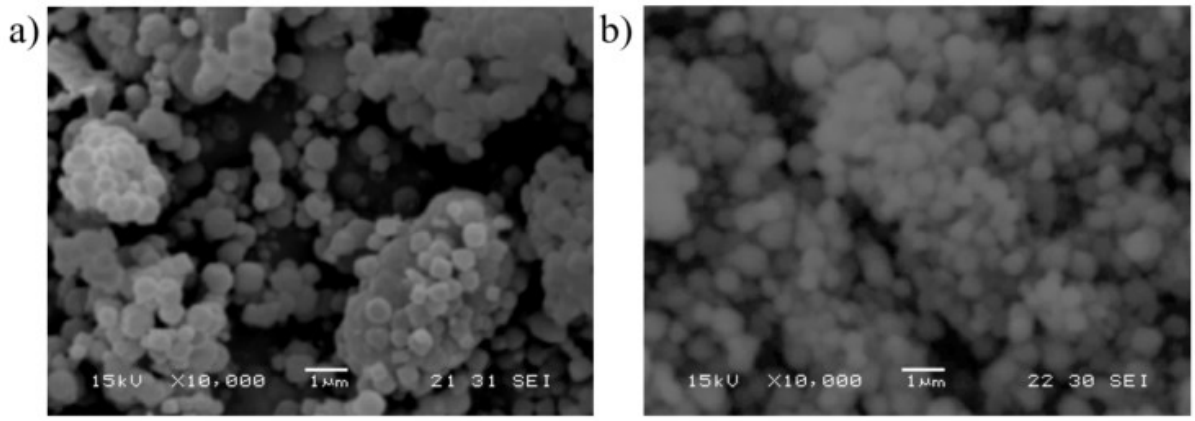

Figure 4-26 Scanning electron microscope of β-zeolite a) before reaction b) after operating 6 hours in sub-critical water at temperature 200 ºC.

Morphology observation (see Figure 4-26) found that the crystal structure remains in rectangular shape as same as before operating in sub-critical water without obvious destructive structure. However, each crystals of β-zeolite are separated to each other, which is different from the fresh β-zeolite that congregate into large particle size. The decreasing of particle size also supported by Scherrer's equation which already explained in XRD section.

Desilication on silanol defect was expected to be the reason of crystallinity decreasing. Normally, β-zeolite has the silanol defect 0.22 mmol/g which is higher than H-ZSM-5 that has 0.04 mmol/g. In the following section 4.2.2, the experiment results also support this hypothesis.

4.2.2 H-ZSM-5

In contrast with β-zeolite, H-ZSM-5 provided the remaining crystallinity nearly 100% (see Table 4-2) in all variation of Si/Al ratio framework under operating in sub-critical condition (200-350 ºC) investigated by XRD analysis (see Figure 4-27, Figure 4-29, Figure 4-31). Morphology observation by SEM analysis also support XRD results that H-ZSM-5 has high structure stability under sub-critical since SEM figures revealed clear crystal structure without the sign of water attack or distortive structure (see Figure 4-28, Figure 4-30, Figure 4-32).

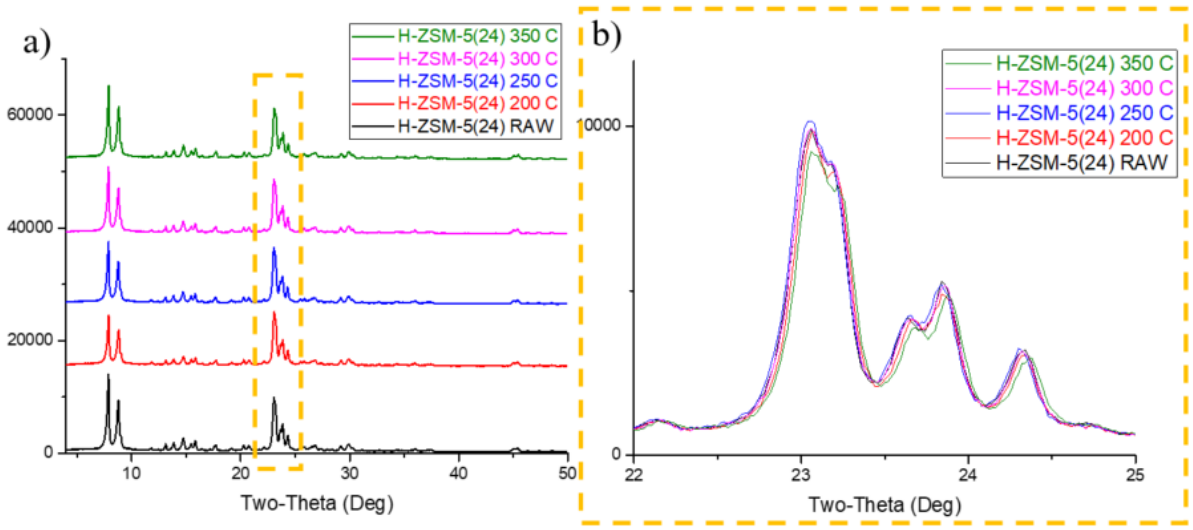

Figure 4-27 a) X-ray pattern (2θ =4º-50º) of H-ZSM-5(24) before operating in sub-critical water (bottom), and after operating in sub-critical water at various temperatures from 200-350 ºC b) X-ray pattern focus in middle angles (2θ =22º-25º).

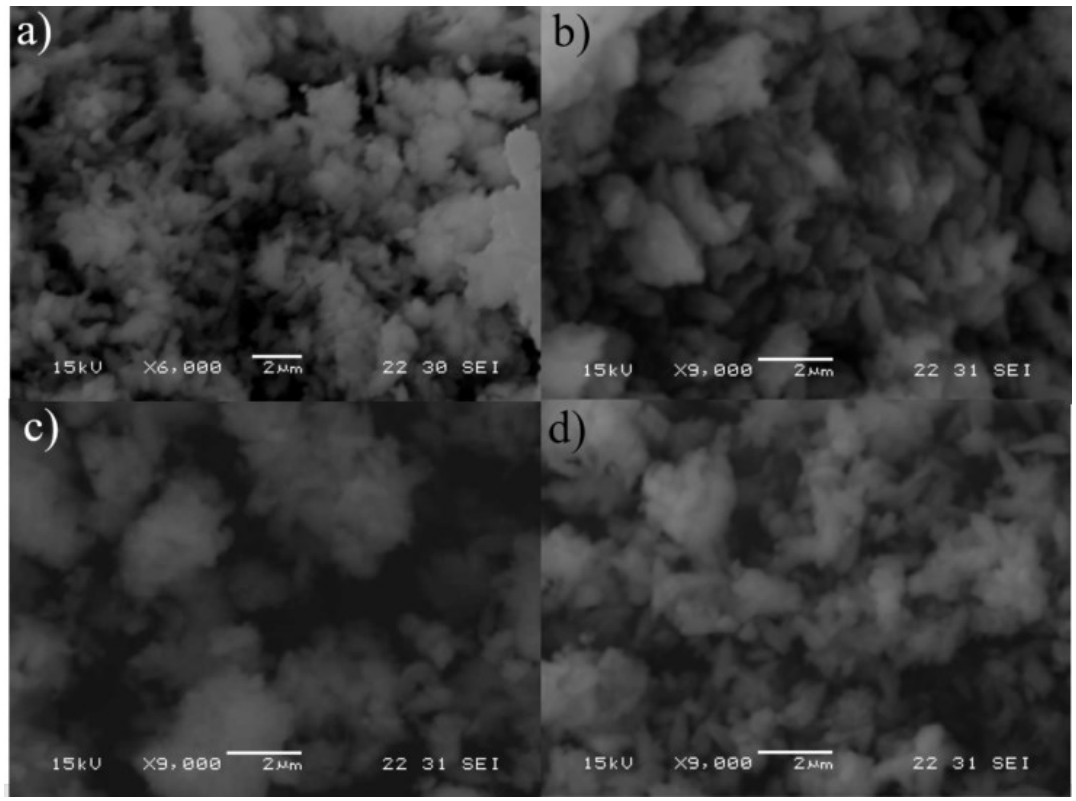

Figure 4-28 Scanning electron microscope of H-ZSM-5(24) operating 6 hours in sub-critical water at temperature a) 200 ºC, b) 250 ºC, c) 300 ºC, and d) 350 ºC

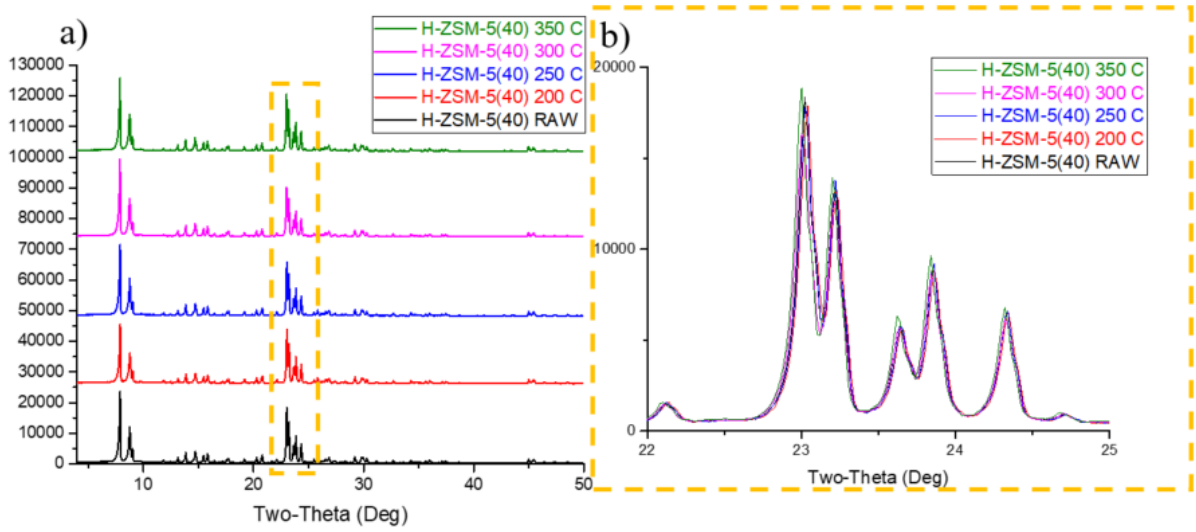

Figure 4-29 a) X-ray pattern (2θ =4º-50º) of H-ZSM-5(40) before operating in sub-critical water (bottom), and after operating in sub-critical water at various temperatures from 200-350 ºC b) X-ray pattern focus in middle angles (2θ =22º-25º).

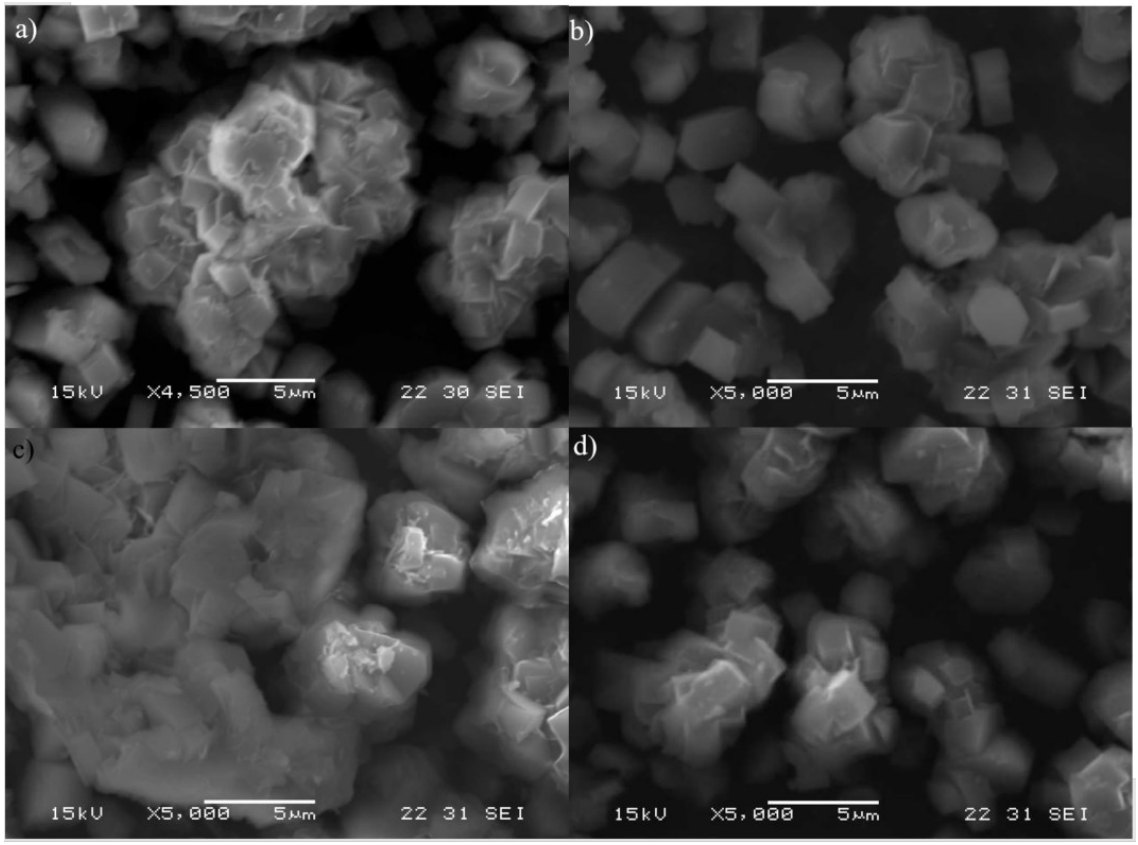

Figure 4-30 Scanning electron microscope of H-ZSM-5(40) operating 6 hours in sub-critical water at temperature a) 200 ºC, b) 250 ºC, c) 300 ºC, and d) 350 ºC

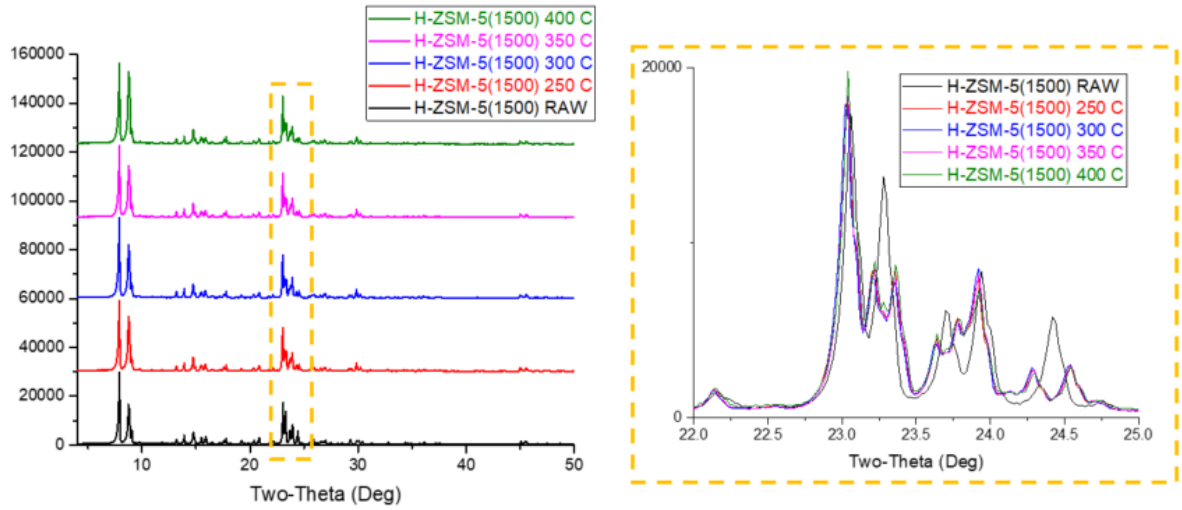

Figure 4-31 a) X-ray pattern (2θ =4º-50º) of H-ZSM-5(1500) before operating in sub-critical water (bottom), and after operating in sub-critical water at various temperatures from 200-350 ºC b) X-ray pattern focus in middle angles (2θ =22º-25º).

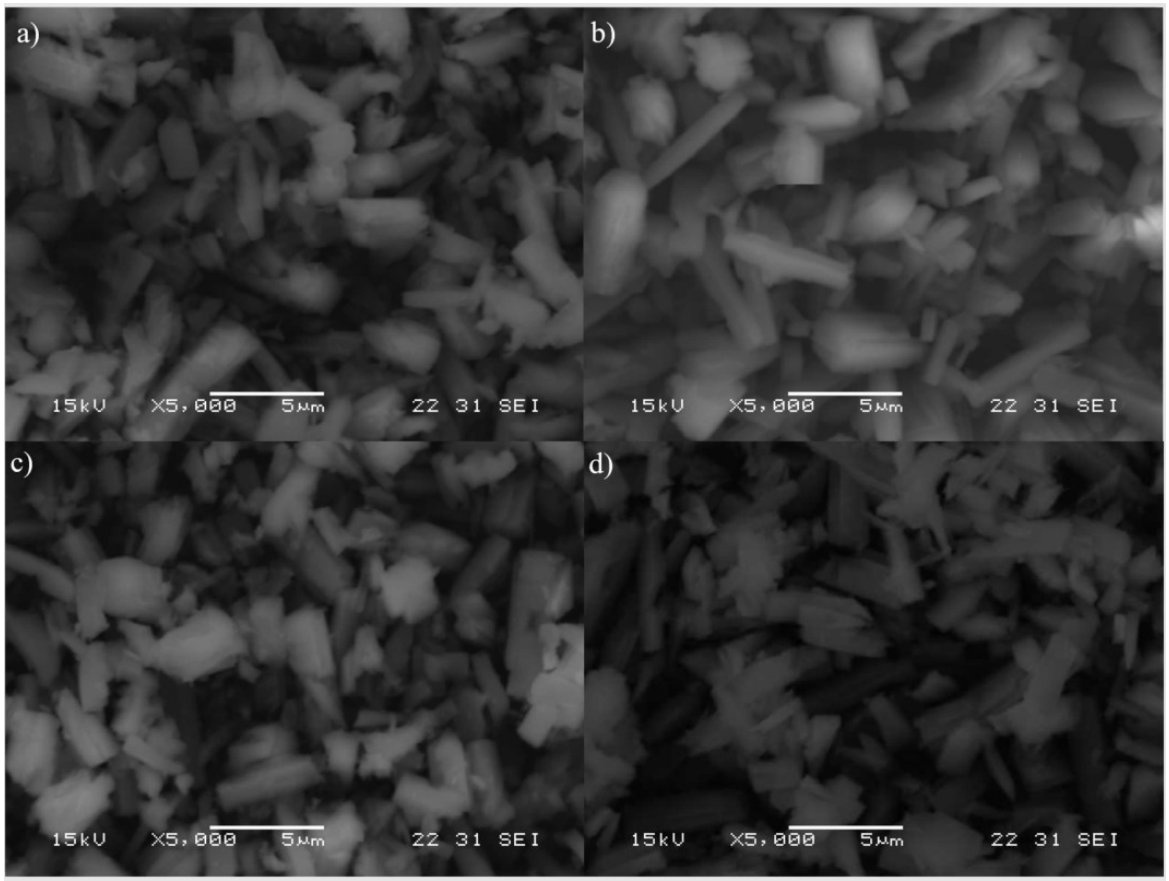

Figure 4-32 Scanning electron microscope of H-ZSM-5(1500) operating 6 hours in sub-critical water at temperature a) 250 ºC, b) 300 ºC, c) 350 ºC, and supercritical d) 400 ºC

In summary, in sub-critical water the structure stabilities are strongly affected by frameworks which related with the number of silanol defect in framework; β-zeolite has decreasing of crystallinity, unlike H-ZSM-5 that has high remaining crystallinity in all Si/Al ratio, which means that water attack on the silanol defected site. In contrast to supercritical water, since destructive structure begins with dealumination to create $Al(OH)_3$, dissociation of EFAL and desilication, Si/Al ratio is strongly affected to the stability.

4.3 Stability of zeolites in sub-critical water of cyclohexene hydration

H-ZSM-5 was selected as the representative zeolites to investigate stability in plug flow reactor (open system) due to high stability in previous batch reactor experiment (see section 4.2). Cyclohexene hydration reaction to product cyclohexanol also selected as reaction model to investigation the overall stability of H-ZSM-5 because 10- membered ring pores structure of ZSM-5 is particularly fit with the size of cyclo-ring which are cyclohexene and cyclohexanol. Which means that H-ZSM-5 should prevent side reaction such as condensation of dimer molecule (Dicyclohexyl ether) (see Figure 4-33).

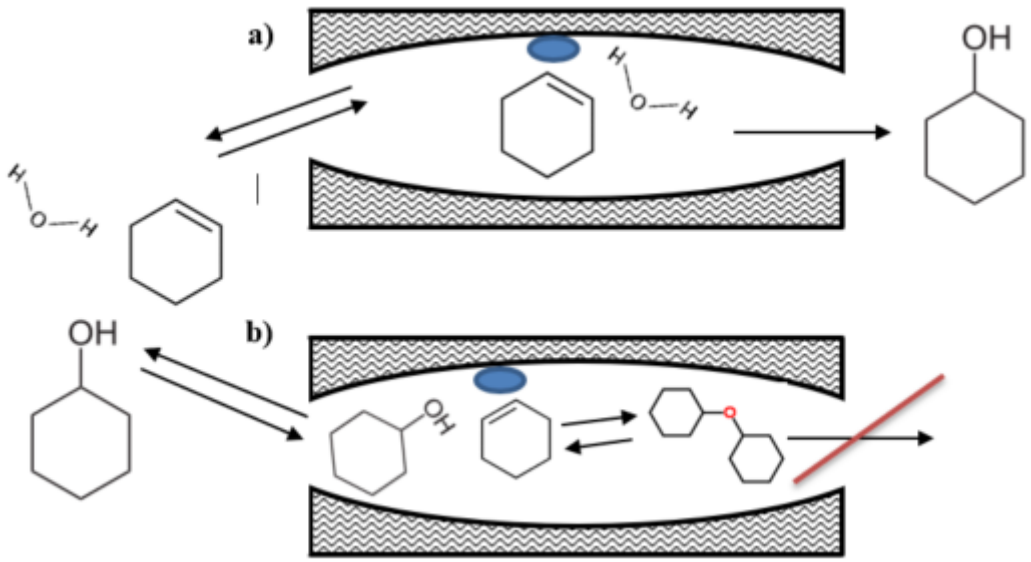

Figure 4-33 a) Main reaction: Hydration reaction of cyclohexene b) Side reaction: Condensation reaction on passing through porous structure of zeolites.

In previous study, applied H-ZSM-5 in cyclohexene hydration at temperature 120 °C was already commercialized by Asahi Kasei company as the intermediate reaction to produce Nylon-6. However, hydration of cyclohexane over zeolite achieve very low yield at 9.5% due

to the extremely low solubility of cyclohexene in water. Moreover, this reaction also suffers from very slow reaction rates; residence time 2 hours in two slurry reaction.

To overcome these problems, hydration of cyclohexene in sub-critical water which can be run in a single dense phase should eliminate the mass transfer limit between organic and water phase and accelerate reaction (see Figure 4-34). However, the overall stability of zeolites need to be investigated to make sure that it can further apply in commercial process.

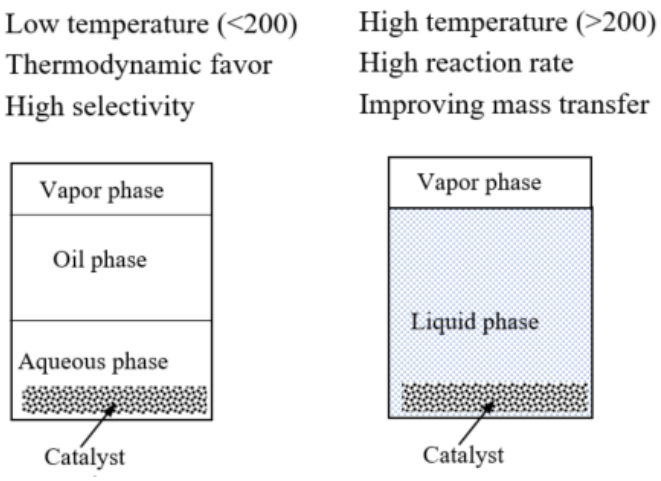

Figure 4-34 Phase systems diagram of cyclohexene hydration at low(left) and high(right) temperature

This experiment aims to investigate overall stability in open system which is different from the previous closed system (batch reactor) that the destructive structure might be limited with Si and Al solution. Moreover, it also aims to find potential to compete with current low temperature operation of cyclohexene hydration over H-ZSM-5. The investigation of activity, solubility of silica and alumina, structure of zeolites, and coking was presented as the following.

4.3.1 Activity

The activity of H-ZSM-5 with three different silica per alumina ratio (24, 40, and 1500) was investigated by GC-FID (see section 3.2.8) using methylcyclohexane as internal standard and pentane as solvent for organic phase, and external standard method for water phase since cyclohexanol product can be dissolved in water phase. Yield of reaction was calculated by %wt. of cyclohexanol production in the sample including organic and water phase. Selectivity in organic phase was calculated by % mol of cyclohexanol divided by the summation of % mole cyclohexanol and % mole methyl cyclopentane because there are only three major detected peaks in product, which are cyclohexene as reactant, cyclohexanol as

primary product, and methyl cyclopentane as by-product. For selectivity to cyclohexanol in water phase, the area normalization method was selected as the roughly estimation method because the peak of cyclohexanol is relatively larger than the other impurity peaks. Moreover, the main objective of this study is the comparison of conversion and selectivity changing over the time.

According to GC-FID analysis results as shown in Figure 4-35, pellet H-ZSM-5 (1500) retained constant cyclohexanol yield at 7% within 4.5 hours operation. However, in pellet H-ZSM-5 (24) and (40), the yield of cyclohexanol decreased from 10% to 7.5% and 7% to 4%, respectively. Methyl cyclopentane which is the major by product from this reaction was found in Pellet H-ZSM-5 (1500) around 0.1-0.15% higher than Pellet H-ZSM-5 (40) around 0.02-0.07%. Pellet H-ZSM-5 (40) and (1500) provided high selectivity and consistency with cyclohexanol product in all collected samples indicated that these zeolites still maintain the porous structure corresponding to the analysis results discuss in section 4.2.2. In case Pellet H-ZSM-5 (24), Methyl cyclopentane was found at the beginning due to heating problem that cannot increase the temperature to reach 200 ºC with 0.5 hour, however, Methyl cyclopentane was decreased over time and remain around 2% at time on stream (TOS) 2.5 hours.

The reaction mechanism of cyclohexene hydration in sub-critical water was presented in Figure 4-36. The reaction mechanism starts with cyclohexene bonding with the acid site to form secondary cyclohexyl carbocation which is consider as unstable compound. After that it will react with the water to form cyclohexanol. However, secondary cyclohexyl carbocation does not immediately react with water. It should quickly rearrange to the tertiary methyl cyclopentyl carbocation, which is much more stable, and then react with water to form methyl cyclopentane. Tertiary methyl cyclopentyl carbocation also consider as the precursor for deactivation of zeolite by coking process in the case that it does not react with water because it could react with cyclohexanol or cyclohexene and create polycyclic hydrocarbons.

The main deactivation reason of Pellet H-ZSM-5 (24) and (40) was expected to be coking on the active site. The TGA analysis in section 4.3.4 also support this hypothesis. The relationship between coking and SiO_2/Al_2O_3 ratio depends on hydrophilic and hydrophobic properties. Hydrophilic zeolites, H-ZSM-5(1500), should prevent the polymerization reactions by surrounding water.

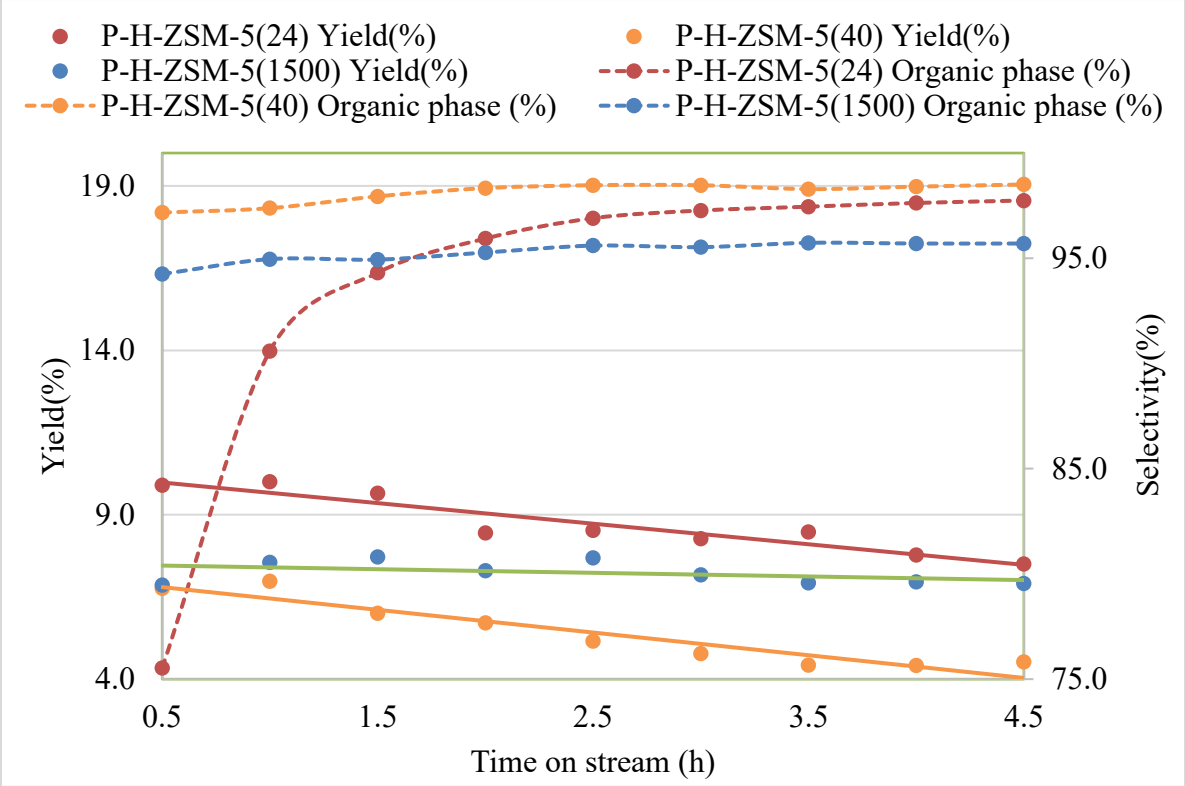

Figure 4-35 Yield and selectivity of cyclohexanol product over cyclohexene hydration at 200 °C, P= 25 MPa, with pellet H-ZSM-5 Si/Al ratio 24, 40, 1500

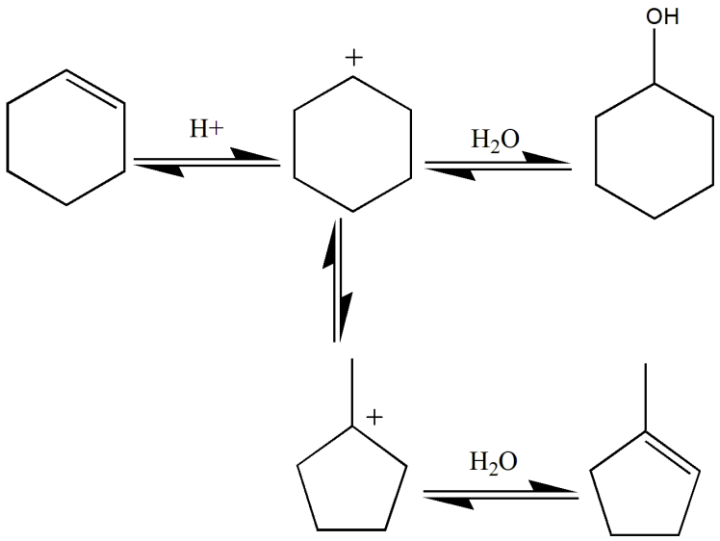

Figure 4-36 Proposed reaction mechanism of cyclohexene hydration in sub-critical water

4.3.2 Solubility of Silica and Alumina

According to ICP-AES analysis (see Figure 4-37), all pellet H-ZSM-5 (Si/Al ratio =24,40, 1500) had silica and alumina dissolving in the effluent samples. Pellet H-ZSM-5 (24)

had the highest Si dissolving at 290 ppm at the first collected sample at 0.5 hour. After that, the solubility of Si slowly decreased at constant rate around -16 ppm/hour. Unlike pellet H-ZSM-5 (24), pellet H-ZSM-5 (40) and (1500) had lower silica dissolving at 120, and 140 ppm, respectively. The result also supported the hypothesis that destructive structure begun with alumina in the framework to generate extra alumina framework (EFAl). After that, EFAl dissociated with water and left the defect structure which created the vulnerable point for destructive structure by desilication reaction. This reaction generated $Si(OH)_4$ to dissolve in water. As a result, high dissolving Si was detected by ICP-AES.

For alumina, it was detected in all samples. Pellet H-ZSM-5 (24) and (40) were detected dissolving Al around 1ppm with slightly increasing in tendency. However, pellet H-ZSM-5 (1500) had the dissolving Al lower at 0.5 ppm with slightly deceasing in tendency. The lower Al dissolving in water was explained by reformation of Al in zeolites framework detected by XRD result (see section).

The calculation of accumulation of Si and Al was summarized in Table 4-3. Accumulated % Si and Al loss in Pellet H-ZSM-5 (24), (40) and (1500) are 23.66, 14.63, and 11.29 ppm over 4.5 hours operation.

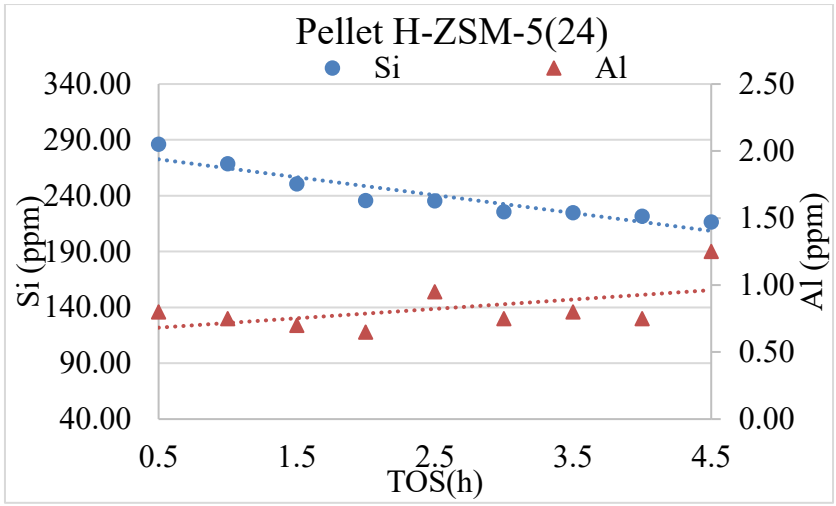

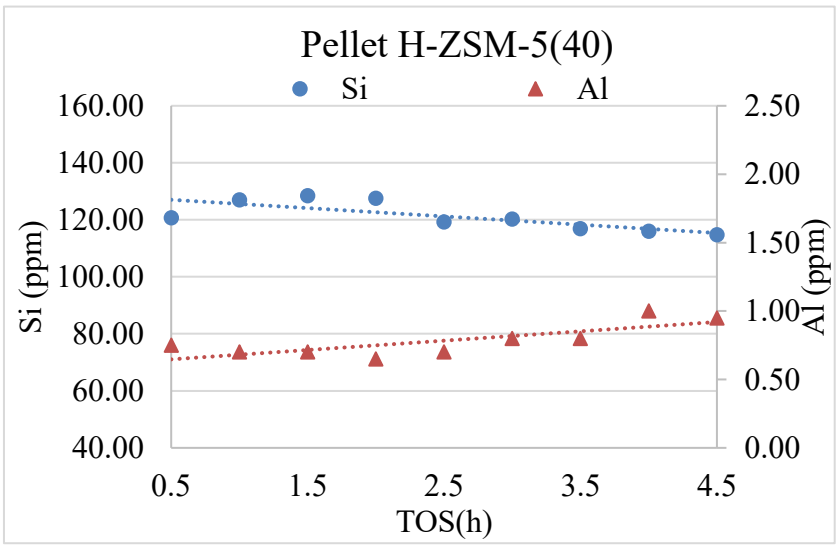

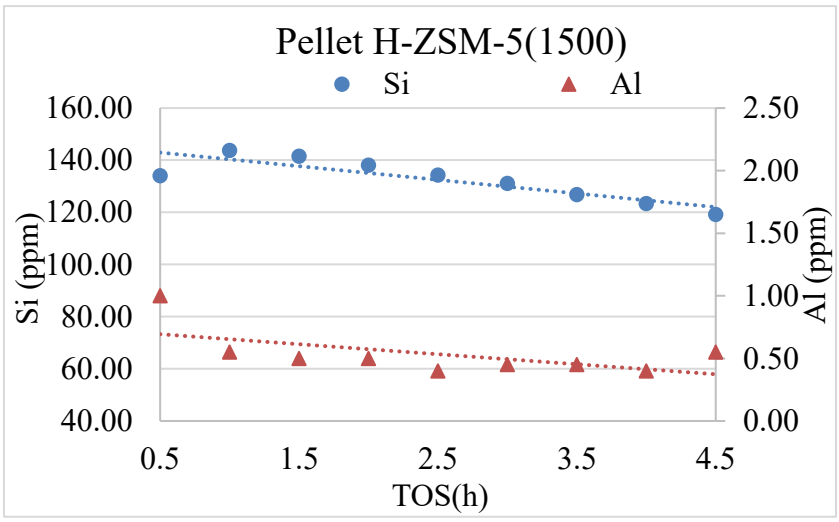

Figure 4-37 Silica and alumina dissolved in the effluence detected by ICP-AES analysis on pellet H-ZSM-5 with Si/Al ratio = 24 (top), 40 (middle), and 1500 (bottom)

Table 4-3 Accumulated % Si and Al weight lost over the time in P-H-ZSM-5(24), (40), and (1500)

Time(h)	P-H-ZSM-5(24)		P-H-ZSM-5(40)		P-H-ZSM-5(1500)	
	Accumulate Si loss (%wt.)	Accumulate Al loss (%wt.)	Accumulate Si loss (%wt.)	Accumulate Al loss (%wt.)	Accumulate Si loss (%wt.)	Accumulate Al loss (%wt.)
0.5	-3.13	-0.02	-1.62	-0.02	-1.27	-0.04
1	-6.06	-0.04	-3.32	-0.04	-2.63	-0.06
1.5	-8.80	-0.06	-5.04	-0.05	-3.97	-0.08
2	-11.38	-0.08	-6.75	-0.07	-5.28	-0.10
2.5	-13.95	-0.10	-8.35	-0.09	-6.55	-0.11
3	-16.41	-0.12	-9.97	-0.11	-7.79	-0.13
3.5	-18.87	-0.14	-11.53	-0.13	-8.99	-0.15
4	-21.29	-0.16	-13.09	-0.15	-10.16	-0.16
4.5	-23.66	-0.19	-14.63	-0.17	-11.29	-0.19

The solubility of Si and Al in P-H-ZSM-5(1500) were further investigated in pure water in plug flow reactor at various temperature from 200 - 400 °C (see Figure 4-38). It found that the solubility of Si and Al are correspond to the disassociation of water (K_w) (see Figure 2-2). At high temperature, the solubility is higher and sharply drop at supercritical water.

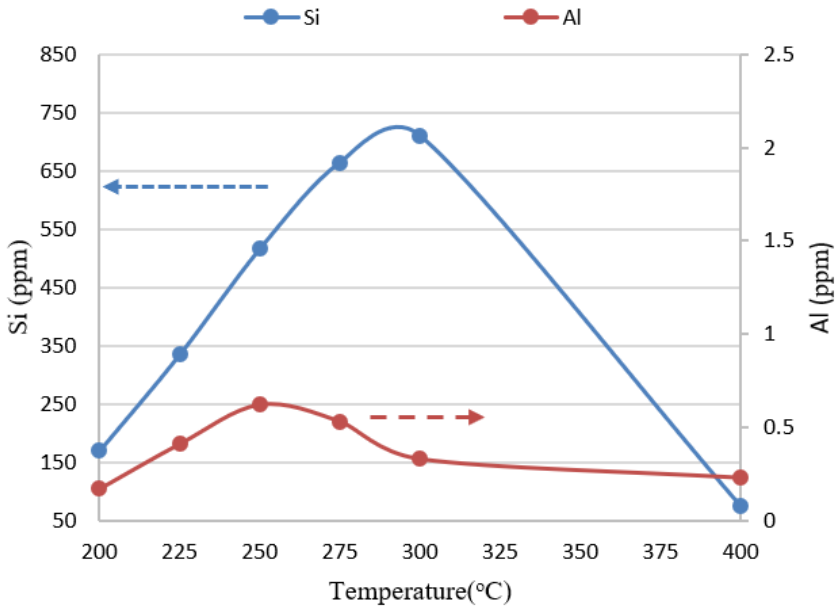

Figure 4-38 Solubility of Si and Al in Pellet H-ZSM-5-(1500) operating in plug flow reactor at various temperatures.

4.3.3 Structure of zeolites

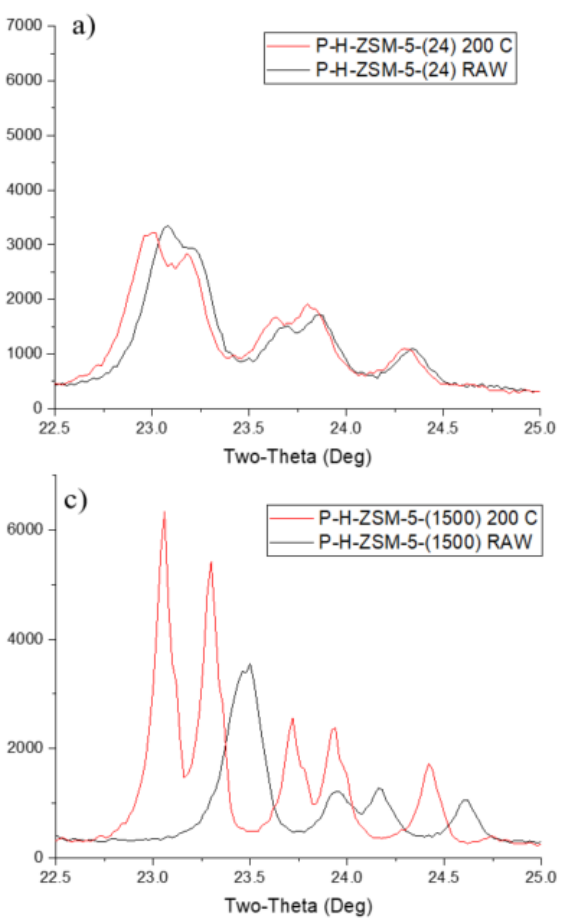

d)

Zeolite	Area (2θ=22.5-25.0)	% Crystallinity
P-H-ZSM-5-(24) RAW	1906.44	
P-H-ZSM-5-(24) 200 C	1994.76	104.63
P-H-ZSM-5-(40) RAW	2423.24	
P-H-ZSM-5-(40) 200 C	2369.89	97.80
P-H-ZSM-5-(1500) RAW	1259.86	
P-H-ZSM-5-(1500) 200 C	2274.43	180.53

Figure 4-39 X-ray diffraction pattern of pellet zeolites (P-H-ZSM-5) with various silica per alumina ratio a) 24 b) 40 c) 1500 d) Area and crystallinity of pellet zeolites (P-H-ZSM-5)

According to XRD analysis results (see Figure 4-39), %Crystallinity in zeolites with Si/Al ratio 20 and 1500 were increased but it decreased in ZSM-5 with Si/Al ratio 40. The result of increasing area caused by the spilt and shift peak effect to lower 2θ. This result indicated that bond length on each crystal of zeolites are increased base on Bragg diffraction equation (Equation 3) (detail of parameter definitions presented in section 3.2.3) due to the substitute reaction of Si with Al, since Si-O has average bond length at 1.64 Å which is lower than average bond length of Al-O at 1.75 Å. During operating in sub-critical water attack the surface of zeolites and remove Al from the framework. However, since pellet zeolites was mixed with alumina binder. The excess alumina re-incorporated with zeolites structure and maintain the zeolites structure as you can see by

the intensity of XRD analysis remain the same as fresh zeolites. The increasing of bond length in atom structure caused the angle of x-ray deceasing base on Bragg equation since n and λ are constant ($n\lambda = 2d \sin\theta$; ↑d -> sinθ↓ -> θ↓)(see Figure 4-40).

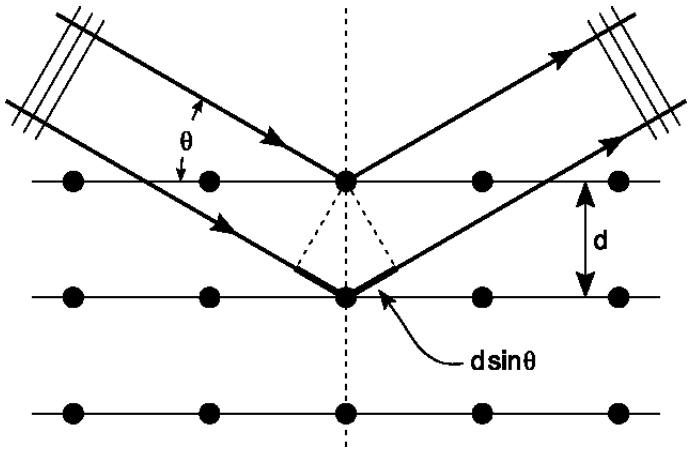

Figure 4-40 Bragg diffraction with two beams with identical wavelength and phase approach a crystalline solid take from Wikipedia under free license agreement.

4.3.4 Coking and surface area (BET)

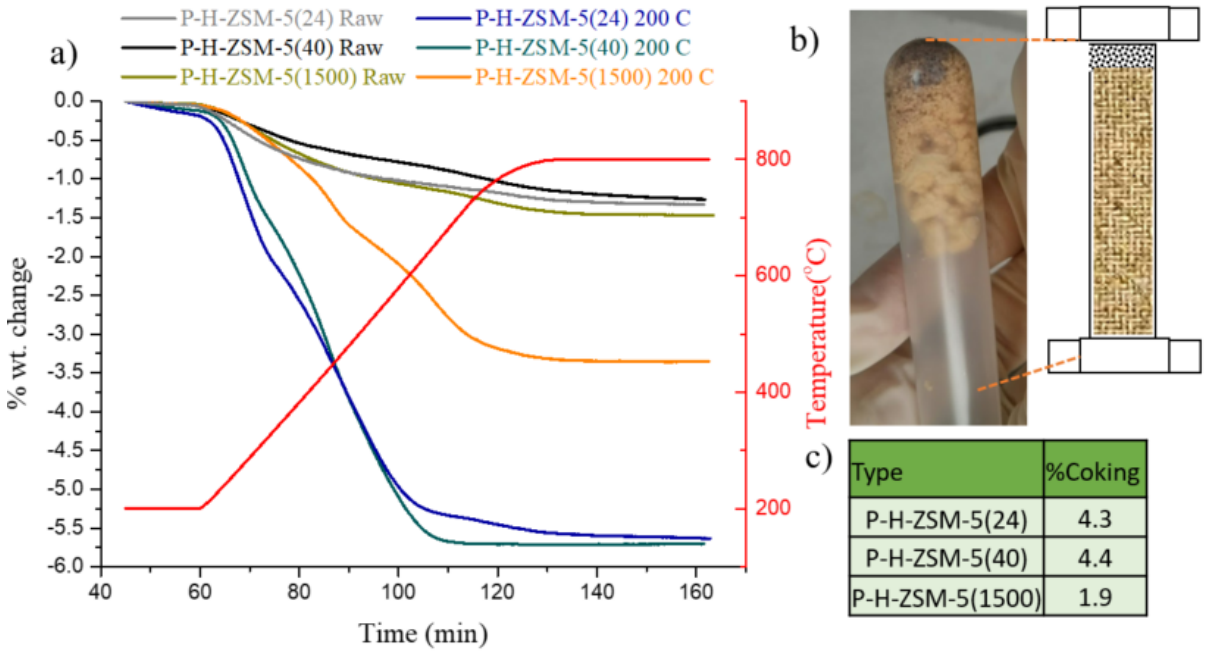

Figure 4-41 a) TGA analysis result on pellet H-ZSM-5 with three Si/Al ratio 24, 40, 1500 before and after reaction at 200 ºC b) Actual photograph of zeolites sample c) % coking on pellet zeolites calculated by the difference of %weight loss before and after reaction.

According to TGA analysis (see Figure 4-41), the coke lay down on pellet H-ZSM-5(1500) was lower than others at 1.9 %wt., whereas pellet H-ZSM-5(24) and (40) had coke lay down about 4.3, and 4.4 %wt., respectively. The relationship between coking and SiO_2/Al_2O_3 ratio depends on hydrophilic and hydrophobic properties. Hydrophilic zeolites, H-ZSM-5(1500), should prevent the polymerization reactions by surrounding water (see Figure 4-42). The appearance of coking was obviously changed by turn to dark pellet observed at the beginning section of reactor (see Figure 4-41b). The coking result also supported the hypothesis that coking is the reason of deceasing of activity in H-ZSM-5(24) and (40) but it did not present in H-ZSM-5(1500) (see section 4.3.1).

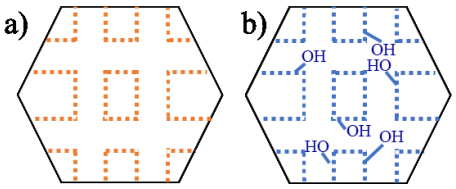

Figure 4-42 Schematic zeolite crystals at internal pore surfaces with a) hydrophobic b) hydrophilic

BET analysis results (see Table 4-4) found that H-ZSM-5(24) and (40) had both deceasing of BET results after operating in sub-critical water. The surface area of H-ZSM-5(24) and (40) decrease around 9.75%, and 9.52% comparing with the fresh zeolites. The deceasing of BET can be explained by coking deposited on the active site of zeolites and blocking N_2 to adsorb on the surface. For P-H-ZSM-5(1500), it had the astonishing results that surface area was increased to 9.4%, which was different from the others, but this result corresponded with XRD pattern changing due to Alumina re-incorporate in framework (see section 4.3.3), and low deposited coking due to hydrophilic property. Normally, Alumina atoms are the source negative change in framework and be consider as the active site that N_2 can be adopted cause the increasing of surface area detected by BET method.

Table 4-4 BET, % crystallinity, and Coking of cyclohexene hydration reaction at 200 ºC

Type	BET (m2/g)			% Crystallinity**	%Coking
	Raw material	After reaction	Change%		
P-H-ZSM-5(20)	316.83	285.95	-9.75	104.63	-
P-H-ZSM-5(40)	341.67	309.15	-9.52	97.80	4.8
P-H-ZSM-5(1500)	286.59	313.52	9.40	180.53	1.5

4.3.5 Morphology

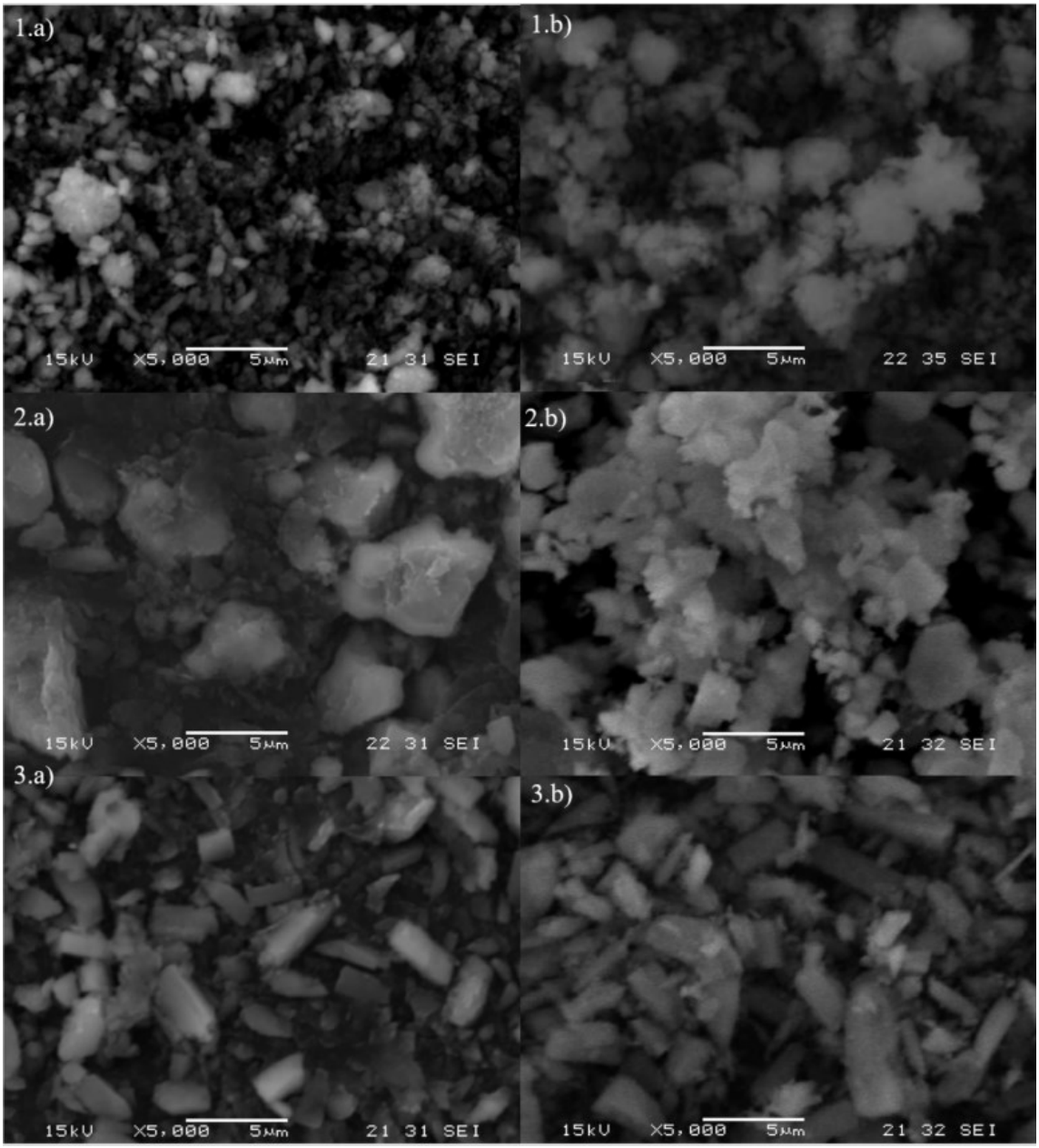

Figure 4-43 Scanning electron microscope of pellet H-ZSM-5 with 1) Si/Al ratio =24, 2) Si/Al ratio =40, and 3) Si/Al ratio 1500 observing at a) before, and b) after cyclohexene hydration at 200 °C

The morphology of all pellet zeolites comparing between before and after reaction as shown in Figure 4-43 are insignificantly different. All SEM result after operating in sub-critical water did not show sign of water attack corresponded to previous study of structure stability of zeolite in section 4.2.2.

In summary, the relationship between coking and SiO_2/Al_2O_3 ratio depended on hydrophilic and hydrophobic properties of zeolites. Hydrophilic zeolites, P-H-ZSM-5(1500), should prevent the polymerization reactions by surrounding water. However, desilication was detected in both residue of both zeolites which may lead to structure collapse in the case that a longer operation.

4.4 Stability of zeolites in supercritical water of cyclohexanol dehydration

To eliminate coke formation which occurred extremely high in preliminary experiment at the same condition with sub-critical water, only 3%wt. of cyclohexanol in water solution mixed with pre-heating water at feed ratio (organic/water) = 10:1. In preliminary experiment without catalyst (see Figure 4-44), cyclohexanol hydration had the conversion relatively low around 1-2 %, and dicyclohexylether also found in product identified by GC-MS. Dicyclohexylether was known as the side reaction from condensation reaction, and porous structure of H-ZSM-5 should prevent this by-product. In this experiment, effect of different Si/Al ratio on pellet H-ZSM-5(40) and (1500) and effect of weight hourly space velocity (WHSV) of catalyst at value 100, 300, and 1500 h^{-1}. WHSV was defined as mass flow rate (g/h) of the reactants divided by the mass of catalyst (g) in the reactor.

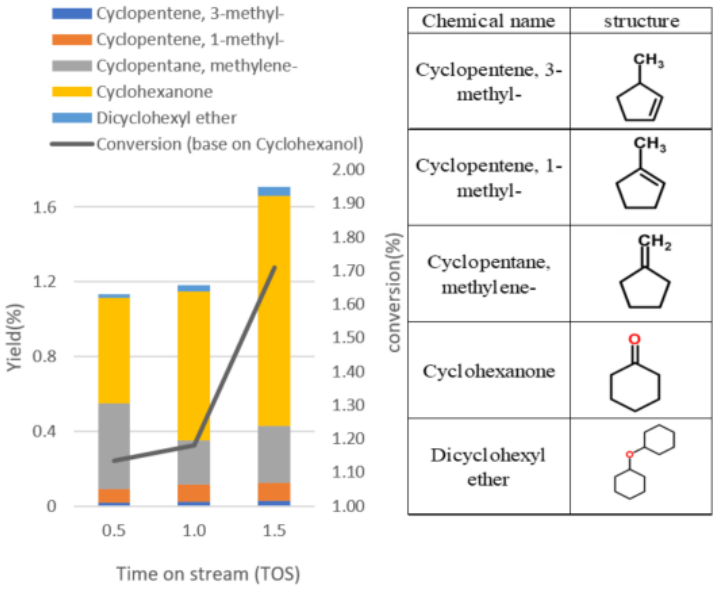

Figure 4-44 GC results of Cyclohexanol dehydration at 400 °C, P= 25 MPa without zeolite

4.4.1 Effect of different Si/Al ratio

Pellet H-ZSM-5(40) and (1500) was filled in plug flow reactor operating in supercritical condition at temperature 400 ºC with WHSV 100 h^{-1}. The qualitative and quantitative analysis on the chemical compound in product was detect by GC-MS and GC-FID, respectively. The detected chemical structure compound by qualitative method was shown in Table 4-5. For quantitative analysis on sample product, both zeolites provided the high conversion close to 100%, and highly stable over 5 hours operation with selective to derivative methyl-cyclopentene around 85-90%. Unlike preliminary non-catalyst experiment, dicyclohexylether cannot be detected in GC-MS in both Si/Al ratio of pellet H-ZSM-5. It means that the porous structure of zeolites can prevent the large molecules such as dimer which was normally generated in general catalyst (see Figure 2-6). XRD pattern also maintained the characteristic peak of ZSM-5 with split and shift to low angle (see Figure 4-46). The reason of peak split and shift already explained in section 4.3.3. Morphology observed by SEM also shown the identical result in both before and after reaction of both zeolites. However, dissolving of Si and Al in all collected sample was found without decreasing tendency (see Figure 4-47). The dissolving of Si in first collected sample was found around 75 ppm at 0.5 hours, and slowly increase to 80 ppm at the last sample collected at 5 hours. For dissolving of Al, it found to be constant at 1.2 ppm over 5 hours. Even the dissolving of Si in supercritical was lower than sub-critical water, and the activity of this reaction maintained high stability, the accumulated %weight loss of Si in the effluence is significant and need to be further investigated (see section 4.4.2). Over 5 hours operation, silica and alumina in zeolites framework was estimated to loss their weight around 7.24%, and 0.43%, respectively.

The mechanism of cyclohexanol dehydration was demonstrated in Figure 4-48. The reaction mechanism has several steps as the following. First, cyclohexanol reacted with acid site of zeolite to form oxonium ion. Second, oxonium ion perform unimolecular elimination to create secondary cyclohexyl carbocation which should be quickly rearrange to the tertiary methyl cyclopentyl carbocation that much more stable. Third, cyclopentyl carbocation loses a proton to form 1-methyl cyclopentene or migration and deprotonate to form 3-methyl cyclopentene and methylene cyclopentane. Some of cyclopentyl carbocation might react with hydroxide ion to form 1-methylcyclopentanol. Undetected cyclohexene in this reaction suggested that bimolecular elimination does not occurred in supercritical water. Moreover, the formation of carbocations becomes increasingly more favorable at higher temperature.

Table 4-5 the detected chemical compound in cyclohexanol dehydration over pellet H-ZSM-5

Chemical name	structure	Chemical name	structure
Cyclopentene, 3-methyl-		Pentanone, 3-methyl-	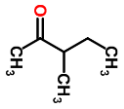
Cyclopentene, 1-methyl-		Cyclopentanol, 1-methyl-	
Cyclopentane, methylene-		Cyclopentanone, 3-methyl-	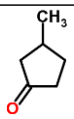
3-Pentanone, 2-methyl-	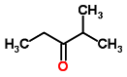	Cyclohexanone	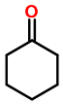

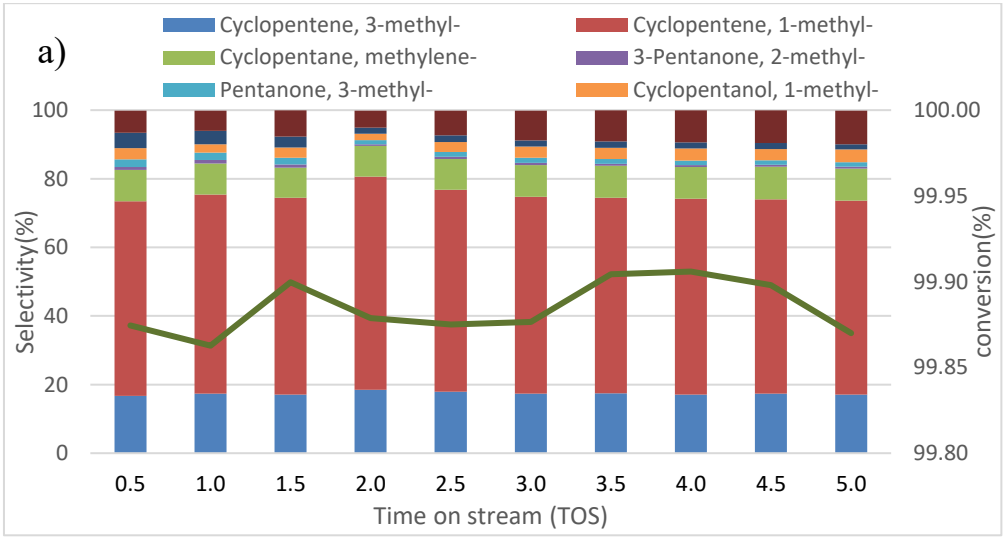

Figure 4-45 GC-FID analysis results of cyclohexanol dehydration at 400 ºC, P= 25 MPa, a) P-H-ZSM-5(1500) b) P-H-ZSM-5(40)

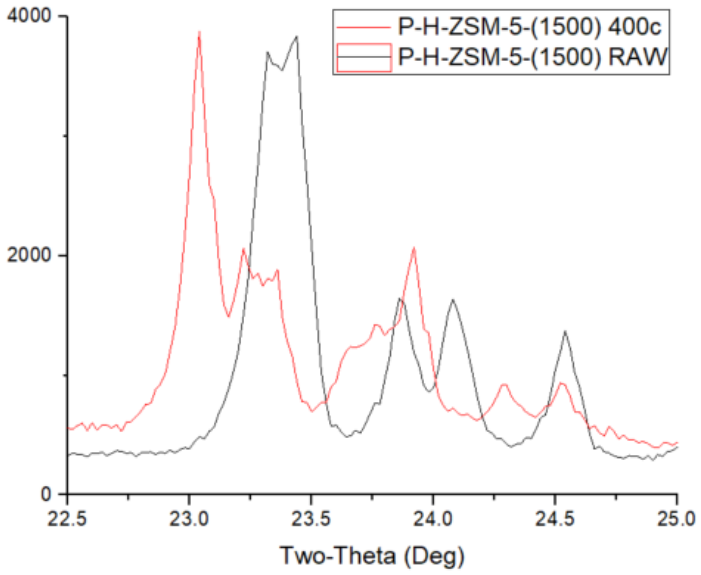

Figure 4-46 X-ray diffraction pattern of pellet zeolites (P-H-ZSM-5-1500) over cyclohexanol dehydration at temperature 400 ºC

a)

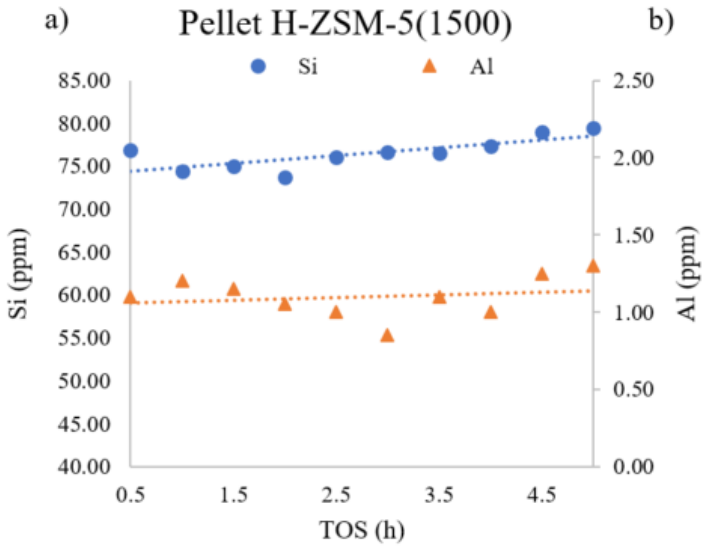

b)

Time(h)	Accumulated Si loss (%wt.)	Accumulated Al loss (%wt.)
0.5	0.73	0.04
1	1.43	0.09
1.5	2.14	0.13
2	2.84	0.17
2.5	3.56	0.21
3	4.29	0.25
3.5	5.01	0.29
4	5.74	0.33
4.5	6.49	0.38
5	7.24	0.43

Figure 4-47 a) Silica and alumina dissolved in the effluence detected by ICP-AES analysis on pellet H-ZSM-5 (1500) over cyclohexanol hydration. b) Estimation accumulated loss of Si and Al (%wt.)

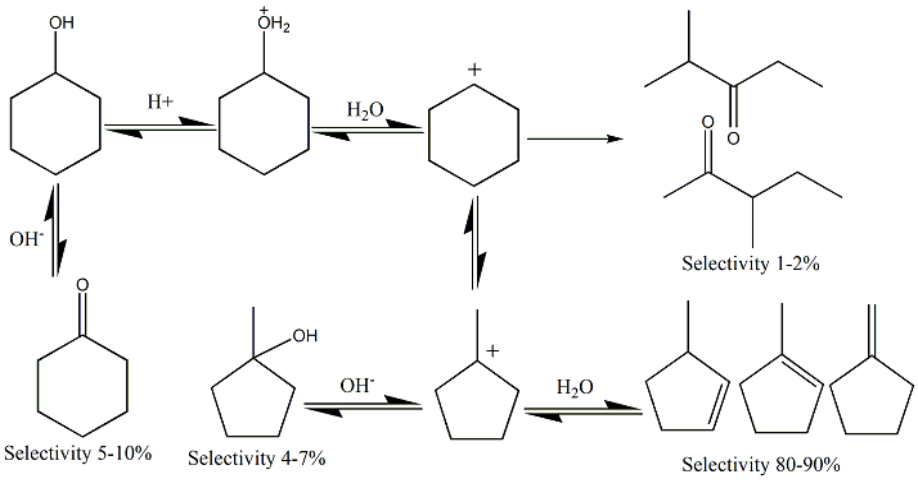

Figure 4-48 Schematic diagram of Cyclohexanol reaction mechanism with zeolite catalyst under supercritical water

4.4.2 Effect of weight hourly space velocity (WHSV)

Since the accumulated %weight loss of Si in the effluence on previous section 0 was found to be relatively high, even it provided high stability. In this chapter, observation on stability of pellet H-ZSM-5 (1500) at higher WHSV was planned to perform at 300, and 1500 h^{-1}. At this operating condition, each particle of zeolites will encounter to the water longer comparing with previous experiment (section 4.4.1), and the degradation tendency will appear faster. This method usually uses to simulate the estimation of catalyst life time for coking deposit instead of running time-on-stream at the actual operating condition that required long time to see the decreasing tendency.

There are two methods to increase the WHSV. First, the reactant flow rate is increased, and second weight of pellet H-ZSM-5 filled in reactor was decreased. Since flow rate of this reaction in previous experiment (section 4.4.1) was already operated at the maximum capacity of pump spec (5ml/min), decreasing weight of filling pellet H-ZSM-5 to 1, and 0.2 grams at WHSV 300, and 1500 h^{-1} was only possible method that can be performed. However, the retrieving zeolites might not be enough to investigate all characterization technique such as XRD, BET, and NH_3-TPD, so the activity of zeolites detected by GC-FID was only method to investigate the stability of zeolites for this section.

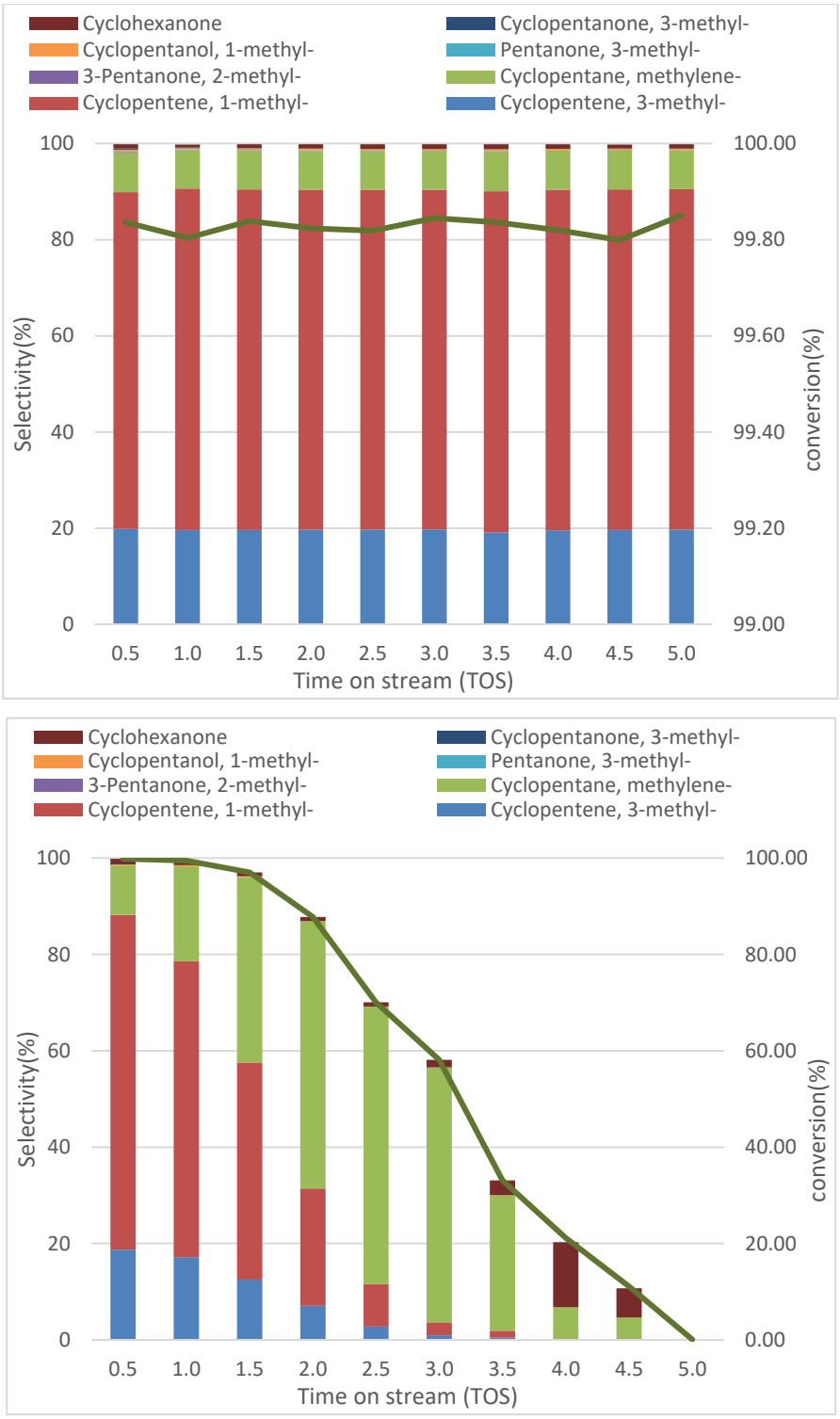

Figure 4-49 GC results of Cyclohexanol dehydration at 400 °C, P= 25 MPa, with zeolite P-H-ZSM-5 (1500) at WHSV 300 h^{-1}, and 1500 h^{-1}

The activity result of both WHSV at 300 and 1500 h^{-1} was presented in Figure 4-49. Pellet H-ZSM-5 still maintain the conversion nearly 100% with improving selectivity to derivative methyl-cyclopentene around 98.5% (selectivity of 3-methyl-cyclopentene, 1-methyl-cyclopentene, and methylene-cyclopentane are 19.5%, 70%, and 8%, respectively).

The accumulation Si loss on pellet H-ZSM-5 over 5 hours at WHSV 300 h^{-1} was estimated around 22% by weight. In case of WHSV 1500 h^{-1}, it was found that conversion was shapely dropped, and the decreasing of conversion begun at 1 hours of time on stream(TOS), and conversion remain only 1 % after 5 hours. Furthermore, no zeolites remained in the reactor after stop the reaction. The estimation of accumulated Si by ICP-AES on the effluence also predicted that pellet H-ZSM-5 (1500) will completely loss from their structure after operating for 4.5 hours. This experimental results proofs that the structure of zeolites was destructed by dealumination and desilication. Undetected destructive tendency of activity (GC-FID) and structure (XRD, BET, and crystallinity) operating with WHSV 100 and 300 h^{-1} were explained by the equilibrium between the disassociation and zeolite structure corresponding to section 4.1.5. The destruction should begin at the entrance zone of pack bed reactor and reach equilibrium of Si/Al solubility which protect the exit zone from destruction. (see Figure 4-50).

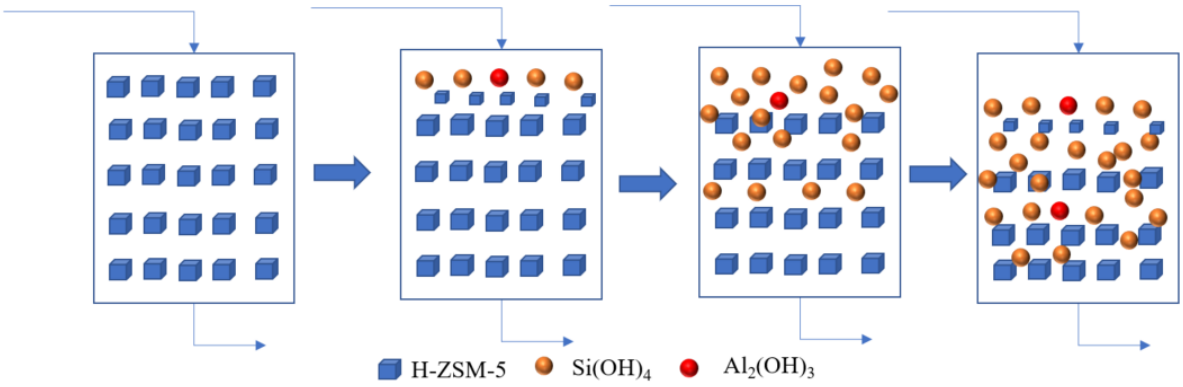

Figure 4-50 Schematic diagrams of water attack on pellet H-ZSM-5 in pack bed reactor.

In summary, unlike close system, pellet zeolites do not have the stability under operating in open system. Solubility of Si and Al play the important role for the destructive structure of zeolites for long term operation. To prevent Si and Al dissolving in the water, pre-filling with Si and Al in water (section 4.1.5) is the possible method that can be applied.

4.5 Acidity of zeolites investigated by NH_3-TPD

Acidity investigated by NH_3-TPD was presented in Table 4-6. All H-ZSM-5 samples have lower acidity comparing with before treatment with water. This result support the hypothesis that water begin to attack and remove alumina framework by dealumination reaction since Al atoms are the source of negative change of zeolites (see section 2.2.3). In case of H-ZSM-5(1500), the acidity deceased to nearly zero since it has already low alumina content

at the beginning. However, pellet H-ZSM-5(1500) provided surprisingly higher acidity than powder form. It was explained by the effect of mixing alumina binder (Al_2O_3) that decreased water attack on alumina framework because of the saturation of alumina ion by dissolving of alumina binder instead. Moreover, XRD pattern of pellet H-ZSM-5(1500) also support this hypothesis by indicated that lactic atoms of zeolite were increased after operating in sub- and supercritical water (section 4.3.3), which should be the result of reconstruction of alumina ion on zeolite framework because the average bond length of alumina with oxygen (Al-O 1.75 Å) is longer than silica with oxygen (Si-O 1.64 Å).

Table 4-6 NH_3-TPD of ZSM-5 after water attack at different condition

Type	Temp (^oC)	Pressure (MPa)	NH3-TPD(mmol/g)	Note**
H-ZSM-5(24)	RT*	Atm.	1.949	1.8
	400	24.1	0.351	
H-ZSM-5(40)	RT*	Atm.	1.551	1.3
	400	24.1	0.627	
H-ZSM-5(1500)	RT*	Atm.	0.372	
	250	saturated	0.015	
	400	24.1	0.000	
	400	26.9	0.003	
Pellet H-ZSM-5(1500)	RT*	Atm.	0.244	
	200	25	0.167	
	400	25	0.029	

*Room temperature(RT), ** Measurement by Tosoh co., Ltd

In summary, H-ZSM-5 loss their acidity under operating in sub- and supercritical water. However, Alumina binder in pellet form can reduced the effect of water attack on acid sites.

4.6 Destructive mechanism of zeolites in sub- and supercritical water

According to various studies on stability of zeolites, various destructive mechanism can be separated in three major categories as the following

4.6.1 Phase transformation

Phase transformation occurred two cases 1. β-zeolite transform to amorphous phase during operate at supercritical water and 2. Minor structure transformation in H-ZSM-5 (1500) that structure change from orthorhombic to monoclinic structure (see Figure 4-15). The reason of structure transformation occurred due to the increasing of stress in structure due to the high temperature and pressure (see Figure 4-51).

In case of β-zeolite transformation, the porous structure of zeolites is destroyed completely, and cannot remain the functional structure as catalyst. However, Minor structure transformation in H-ZSM-5 (1500) does not directly affect the property of zeolites as catalyst since the structure remain in porous shape.

Phase transformation directly related to the structure strength which caused by thermodynamic property such as energy of formation and steric effect in structure (see section 2.2.6)

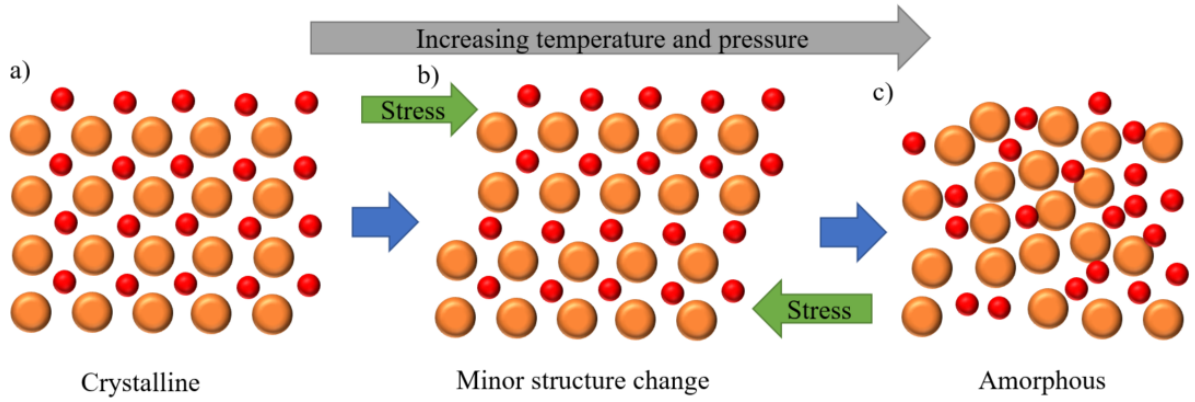

Figure 4-51 phase transformation on zeolites at sub- and supercritical water.

4.6.2 Coking

Coking is the general and well-known deactivation of catalyst appear in many hydrocarbon processes. According to Bartholomew study(Argyle & Bartholomew, 2015), at temperature lower 500 ºC slow polymerization of hydrocarbon radicals is generated to block active site or it call encapsulating film type which cause from low water/organic phase ratio or aromatic presence in feed. The presence of coke can also block the pore channel inside framework which directly effect to the activity of zeolite. By the way, coking effect can be eliminated by operating in supercritical water at high water/organic phase ratio.

Hydrophilic and hydrophobic zeolites also play the important role for amount of coking deposited on their structure (see section 4.2.2). Hydrophilic zeolites, Pellet H-ZSM-5 (1500), was found to have significant lower deposition of coke comparing with hydrophobic zeolites.

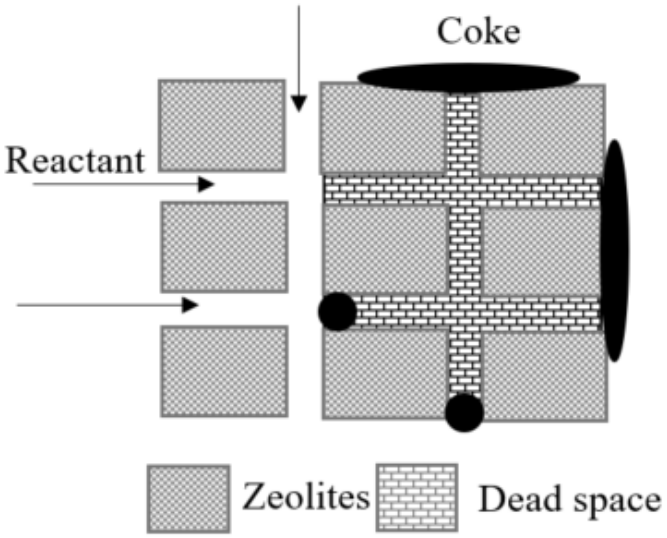

Figure 4-52 Schematic representation of a H-ZSM-5 structure, showing the coke depositions in the dehydration reaction over H-ZSM-5

4.6.3 Dissolving of Si and Al

Dissolving of Si and Al was found in both sub- and supercritical water. In previous study(Gounder, 2014), dealumination was found to occur in vapor phase, and in hot liquid water (<200 ºC) desilication was believed to occur.

However, in this study, various characterization techniques indicted that both dealumination and desilication occur in both sub- and supercritical water. For example, the intensity of XRD pattern in low angle was increased which indicted dealumination reaction, SEM-EDX found all zeolites sample had lower Si/Al ratio which indicted desilication reaction, NH_3-TPD result demonstrated that acidity of zeolites was decreased which indicted dealumination reaction, and ICP-AES found that both Si and Al dissolving in water, but silica was found higher than alumina. With gathering all information together, the destructive structure mechanism was proposed in Figure 4-53.

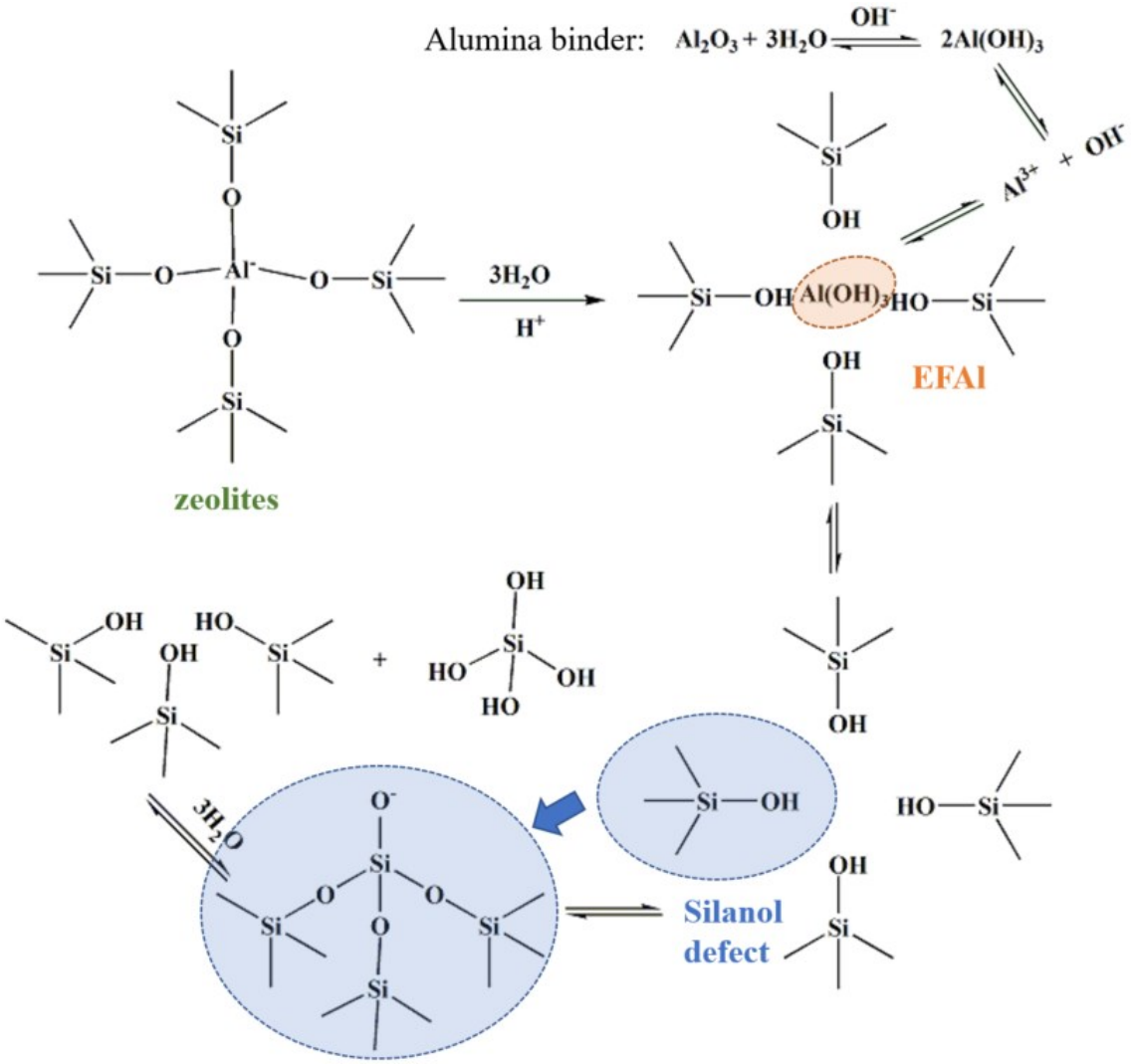

Figure 4-53 Schematic diagram of destructive structure of zeolites by water attack

Detail of destructive mechanism was explained in step-by-step as the following

1st Step: Dealumination to create $Al(OH)_3$ or EFAl.

Since alumina atoms have three valance electrons but it bonds with four atoms of silica in zeolites structure, alumina in structure framework will produce the negative change or acid sites. After water attacked and reduced, alumina will leave from zeolites structure, and create extra-framework alumina (EFAl) which still deposited on zeolites structure and encapsulate the vulnerable silanol defect. At this step, totally acidity was decreased, the intensity of XRD in low angles (2θ =4°-10°) was increased (Viswanadham et al., 2006), and SEM-EDX still provide the same result because alumina does not detract from structure.

2nd Step: Dissociation of EFAl and Binder

Extra-framework alumina (EFAl) can be dissolved and remove from the framework by acid or base (Fan, Bao, Lin, Shi, & Liu, 2006). In sub- and supercritical water, water can act

itself as acid (H^+) or base (OH^-) to dissolve EFAl into alumina ion. This reaction directly relates with the dissociation of water, which means that this reaction also temperature dependence. Since alumina slightly found in the effluence, it indicated that it has the equilibrium between EFAl and Alumina ion. Moreover, this reaction is favor to reactant side (EFAl). This hypothesis explained the reason that high crystallinity was found in close system but not in the open system at high WHSV. In plug flow reactor, adding alumina binder create extra alumina ion which block the dissolving of EFAl. In addition, alumina ion was found to re-associate with the framework (see section 4.3.3).

3rd Step: Desilication (1 $Al(OH)_3$ ---> 4 Silanol defect(Si-OH))

After one EFAl is dissolved in the water, four silanol defect will be created. This functional group are vulnerable to be attacked by water and produces $Si(OH)_4$.

4th Step: Chain reaction of desilication

After water attacked at one silanol defect site, it generates three more silanol defect site. The reaction will stop after reach equilibrium between silica in framework and silica ion.

CHAPTER 5 CONCLUSION AND RECOMMENDATION

5.1 Conclusion

The structure stability of zeolites strongly depended on their framework and SiO_2/Al_2O_3 ratio. It was found that β-zeolites completely transform to amorphous phase. However, H-ZSM-5 maintain mostly their structure in supercritical water, especially H-ZSM-5 with higher SiO_2/Al_2O_3 ratio providing infinitesimal change of crystallinity. Nevertheless, dissolving of Si and Al was observed by ICP-AES, and decreasing of acidity was found by NH_3-TPD in both sub- and supercritical water, which indicated that desilication and dealumination occurred. The reason why structure of zeolites remained in sub- and supercritical water was explained by the saturation of Si and Al in the effluence which stop desilication and dealumination to proceed. To improve the structure stability, pre-filling with Si and Al in water was found to increase the remaining crystallinity.

Deactivation by coking also appeared in cyclohexene hydration in sub-critical water. it found that amount of deposited coking was depend on SiO_2/Al_2O_3 ratio of zeolites. Hydrophilic zeolites, P-H-ZSM-5(1500), have lower deposited coking due to effect of water surrounding preventing the polymerization reaction.

The destructive mechanism was separated in three types including phase transformation, coking, and dissolving of Si and Al. Phase transformation to amorphous phase occurred in β-zeolites operating at supercritical water, coking was severe appeared in hydrophobic zeolites, and dissolving of Si and Al begun with dealumination, and following by desilication reaction.

5.2 Recommendation

High silica per alumina ratio of H-ZSM-5 exhibits excellent stability and performance in both cyclohexene hydration and cyclohexanol dehydration in sub- and supercritical water. However, dissolving of silica and alumina might be the major drawback for applied in actual process application. Nevertheless, since dissolving of silica and alumina was confirmed that it has the equilibrium between in the framework and water, applied water to pre-encounter with SiO_2 and Al_2O_3 combining with recycle line that generally use in industrial processes is the one possible method to improve the life time of catalyst (see Figure 5-1).

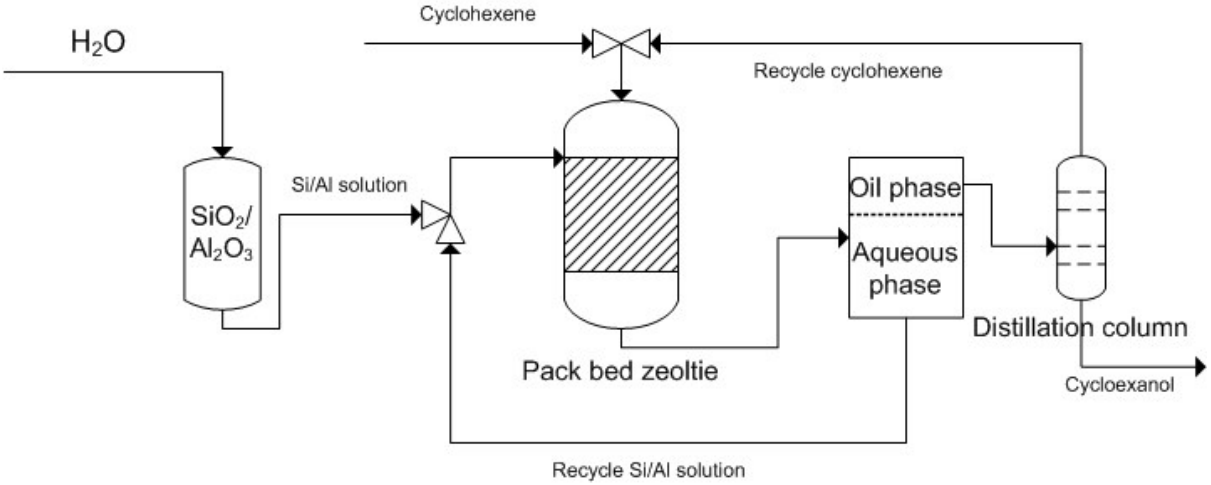

Figure 5-1 Process flow diagram of cyclohexene hydration by applied saturation concept.

REFERENCES

Akiya, N., & Savage, P. E. (2001). Kinetics and Mechanism of Cyclohexanol Dehydration in High-Temperature Water. *Industrial & Engineering Chemistry Research*, *40*, 1822–1831. https://doi.org/10.1021/ie000964z

Akiya, N., & Savage, P. E. (2002). Roles of Water for Chemical Reactions in High-Temperature Water. *Chemical Reviews*, *102*(8), 2725–2750. https://doi.org/10.1021/cr000668w

Akizuki, M., Fujii, T., Hayashi, R., & Oshima, Y. (2014). Effects of water on reactions for waste treatment, organic synthesis, and bio-refinery in sub- and supercritical water. *Journal of Bioscience and Bioengineering*, *117*(1), 10–18. https://doi.org/10.1016/j.jbiosc.2013.06.011

Akizuki, M., & Oshima, Y. (2012). Kinetics of glycerol dehydration with WO 3/TiO 2 in supercritical water. *Industrial and Engineering Chemistry Research*, *51*(38), 12253–12257. https://doi.org/10.1021/ie301823f

Akizuki, M., & Oshima, Y. (2017). Acid catalytic properties of TiO 2 , Nb 2 O 5 , and NbO X /TiO 2 in supercritical water. *The Journal of Supercritical Fluids*. https://doi.org/10.1016/j.supflu.2017.12.009

Akizuki, M., Tomita, K., & Oshima, Y. (2011). Kinetics of solid acid catalyzed 1-octene reactions with TiO2 in sub- and supercritical water. *Journal of Supercritical Fluids*, *56*(1), 14–20. https://doi.org/10.1016/j.supflu.2010.11.015

Ardit, M., Martucci, A., & Cruciani, G. (2015). Monoclinic orthorhombic phase transition in ZSM 5 zeolite: Spontaneous strain variation and thermodynamic properties. *Journal of Physical Chemistry C*, *119*(13), 7351–7359. https://doi.org/10.1021/acs.jpcc.5b00900

Argyle, M., & Bartholomew, C. (2015). Heterogeneous Catalyst Deactivation and Regeneration: A Review. *Catalysts*, *5*(1), 145–269. https://doi.org/10.3390/catal5010145

Astmd5758-01. (2011). Standard Test Method for Determination of Relative Crystallinity of Zeolite ZSM-5 by, *1*(Reapproved 2011), 6–9. https://doi.org/10.1520/D5758-01R11E01.2

Baerlocher, C. (2017). Database of Zeolite Structures. Retrieved December 28, 2017, from http://www.iza-structure.org/databases/

Baerlocher, C., McCusker, L., & Olson, D. (2007). *Atlas of zeolite framework types*. *Sensors* (Vol. 12). https://doi.org/10.1016/B978-044453064-6/50287-5

Bandura, A. V., & Lvov, S. N. (2006). The ionization constant of water over wide ranges of temperature and density. *Journal of Physical and Chemical Reference Data*, *35*(1), 15–30. https://doi.org/10.1063/1.1928231

Brunner, G. (2009). Near critical and supercritical water. Part I. Hydrolytic and hydrothermal processes. *Journal of Supercritical Fluids*, *47*(3), 373–381. https://doi.org/10.1016/j.supflu.2008.09.002

Camblor, M. A., & Pérez-Pariente, J. (1991). Crystallization of zeolite beta: Effect of Na and K ions. *Zeolites*, *11*(3), 202–210. https://doi.org/10.1016/S0144-2449(05)80220-9

Čejka, J., Corma, A., & Tacey, Z. (2010). *Zeolites and Catalysis*. (J. Čejka, A. Corma, & S. Zones, Eds.). Weinheim, Germany: Wiley-VCH Verlag GmbH & Co. KGaA. https://doi.org/10.1002/9783527630295

Chakinala, A. G., Chinthaginjala, J. K., Seshan, K., Van Swaaij, W. P. M., Kersten, S. R. A., & Brilman, D. W. F. (2012). Catalyst screening for the hydrothermal gasification of aqueous phase of bio-oil. *Catalysis Today*, *195*(1), 83–92. https://doi.org/10.1016/j.cattod.2012.07.042

Chareonlimkun, A., Champreda, V., Shotipruk, A., & Laosiripojana, N. (2010). Catalytic conversion of sugarcane bagasse, rice husk and corncob in the presence of TiO2, ZrO2 and mixed-oxide TiO2-ZrO2 under hot compressed water (HCW) condition. *Bioresource Technology*, *101*(11), 4179–4186. https://doi.org/10.1016/j.biortech.2010.01.037

Chheda, J. N., & Dumesic, J. a. (2006). Production of Hydroxymethylfurfural from Fructose. *Science*, *312*(4), 1933. https://doi.org/10.1126/science.1126337

Corma, A., Iborra, S., & Velty, A. (2007). Chemical routes for the transformation of biomass into chemicals. *Chemical Reviews*, *107*(6), 2411–502. https://doi.org/10.1021/cr050989d

de Vlieger, D. J. M., Chakinala, A. G., Lefferts, L., Kersten, S. R. A., Seshan, K., & Brilman, D. W. F. (2012). Hydrogen from ethylene glycol by supercritical water reforming using noble and base metal catalysts. *Applied Catalysis B: Environmental*, *111–112*, 536–544. https://doi.org/10.1016/j.apcatb.2011.11.005

De Vlieger, D. J. M., Mojet, B. L., Lefferts, L., & Seshan, K. (2012). Aqueous Phase Reforming of ethylene glycol - Role of intermediates in catalyst performance. *Journal of Catalysis*, *292*, 239–245. https://doi.org/10.1016/j.jcat.2012.05.019

Degnan, Jr., T. F. (2000). Applications of zeolites in petroleum refing. *Topics in Catalysis*, *13*(4), 349–356. https://doi.org/10.1023/A:1009054905137

Dimitrijevic, R., Lutz, W., & Ritzmann, A. (2006). Hydrothermal stability of zeolites: Determination of extra-framework species of H-Y faujasite-type steamed zeolite. *Journal of Physics and Chemistry of Solids*, *67*(8), 1741–1748. https://doi.org/10.1016/j.jpcs.2006.03.014

Eckert, C. A., Liotta, C. L., Bush, D., Brown, J. S., & Hallett, J. P. (2004). Sustainable reactions in tunable solvents. *Journal of Physical Chemistry B*, *108*(47), 18108–18118. https://doi.org/10.1021/jp0487612

external standard in chromatography. (n.d.). In *IUPAC Compendium of Chemical Terminology*. Research Triagle Park, NC: IUPAC. https://doi.org/10.1351/goldbook.E02290

Fan, Y., Bao, X., Lin, X., Shi, G., & Liu, H. (2006). Acidity adjustment of HZSM-5 zeolites by dealumination

and realumination with steaming and citric acid treatments. *Journal of Physical Chemistry B*, *110*(31), 15411–15416. https://doi.org/10.1021/jp0607566

Fernández, D. P., Goodwin, A. R. H., Lemmon, E. W., Levelt Sengers, J. M. H., & Williams, R. C. (1997). A Formulation for the Static Permittivity of Water and Steam at Temperatures from 238 K to 873 K at Pressures up to 1200 MPa, Including Derivatives and Debye–Hückel Coefficients. *Journal of Physical and Chemical Reference Data*, *26*(4), 1125–1166. https://doi.org/10.1063/1.555997

Fournier, R. O., & Rowe, J. j. (1977). The solubility of amorphous silica in water at high temperatures and high pressures. *American Mineralogist*, *62*, 1052–1056. Retrieved from http://www.minsocam.org/ammin/AM62/AM62_1052.pdf

Gayubo, A. G., Alonso, A., Valle, B., Aguayo, A. T., & Bilbao, J. (2010). Selective production of olefins from bioethanol on HZSM-5 zeolite catalysts treated with NaOH. *Applied Catalysis B: Environmental*, *97*(1–2), 299–306. https://doi.org/10.1016/j.apcatb.2010.04.021

Gounder, R. (2014). Hydrophobic microporous and mesoporous oxides as Bronsted and Lewis acid catalysts for biomass conversion in liquid water. *Catal. Sci. Technol.*, *4*(9), 2877–2886. https://doi.org/10.1039/C4CY00712C

Hirth, T., & Franck, E. U. (1993). Oxidation and Hydrothermolysis of Hydrocarbons in Supercritical Water at High Pressures. *Berichte Der Bunsengesellschaft Für Physikalische Chemie*, *97*(9), 1091–1097. https://doi.org/10.1002/bbpc.19930970905

Huber, G. W., Iborra, S., & Corma, A. (2006). Synthesis of transportation fuels from biomass: Chemistry, catalysts, and engineering. *Chemical Reviews*, *106*(9), 4044–4098. https://doi.org/10.1021/cr068360d

internal standard in chromatography. (n.d.). In *IUPAC Compendium of Chemical Terminology*. Research Triagle Park, NC: IUPAC. https://doi.org/10.1351/goldbook.I03108

Jongerius, A. L., Copeland, J. R., Foo, G. S., Hofmann, J. P., Bruijnincx, P. C. A., Sievers, C., & Weckhuysen, B. M. (2013). Stability of Pt/γ-Al2O3 catalysts in lignin and lignin model compound solutions under liquid phase reforming reaction conditions. *ACS Catalysis*, *3*(3), 464–473. https://doi.org/10.1021/cs300684y

Katritzky, A. R., Allin, S. M., & Siskin, M. (1996). Aquathermolysis: Reactions of Organic Compounds with Superheated Water. *Accounts of Chemical Research*, *29*(8), 399–406. https://doi.org/10.1021/ar950144w

Kokotailo, G. T., Lawton, S. L., Olson, D. H., & Meier, W. M. (1978). Structure of synthetic zeolite ZSM-5. *Nature*, *272*(5652), 437–438. https://doi.org/10.1038/272437a0

Luo, C., Wang, S., & Liu, H. (2007). Cellulose conversion into polyols catalyzed by reversibly formed acids and supported ruthenium clusters in hot water. *Angewandte Chemie - International Edition*, *46*(40), 7636–7639. https://doi.org/10.1002/anie.200702661

Luo, N., Fu, X., Cao, F., Xiao, T., & Edwards, P. P. (2008). Glycerol aqueous phase reforming for hydrogen generation over Pt catalyst - Effect of catalyst composition and reaction conditions. *Fuel*, *87*(17–18), 3483–3489. https://doi.org/10.1016/j.fuel.2008.06.021

Lutz, W., Toufar, H., Kurzhals, R., & Suckow, M. (2005). Investigation and modeling of the hydrothermal stability of technically relevant zeolites. *Adsorption*, *11*(3–4), 405–413. https://doi.org/10.1007/s10450-005-5406-9

Lynd, L. R., Wyman, C. E., & Gerngross, T. U. (1999). Biocommodity engineering. *Biotechnology Progress*, *15*(5), 777–793. https://doi.org/10.1021/bp990109e

Matsumura, Y., Minowa, T., Potic, B., Kersten, S. R. A., Prins, W., Van Swaaij, W. P. M., … Antal, M. J. (2005). Biomass gasification in near- and super-critical water: Status and prospects. *Biomass and Bioenergy*, *29*(4), 269–292. https://doi.org/10.1016/j.biombioe.2005.04.006

McCusker, L. B. (1998). Product characterization by X-ray powder diffraction. *Microporous and Mesoporous Materials*, *22*(4–6), 527–529. https://doi.org/10.1016/S1387-1811(98)80016-4

Mo, N., & Savage, P. E. (2014). Hydrothermal Catalytic Cracking of Fatty Acids with HZSM - 5. *ACS Sustainable Chemistry & Engineering*, *2*, 88−94. https://doi.org/10.1021/sc400368n

Peterson, A. A., Vogel, F., Lachance, R. P., Fröling, M., Antal, Jr., M. J., & Tester, J. W. (2008). Thermochemical biofuel production in hydrothermal media: A review of sub- and supercritical water technologies. *Energy & Environmental Science*, *1*(1), 32. https://doi.org/10.1039/b810100k

Pham, H. N., Anderson, A. E., Johnson, R. L., Schmidt-Rohr, K., & Datye, A. K. (2012). Improved hydrothermal stability of mesoporous oxides for reactions in the aqueous phase. *Angewandte Chemie - International Edition*, *51*(52), 13163–13167. https://doi.org/10.1002/anie.201206675

Pham, H. N., Pagan-Torres, Y. J., Serrano-Ruiz, J. C., Wang, D., Dumesic, J. A., & Datye, A. K. (2011). Improved hydrothermal stability of niobia-supported Pd catalysts. *Applied Catalysis A: General*, *397*(1–2), 153–162. https://doi.org/10.1016/j.apcata.2011.02.026

Rabo, J. A., & Schoonover, M. W. (2001). Early discoveries in zeolite chemistry and catalysis at Union Carbide, and follow-up in industrial catalysis. *Applied Catalysis A: General*, *222*(1–2), 261–275. https://doi.org/10.1016/S0926-860X(01)00840-7

Ramasamy, K. K., Gerber, M. A., Flake, M., Zhang, H., & Wang, Y. (2014). Conversion of biomass-derived small oxygenates over HZSM-5 and its deactivation mechanism. *Green Chemistry*, *16*(2), 748–760. https://doi.org/10.1039/C3GC41369A

Ramos, L., Kristenson, E. M., & Brinkman, U. T. (2002). Current use of pressurised liquid extraction and subcritical water extraction in environmental analysis. *Journal of Chromatography A*, *975*(1), 3–29. https://doi.org/10.1016/S0021-9673(02)01336-5

Ravenelle, R. M., Copeland, J. R., Kim, W. G., Crittenden, J. C., & Sievers, C. (2011). Structural Changes of γ-Al2O3-Supported Catalysts in Hot Liquid Water. *ACS Catalysis*, *1*(5), 552–561. https://doi.org/10.1021/cs1001515

Ravenelle, R. M., Schübler, F., Damico, A., Danilina, N., Van Bokhoven, J. A., Lercher, J. A., … Sievers, C. (2010). Stability of zeolites in hot liquid water. *Journal of Physical Chemistry C*, *114*(46), 19582–19595. https://doi.org/10.1021/jp104639e

Savage, P. E. (2009). A perspective on catalysis in sub- and supercritical water. *Journal of Supercritical Fluids*, *47*(3), 407–414. https://doi.org/10.1016/j.supflu.2008.09.007

Shafiee, S., & Topal, E. (2009). When will fossil fuel reserves be diminished? *Energy Policy*, *37*(1), 181–189. https://doi.org/10.1016/j.enpol.2008.08.016

Tanabe, K. (1999). Industrial application of solid acid–base catalysts. *Applied Catalysis A: General*, *181*, 399–434. https://doi.org/10.1016/S0926-860X(98)00397-4

Vilcocq, L., Cabiac, A., Especel, C., Lacombe, S., & Duprez, D. (2011). Study of the stability of Pt/SiO2-Al2O3 catalysts in aqueous medium: Application for sorbitol transformation. *Catalysis Communications*, *15*(1), 18–22. https://doi.org/10.1016/j.catcom.2011.08.002

Viswanadham, N., Gupta, J. K., Dhar, G. M., & Garg, M. O. (2006). Effect of Synthesis Methods and Modification Treatments of ZSM-5 on Light Alkane Aromatization, (15), 1806–1814.

Wagner, W., & Pruß, A. (2002). The IAPWS Formulation 1995 for the Thermodynamic Properties of Ordinary Water Substance for General and Scientific Use. *Journal of Physical and Chemical Reference Data*, *31*(2), 387–535. https://doi.org/10.1063/1.1461829

Wawrzetz, A., Peng, B., Hrabar, A., Jentys, A., Lemonidou, A. A., & Lercher, J. A. (2010). Towards understanding the bifunctional hydrodeoxygenation and aqueous phase reforming of glycerol. *Journal of Catalysis*, *269*(2), 411–420. https://doi.org/10.1016/j.jcat.2009.11.027

Weingärtner, H., & Franck, E. U. (2005). Supercritical Water as a Solvent. *Angewandte Chemie International Edition*, *44*(18), 2672–2692. https://doi.org/10.1002/anie.200462468

Xiong, H., Pham, H. N., & Datye, A. K. (2013). A facile approach for the synthesis of niobia/carbon composites having improved hydrothermal stability for aqueous-phase reactions. *Journal of Catalysis*, *302*, 93–100. https://doi.org/10.1016/j.jcat.2013.03.007

Yu, J., & Savage, P. E. (2001). Catalyst activity, stability, and transformations during oxidation in supercritical water. *Applied Catalysis B: Environmental*, *31*(2), 123–132. https://doi.org/10.1016/S0926-3373(00)00273-3

Yu, Y., Lou, X., & Wu, H. (2008). Some Recent Advances in Hydrolysis of Biomass in Hot-Compressed Water and Its Comparisons with Other Hydrolysis Methods †. *Energy & Fuels*, *22*(1), 46–60.

https://doi.org/10.1021/ef700292p

Yuan, P., Liu, Y., Bai, F., Xu, L., Cheng, Z., & Yuan, W. (2011). Hydration of cyclohexene in sub-critical water over WO x – ZrO 2 catalysts. *CATCOM*, *12*(8), 753–756. https://doi.org/10.1016/j.catcom.2011.01.009

Zapata, P. A., Huang, Y., Gonzalez-Borja, M. A., & Resasco, D. E. (2013). Silylated hydrophobic zeolites with enhanced tolerance to hot liquid water. *Journal of Catalysis*, *308*, 82–97. https://doi.org/10.1016/j.jcat.2013.05.024

Zhang, L., Chen, K., Chen, B., White, J. L., & Resasco, D. E. (2015). Factors that Determine Zeolite Stability in Hot Liquid Water. *Journal of the American Chemical Society*, *137*(36), 11810–11819. https://doi.org/10.1021/jacs.5b07398

Zimmermann, N. E. R., & Haranczyk, M. (2016). History and Utility of Zeolite Framework-Type Discovery from a Data-Science Perspective. *Crystal Growth and Design*, *16*(6), 3043–3048. https://doi.org/10.1021/acs.cgd.6b00272

ACKNOWLEDGEMENTS

First and foremost, I would like to express my sincere and gratitude to my advisor, Professor Yoshito Oshima for giving me an opportunity to study on the stability of zeolites with a great help, advice, and support during two years of my master studies. His expertise on sub- and supercritical water are outstanding and allow me to understand the behavior of water in the new aspects that I never experience. Moreover, I would like to thank Assistant Professor Makoto Akizuki for his advice, feedback, support and deeply discussion about my research. He also created plug flow system and NH_3-TPD unit that I use to investigate the catalytic stability of zeolites. Without his contribution, my study could lack of the concrete evidence to investigate the stability of zeolites.

I would like to gratefully acknowledge my thesis co-advisor Professor Tomochika Tokunaga for good advices and comments including a very useful contact for special analysis equipment (Solid-state NMR) that is necessary for my future research.

I would like to take this opportunity to thank Associate Professor Junichiro Otomo. During joint seminar presentation, he gives a helpful instruction for my research. In addition, he also allows me to use BET and TGA analysis equipment for investigate the surface area of zeolites and the deposited coking. Assistant Professor Fumihiko Kosaka also sacrifice his time to help and teach me how to use BET and TGA which I deeply appreciate for his contribution.

I have received great support from many people in the Institute for Solid State Physics (ISSP) and Environment and Safety Research Center in the University of Tokyo for teaching and allow me to use various characterization equipment such as Assistant Professor Osamu Sawai for GC-MS, Assistant Professor Takeshi Yajima for XRD analysis, Dr. Daisuke Hamane for TEM, SEM and EDX, and Masayoshi Koike for ICP-AES. I really appreciate all of them for the tremendous support and kindness.

I am extremely grateful for everyone in Oshima and Otomo laboratory members that help me in many ways such as translating Japanese document or teaching me how to handle the equipment in our laboratory.

I would like to thank Monbukagakusho (MEXT) scholarship for financial support during I stay in Japan, and I am grateful to Tosoh corporation for provide free samples of all pellet zeolites that used in this report.

Lastly, I would like to dedicate the achievement of my work to my family. Without their support, it will be hard for me to accomplish this work.